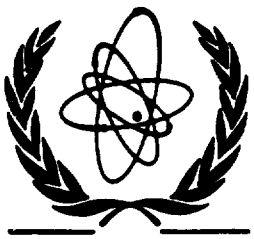

International Atomic Energy Agency

INDC(BLR)-005
Distr. G

INDC INTERNATIONAL NUCLEAR DATA COMMITTEE

EVALUATION OF NEUTRON DATA FOR AMERICIUM-241

V.M. Maslov, E.Sh. Sukhovitskij, Yu.V. Porodzinskij,
A.B. Klepatskij, G.B. Morogovskij

Radiation Physics & Chemistry Problems Institute
220109, Minsk-Sosny, Belarus

October 1996

IAEA NUCLEAR DATA SECTION, WAGRAMERSTRASSE 5, A-1400 VIENNA

Reproduced by the IAEA in Austria
October 1996

INDC(BLR)-005
Distr. G

EVALUATION OF NEUTRON DATA FOR AMERICIUM-241

V.M. Maslov, E.Sh. Sukhovitskij, Yu.V. Porodzinskij,
A.B. Klepatskij, G.B. Morogovskij

Radiation Physics & Chemistry Problems Institute
220109, Minsk-Sosny, Belarus

Abstract

The evaluation of neutron data for ^{241}Am is made in the energy region from 10^{-5} eV to 20 MeV. The results of the evaluation are compiled in the ENDF/B-VI format.

This work is performed under the Project Agreement CIS-03-95 with the International Science and Technology Center (Moscow). The Financing Party for the Project is Japan. The evaluation was requested by Y. Kikuchi (JAERI).

Date of Manuscript: May 8, 1996

Contents

1. **Introduction** 7

2. **Resolved resonance region** 7
   - 2.1 Previous evaluations of resolved resonance parameters 7
   - 2.2 Measured data fitting 8
     - 2.2.1 Total cross section 8
     - 2.2.2 Fission cross section 9
     - 2.2.3 Radiative capture cross section 9
     - 2.2.4 Absorption cross section 9
     - 2.2.5 Energy region below 0.1 eV 9
     - 2.2.6 Energy region 0.1 ÷ 150 eV 9
     - 2.2.7 Resonance parameter analysis 10

3. **Unresolved resonance region** 11
   - 3.1 Review 11
   - 3.2 The s-wave average resonance parameter evaluation 11
     - 3.2.1 Estimate of resonance level missing influence on $< D_{obs} >$ and $< S_0 >$ 11
     - 3.2.2 Evaluation of $< D_{obs} >$, $< S_0 >$, $< \Gamma_\gamma >$ and $< \Gamma_f >$ based on the resonance parameters 12
   - 3.3 The s-, p- and d-wave average resonance parameter evaluation 12
     - 3.3.1 Neutron width 12
     - 3.3.2 Neutron resonance spacing 13
     - 3.3.3 Fission width 13
     - 3.3.4 Radiative capture width 13
   - 3.4 Cross section evaluation in the region 0.15 - 41.3483 keV 14
     - 3.4.1 Fitting of fission cross section structure 14
     - 3.4.2 Capture cross section energy dependence 14
     - 3.4.3 Comparison of current and JENDL-3 and ENDF/B-VI evaluated data 15

4. **Fast neutron cross sections** 15
   - 4.1 Optical potential 16
   - 4.2 Fission cross section 17
     - 4.2.1 Status of the experimental data 17
     - 4.2.2 Statistical model calculation of fission cross section 19
     - 4.2.3 Fission transmission coefficient, level density and transitition state spectrum 20
     - 4.2.4 Fission cross section above emissive fission threshold 22
   - 4.3 Inelastic scattering cross section 23
     - 4.3.1 Levels of ^{241}Am 23
     - 4.3.2 ^{241}Am level density 23
     - 4.3.3 Compound inelastic scattering 23
     - 4.3.4 Direct inelastic scattering 24

4.3.5 ^{242}Am level density 24
4.4 Radiative capture cross section 25
4.5 Cross sections of (n,2n) and (n,3n) reactions 26

5. Energy distributions of secondary neutrons 26
5.1 Model calculations of (n,nx) reaction spectra 26
5.2 Prompt fission neutron spectra 27
5.2.1 Model calculations of prompt fission neutron spectra 27
5.2.2 Other parameters 28
5.2.3 Prompt fission neutron spectra evaluation 28

6. Number of neutrons per fission 30

7. Angular distributions of secondary neutrons 31

8. Conclusions 31

9. References 32

10. Figure captions 35

1 Introduction

The advanced nuclear fuel cycle studies request the nuclear data of transplutonium isotopes.[1] The neutron data for americium isotopes are especially important in this respect. Recently we have evaluated the data for ^{243}Cm, ^{245}Cm and ^{246}Cm. In this work the evaluation of ^{241}Am neutron data is performed. The next isotope, which neutron data would be evaluated is ^{243}Am. The curium and americium isotopes data to be evaluated were requested by the General Manager of Japan Nuclear data Center Dr. Y. Kikuchi. The quantities evaluated are resolved and unresolved resonance parameters, total, elastic and inelastic scattering, fission, capture, (n,2n) and (n,3n) reaction cross sections, angular and energy distributions of secondary neutrons, including partial (n,xn) and (n,xnf) reaction spectra, fission spectra and number of neutrons per fission. The incident neutron energy range covered is from 10^{-5} eV up to 20 MeV. The evaluated quantities are compared with JENDL-3 evaluation.[2]

2 Resolved resonance region

The measured data base has not changed essentially since the JENDL-3 and ENDF/B-VI evaluations were completed. Although the high level of subthreshold fission cross section of Seeger et al.[4] was discarded, the recent data of Kobayashi et al.[5] attracted attention to this problem once again. The latter data are still unaccessible up to now, maybe because they need more sophisticated analysis of ^{241}Am sample impurities.

2.1 Previous evaluations of resolved resonance parameters

The evaluated single-level Breit-Wigner resonance parameters of ENDF/B-VI[3] are based on the resonance parameters by Derrien and Lucas[6], Weston and Todd[7] and Kalebin et al.[8] from 10^{-5} eV up to 150 eV. Since the first few resonance parameters given by these authors are quite compatible, the evaluated resonance parameters are the average values of initial resonance parameters.[6,7,8] The weights take into account the appropriate measurement errors. The resulted 195 resonance parameters, including 5 negative resonances, are obtained assuming radiation width Γ_γ = 44.2 meV for 70% of the resonances. The scatter of radiation width values is from 10 meV up to 94 meV. In the energy region 142.5-150 eV a background radiative capture cross section of 12.2 barns is employed. The average resonance parameters,

thermal cross sections and resonance integral data are given in Table 2.1. Thermal total cross section is compatible with Kalebin et al.[8] data.

The multi-level Breit-Wigner resonance parameters of JENDL-3 evaluation[2] are actually parameters, provided by Derrien and Lucas.[6] Since the fission width values are provided by Derrien and Lucas[6] only up to 40 eV, at higher energies average fission width value of 0.229 meV was adopted. The radiation width $\Gamma_\gamma = 43.77$ meV was assumed for 102 resonances out of total number of 194 resonances. In the energy interval of 55 - 67 eV the radiation width Γ_γ was increased arbitrarily by 100 meV, this leads to severe discrepancies of ENDF/B-VI and JENDL-3 evaluated capture cross sections. Thermal total and capture cross sections are compatible with Lynn et al.[9] evaluation.

2.2 Measured data fitting

The purpose of current resonance parameter evaluation is to extract resolved resonance parameters up to 150 eV by consistent analysis of available data on total, fission, absorption and capture data. The incident neutron energies range is divided rather arbitrarily into two intervals: 10^{-5} - 0.1 eV and 0.1 - 150 eV. The energy point of 0.1 eV was chosen because the negative resonances define the cross sections below 0.1 eV, while contributing mainly to the thermal cross section values. The multi-level Breit-Wigner formalism is employed. The assigning of resonance spins was done as follows. Two assumptions were adopted: the number of resonances with spin J is proportional to $(2J+1)$, reduced neutron width distribution should obey that of Porter-Thomas, neutron resonance spacing distribution should obey that of Wigner.

2.2.1 Total cross section

The total cross section data of Derrien and Lucas[6] are available in the energy region of 0.785 eV - 150 eV, Adamchuk et al.[10] data are available in the energy region of 0.0063 eV - 82 eV and Belanova et al.[11] data are available in the energy region of 0.0212 eV - 150 eV. Two former data sets[6,10] are compatible in the energy interval of 0.785 eV - 1 eV, while the latter data set is systematically higher by about $40 \div 50$ barns below 1 eV (see fig. 2.1). The same is true at higher energies (see fig. 2.2), however the data shapes are similar. Moreover, the thermal total cross section of Belanova et al.[11] is essentially higher than other available data. We suppose that there is a systematic error in data of Belanova et al.[11], so we omit them henceforth from the analysis.

2.2.2 Fission cross section

Fission cross section was measured in the energy region of 1 eV - 40 eV by Derrien and Lucas[6], in the energy region above 0.01883 eV by Dabbs et al.[12], in the energy region of 0.0321 eV - 150 eV by Bowman et al.[13] and in the energy region of 0.0231 eV - 50 eV by Gerasimov et al.[14] All data sets, excluding data of Dabbs et al.[12], were normalized to the thermal fission cross section value of ~3.13 eV.

2.2.3 Radiative capture cross section

Radiative capture cross section was measured in the energy region of 0.68 eV - 150 eV by Vanpraet et al.[15]

2.2.4 Absorption cross section

Absorption cross section was measured in the energy region of 0.01 eV - 370 keV by Weston and Todd.[7] The cross section was normalized at thermal neutron energies (0.2-0.3 eV).

2.2.5 Energy region below 0.1 eV

The negative resonances define the cross section values in this energy region. We adopted the following thermal values of: total $\sigma_t = 599.5$ barns, absorption $\sigma_a = 582.78$ barns and fission $\sigma_f = 3.136$ barns cross sections, evaluated from the measured data. The potential scattering radius, calculated with the coupled channel approach $R_p = 9.157$ fm. The resonance contribution to the thermal scattering cross section is about 1 barn, the absorption cross section data of Weston and Todd[7] should be renormalized to the value of thermal absorption cross section $\sigma_a = \sigma_t - \sigma_n \simeq 588$ barns. Consistent fitting of total, absorption and fission data gives the appropriate values, given in Table 2.1

The negative resonance parameters due to Lynn et al.[9]are adopted. Thermal cross section values and cross section data below 0.1 eV are fitted with present resonance parameters.

2.2.6 Energy region 0.1 ÷ 150 eV

There is a systematic difference in the energy interval of 15 eV - 39.8 eV between fission data by Derrien and Lucas[6] and by Dabbs et al.[12], the latter being ~30% higher. However, for narrower intervals (~5 eV), the difference may exceed ~40%. To "reconcile" both data sets we assumed the total error of data of Dabbs et al.[12] ~3 times as large as original total error. The resolution function of Dabbs et al.[12] measurement was modelled[16], while the resolution parameter was extracted from the comparison of the original

data and reconstructed with modelled resolution function of data by Dabbs et al.[12]

The resolution function of Vanpraet[15] capture cross section measurement was also modelled[16], while the resolution parameter was extracted from the data shape analysis. It was increased ~5 times in the interval 56.5 - 79 eV, ~4 times in the interval 79 eV - 110.7 eV, ~3 times in the interval 110.7 eV – 150 eV. We suppose that the total error must be about that of the absorption measurement by Weston and Todd.[7] Hence, the original error was increased ~2.3 times.

2.2.7 Resonance parameter analysis

We have got parameters for 195 resonances up to 150 eV. They describe the measured data on total, fission and capture cross sections within the attributed errors. The average resonance parameters, thermal cross sections and resonance integrals are presented in Table 2.1. Figures 2.3, 2.4, 2.5

Table 2.1

	ENDF/B-VI	JENDL-3	This evaluation
$\langle\Gamma_n^0\rangle$, meV	0.1462	0.1467	0.1451
$\langle\Gamma_f\rangle$, meV	0.301	0.229	0.324
$\langle\Gamma_\gamma\rangle$, meV	45.06	54.62	48.33
$\langle D\rangle$, eV	0.771	0.775	0.771
$S_0 \times 10^4$	0.9528	0.9535	0.9345
σ_t , barn	633.20	614.584	599.469
σ_γ , barn	618.758	600.436	584.802
σ_f , barn	3.1385	3.018	3.1358
σ_n , barn	11.303	11.130	11.531
g_γ	1.00357	1.00287	1.00722
g_f	1.01646	1.01665	1.02783
I_γ , barn	1387.69	1305.80	1351.20
I_f , barn	14.994	13.862	14.508

demonstrate the data fits below 0.1 eV. Figures 2.1 and 2.2 demonstrate the measured total data fits up to 8 eV. The fig. 2.6 shows the comparison of distribution of radiative capture widths for positive resonances with Porter-Thomas distribution. The resonance missing as well as reduced neutron width $\langle\Gamma_n^0\rangle$ and neutron resonance spacing $\langle D\rangle$ distributions are discussed below. Table 2.1 shows that for different evaluations $s-$wave neutron strength function S_0 and reduced neutron width $\langle\Gamma_n^0\rangle$ values are close to each other. It is not the case for average fission width, which are rather

discrepant. Present average fission width value is appreciably higher than that of JENDL-3 evaluation, since for all resonances above 40 eV the value of 0.229 meV was adopted. In ENDF/B-VI evaluation the radiative width was kept constant (44.2 meV) for most of the resonances. In JENDL-3 evaluation the radiative width is rather high for resonances in the interval 55 - 67 eV. Thermal cross sections and resonance integrals are fairly compatible with respective measured data.

The thermal total σ_t, capture σ_γ, and scattering σ_n cross sections, $g_\gamma-$, and g_f-factors, as well as resonance integrals $I\gamma$ and I_f values are calculated with a code INTER.[17] In case of JENDL-3 and present evaluations the multi-level Breit-Wigner formalism was used, while for ENDF/B-IV evaluation single-level formula was employed.

3 Unresolved resonance region

3.1 Review

Unresolved resonance region of ^{241}Am is supposed to be from 0.15 keV up to 41.3483 keV. The lower energy is the end-point of resolved resonance region, the upper energy is the threshold energy of the inelastic scattering. We suppose $s-$, $p-$ and $d-$wave neutron-nucleus interactions to be effective.

3.2 The s-wave average resonance parameter evaluation

3.2.1 Estimate of resonance level missing influence on $\langle D_{obs}\rangle$ and $\langle S_0\rangle$

The preliminary estimates of average partial widths were obtained by averaging the evaluated resolved resonance parameters. Figure 3.1 shows the cumulative sum of resolved resonance levels. The averaged parameters for positive resolved resonances are as follows:

$$\begin{aligned}\langle\Gamma_n^0\rangle &= 1.444\times10^{-4}\ (\mathrm{eV})^{1/2}\\ \langle\Gamma_f\rangle &= 0.327\ \mathrm{meV}\\ \langle D_{obs}\rangle &= 0.787\ \mathrm{eV}\\ \langle\Gamma\gamma\rangle &= 48.4\ \mathrm{meV}\end{aligned}$$

Due to missing of weak resonances these average values overestimate actual reduced neutron width $\langle g\Gamma_n^0\rangle$ and neutron resonance spacing $\langle D_{obs}\rangle$. To get a physically justified values of $\langle g\Gamma_n^0\rangle$ and $\langle D_{obs}\rangle$ we employ a method, which is described elsewhere.[18] Both reduced neutron width and neutron resonance spacing distributions are obtained in a unified approach. We take into account the correlation of weak resonance missing and resonance missing

due to poor experimental resolution. The resolution function parameters as well as $\langle g\Gamma_n^0 \rangle$ and $\langle D_{obs} \rangle$ values are obtained by maximum likelihood method when comparing experimental distributions of reduced neutron width and resonance spacing with Porter-Thomas and Wigner distributions, modified for the resonance missing. The latter distributions will be called expected distributions.

3.2.2 Evaluation of $\langle D_{obs} \rangle$, $\langle S_0 \rangle$, $\langle \Gamma_\gamma \rangle$ and $\langle \Gamma_f \rangle$ based on the resonance parameters

To evaluate average neutron resonance spacing $\langle D_{obs} \rangle$ and s-wave neutron strength function S_0 we apply our method[18] to the resolved resonance data base. We suppose that data up to 150 eV should be taken into account. Figure 3.1 shows the cumulative sum of resolved resonance levels. Dashed lines above and below the solid line show the dependence of the error of $\langle D_{obs} \rangle$ and the number of resonances. The missing of levels is evident at very low energies. Energy intervals denoted as I and II, corresponding to different experimental resolution are shown. Figure 3.2 demonstrates cumulative sum of reduced neutron widths. Here again, dashed lines above and below the solid line show the $s-$wave neutron strength function error. The evaluated values are:

$$\langle S_0 \rangle = (\ 0.864 \pm 0.131) \times 10^{-4}\ (\mathrm{eV})^{-1/2}$$
$$\langle D_{obs} \rangle = (0.505 \pm 0.042)\ \mathrm{eV}$$

Figure 3.3 shows the comparison of expected and experimental reduced neutron width distributions. Figure 3.4 shows the comparison of distributions for neutron resonance spacing. All the figures are obtained for energy interval 0-150eV. The expected distributions shown on the figures 3.2 and 3.3 demonstrate the effect of resonance missing. There is evidence that the expected distributions are consistent within statistical errors with the experimental data for energy interval 0-150 eV. That is the reason to consider the $\langle D_{obs} \rangle$ and S_0 estimates reliable.

3.3 The s-, p- and d-wave average resonance parameter evaluation

3.3.1 Neutron width

Average neutron width is calculated as follows

$$\langle \Gamma_n^{lJ} \rangle = S_l \langle D_J \rangle E_n^{1/2} P_l,$$

where P_l is the transmission factor for the lth partial wave, which was calculated within black nucleus model. The p-wave neutron strength function $S_1 = 2.204 \times 10^{-4}$ (eV)$^{-1/2}$ was calculated with the optical model, using the deformed optical potential, described below. According to the results of optical model calculations S_0 was assumed to decrease linearly to the value of S_0=0.807×10^{-4}(eV)$^{-1/2}$ for neutron energy of 41.3483 keV. The d-wave neutron strength function was taken from optical model calculations: S_2 = 1.022×10^{-4} (eV).$^{-1/2}$ Since the d-wave contribution is rather small, the impact of any reasonable approximation on calculated values is negligible

3.3.2 Neutron resonance spacing

Neutron resonance spacing $\langle D_J \rangle$ was calculated with the phenomenological model[19], which takes into account the shell, pairing and collective effects. The main parameter of the model $\tilde{a}$ was normalized to the observed neutron resonance spacing $\langle D_{obs} \rangle$ =0.505 eV.

3.3.3 Fission width

Fission widths are calculated within a double-humped fission barrier model. Energy and angular momentum dependence of fission width is defined by the transition state spectra at inner and outer barrier humps. We constructed transition spectra by supposing the triaxiality of inner saddle and mass asymmetry at outer saddle. They will be described below. The calculated fission widths $\langle \Gamma_f^{2-} \rangle$ and $\langle \Gamma_f^{3-} \rangle$ for $s-$wave neutrons are normalized to the average fission width $\langle \Gamma_f \rangle$ =0.38 meV at 0.15 keV incident neutron energy, which allows to describe fission measured data. This value of $\langle \Gamma_f \rangle$ is somewhat higher than average resolved resonance fission width.

3.3.4 Radiative capture width

Energy and angular momentum dependences of radiative capture width are calculated within a two-cascade γ-emission model with allowance for the (n,γf) and (n,γn') reaction competition to the (n,$\gamma\gamma$) reaction. In this energy region (n,γ) reaction appears to be a radiative capture reaction. The radiative capture width is normalized to the value of $\langle \Gamma_\gamma \rangle$ =48.4 meV. (For details see Chapter IV).

3.4 Cross section evaluation in the region 0.15-41.3483 keV

3.4.1 Fitting of fission cross section structure

Experimental fission cross-sections in the unresolved resonance region are measured by Bowman et al.[20], Shpak et al.[21], Gayther and Thomas[22], Wisshak and Kappeler[23], Hage et al.[24], Knitter and Budtz-Jorgensen[25], Dabbs et al.[12] and Kobayashi et al.[5] Data of Wisshak and Kappeler[23], Hage et al.[24] and Dabbs et al.[12] are fitted in present evaluation. Dabbs et al.[12]data were chosen to be the base of fission cross section evaluation in the unresolved resonance region (for details see Chapter IV). An argument in the support of data by Dabbs et al.[12] gives calculation with fission width normalized to the resolved resonance fission value of $\langle\Gamma_f\rangle$ =0.327 meV. The resulted cross section values are even somewhat lower than data of Dabbs et al.[12] In our evaluation we described data by Dabbs et al.[12] with fission widths normalized to $\langle\Gamma_f\rangle$=0.38 value at 0.15 keV. Structure observed in data by Dabbs et al.[12] is fitted by adjusting fission width in l=0, J=2^- entrance channel. Comparison of evaluated and experimental fission cross sections in the unresolved resonance energy region is given on Fig3.5. Below 10 keV the problem of discrepancies between earlier and recent data was addressed by Kobayashi et al.[5] This data tend to support Gayther and Thomas[22] data, which are ~3 times higher than data of Dabbs et al.[12] below 10 keV. The data of Knitter and Budtz-Jorgensen[25] are lying ~10 times lower than data of Dabbs et al.[12] around 1 keV. The most disturbing is the discrepancy of evaluated curve with data of Knitter and Budtz-Jorgensen[25], since they were obtained with different technique as compared with measurements of Wisshak and Kappeler[23] and Hage et al.[24] That means at least new measurements are highly desirable below ~100 keV.

3.4.2 Capture cross section energy dependence

Capture cross section in the energy region of interest is measured by Gayther and Thomas[22], Wisshak and Kappeler[23] and Vanpraet et al.[15]. Absorption data of Weston and Todd[7] can be also used as fission cross-sections is very small in this region. All the experimental data sets are compatible with each other below 10 keV, although Vanpraet et al.[15] data are lying somewhat higher than others. Above 10keV data of Wisshak and Kappeler[23] are in good agreement with data of Gayther and Thomas[22] while the data of Weston and Todd[7] and Vanpraet et al.[15] are essentially lower. In present evaluation we adopted capture data of Gayther and Thomas[22] and Wisshak and Kappeler[23] since the data trends above 10 keV are consistent with our calculated cross sections with the adopted average resonance paremeters. Comparison of evaluated and measured capture cross-sections in unresolved resonance region is given on Fig 3.6. We consider non-feasible the repro-

duction of structure, observed in data of Gayther and Thomas[22] below ~1.5 keV.

3.4.3 Comparison of current and JENDL-3 and ENDF/B-VI evaluated data

Evaluated fission cross sections of this work is consistent with JENDL-3 and ENDF/B-VI in the unresolved resonance region as they are based on the same data of Dabbs et al.[12] Figure 3.5 shows the comparison of fission cross sections σ_f for both evaluations. The discrepancies are noticed when comparing the (n,γ) reaction cross sections (see fig. 3.6) Current evaluated capture cross section is $\approx$ 25% lower at the lower edge of unresolved resonance region then JENDL-3 and ENDF/B-VI evaluations and almost coincide above 10keV. Fig 3.6 gives comparison of evaluated capture cross section with measured data. Comparison of the evaluated fission and capture cross-sections is given in Table 3.1.

Table 3.1 Comparison of the evaluated fission and capture cross sections

Energy, keV	$\sigma\gamma, b$			σ_f, b		
	present	JENDL-3	ENDF/B-VI	present	JENDL-3	ENDF/B-VI
0.175	25.26	31.24	26.07	0.165	0.161	0.168
0.350	17.47	22.98	22.29	0.147	0.147	0.152
0.550	13.78	17.55	14.29	0.084	0.093	0.078
0.650	12.59	15.70	13.80	0.100	0.084	0.079
0.850	10.93	13.20	11.27	0.065	0.071	0.069
1.250	8.9	10.73	11.16	0.065	0.053	0.064
1.750	7.46	9.01	8.43	0.041	0.043	0.043
3.5	5.24	6.10	5.92	0.037	0.037	0.035
4.5	4.65	5.00	4.85	0.031	0.031	0.033
8.5	3.53	3.73	3.72	0.021	0.022	0.021
12.5	3.06	3.11	3.25	0.020	0.019	0.019
17.5	2.76	2.81	2.85	0.017	0.017	0.016
22.5	2.58	2.58	2.54	0.016	0.016	0.016
27.5	2.45	2.39	2.38	0.016	0.016	0.015
41.3483	2.22	2.08	2.11	0.014	0.015	0.014

4 Fast neutron cross sections

The measured neutron data in fast energy region, i.e. above ~41 keV are available for total, capture, fission and (n,2n) reaction cross sections. There is a lot of discrepancies in fission data in a deep subthreshold region, in a

plateau region and at higher energies, especially around 14.6 MeV. Nonetheless, the available fission and capture data fit would be used as constraint for (n,n') and $(n,2n)$ reaction cross sections calculation. We reproduce also the average resonance fission width within double-humped fission barrier model. To fix fission channel parameters the systematic trends are used.

4.1 Optical potential

The deformed optical potential for n+^{241}Am interaction is employed. The data of Phillips et al.[26] on total cross section are fitted, having in mind the systematic error of 0.6 barn. The starting values for the potential parameters were those for n+^{238}U interaction.[27] The isotopic dependences of real and imaginary parts of the potential were calculated using the optical potential parameter systematics.[28] Previously we modified the original potential geometry parameters[27] to fit total cross section and differential scattering data for N-odd and even targets above 10 MeV. This procedure of parameter fitting is well tested in case of and ^{233}U, ^{239}Pu, ^{235}U, ^{232}Th and ^{238}U targets. Four levels of the ground state rotational band ($5/2^-$,$7/2^-$,$9/2^-$,$11/2^-$) are coupled. The deformation parameters β_2 and β_4 are obtained by fitting $s-$wave neutron strength function S_0 value of 0.864×10^{-4} $(\mathrm{eV})^{-1/2}$ and p-wave neutron strength function S_1 value of 2.00×10^{-4} $(\mathrm{eV}).^{-1/2}$ The p-wave neutron strength function S_1 was obtained by fitting capture cross section data of Gayther and Thomas[22] and Wisshak and Kappeler[23] in 20 - 300keV energy region. This low value of S_1 was obtained by slight changing of V_R and W_D values to get low compound reaction cross section. The potential parameters are as follows:

$$V_R = 46.15 - 0.3E, MeV, r_R = 1.26\ fm, a_R = 0.615\ fm$$
$$W_D = \begin{cases} 3.56 + 0.4E, MeV, & E \leq 10 MeV, r_D = 1.24\ fm, a_D = 0.5\ fm \\ 7.56\ MeV, & E > 10\ MeV \end{cases}$$
$$V_{SO} = 6.2\ MeV, r_{SO} = 1.12\ fm, a_{SO} = 0.47\ fm, \beta_2 = 0.181, \beta_4 = 0.076$$

The s-, p-, and d-wave neutron strength functions and potential scattering cross section, calculated with this potential parameters in a coupled channel approach at incident neutron energy of 150 eV are:

$$S_0 = 0.851 \times 10^{-4}(\mathrm{eV})^{-1/2} \quad , \quad R' = 9.157 \text{ fm}$$

and at 41.3483 keV are:

$$S_0 = 0.807 \times 10^{-4}(\mathrm{eV})^{-1/2} \quad S_1 = 2.204 \times 10^{-4}(\mathrm{eV})^{-1/2} \quad S_2 = 1.022 \times 10^{-4}(\mathrm{eV})^{-1/2}$$

The reaction cross sections, calculated with deformed optical potential and spherical optical potential, which is used in JENDL-3 evaluation, are

compared on fig. 4.1. The significant differences below 1 MeV and above 10 MeV would be manifested in inelastic scattering cross section and $(n, 3n)$ cross section. The total cross section seem rather different (see fig. 4.2), especially at low energies, although they fit the data of Phillips and Howe[26] within errors. The discrepancy of elastic scattering cross sections, shown on fig. 4.2 is similar to that, observed in case of total cross section. The differences at low energies are due to rather low value of $s-$wave strength function adopted in present evaluation.

4.2 Fission cross section

4.2.1 Status of the experimental data

A number of measurements are available for fission cross section, but most of them are discrepant with each other. We will divide the data into four groups: deep subthreshold region, threshold region, plateau region and region above emissive fission threshold (see figs. 4.4, 4.5, 4.6, 4.7).

Fission cross section of ^{241}Am was measured by Seeger et al.[4] from 20 eV to 1 MeV at the bomb-shot. Above 10 keV ratio of fission cross sections of ^{241}Am and ^{235}U was obtained. Fission cross section of ^{241}Am was measured at linac[20] as a ratio to fission cross section of ^{239}Pu. BF_3-counter was used as a flux monitor.

Shpack et al.[21] defined fission cross section of ^{241}Am in the energy region from 3 keV to 4 MeV. They have measured shape of fission cross sections ratio of ^{241}Am and ^{239}Pu. Then the shape of ^{241}Am fission cross section was defined, using fission cross section of ^{239}Pu. Eventually absolute fission cross section of ^{241}Am was obtained by normalizing to data of Fomushkin et al.[29] The anomalous trend of fission cross section deep below threshold, observed by Seeger et al.[4] was discarded by these data as early as in 1969.

Fission cross section ratio of ^{241}Am and ^{235}U was defined by Fomushkin et al.[29] in the range of incident neutron energy from 0.44 MeV to 3.62 MeV. They have used mica detectors. The sample weight was defined using $T_{\alpha_{1/2}}$ =458.1 years, so their results should be renormalized to new value of $T_{\alpha_{1/2}}$ =432 years.

The ratio of fission cross sections of ^{241}Am and ^{239}Pu was measured in the energy range from 0.13 to 7.0 MeV by Kupriyanov et al.[30] The energy dependence of fission ratios was defined using ionization fission chambers. The absolute values of fission ratios were obtained using mica detectors. The ratios of fission cross sections of ^{241}Am and ^{235}U we obtained from the original data with the aid of ratio of fission cross sections of ^{239}Pu and ^{235}U by Fursov et al.[31]

The absolute fission cross section was obtained by Aleksandrov et al.[32] at 2.5 MeV neutron energy with the time-correlated associated particle method.

Neutrons were produced via D(d,n)^{3}He reaction.

The fission cross section ratio of ^{241}Am and ^{235}U was measured by Knitter and Budtz-Jorgensen[25] in the energy range from 100 eV to 5.3 MeV. Fission events of ^{241}Am were registered by fragment detection using an ionization chamber with intrinsic suppression of alpha background. Monoenergetic neutrons were produced via ^{7}Li(p,n) (0.153-1.3 MeV), T(p,n) (1-4.5 MeV), D(d,n) (4.5-5.3 MeV). Below 300 keV down to 5 keV the measurements were executed with pulsed Van de Graaff accelerator. Neutrons of energies from 1.28 eV to 2.5 MeV were produced with the linac. Absolute values of the ^{241}Am fission cross section were obtained using ^{235}U reference fission cross section of ENDF/B-VI.[3]

Gaythe and Thomas[22] have measured average fission cross section in the range of incident neutron energy from 50 eV to 10 keV by observing prompt fission neutrons at 45 MeV linac. The ^{235}U measurement was used to establish an absolute scale for the ^{241}Am fission cross section. The average ^{235}U fission yield in the 1 keV to 2 keV range of incident neutron energies of 7.167 barns was used to normalize the ^{235}U fission cross section measurement.

Subthreshold fission cross section was measured in the energy range from 10 to 250 keV, using ^{235}U as a standard, by Wisshak and Käppeler.[23] Neutrons were produced via ^{7}Li(p,n) (10-150 keV) and the T(p,n) (50-150 keV) reaction with the Van de Graaff accelerator. Fission events were detected by a fission neutrons detector (liquid scintillator). The fission ratio was converted into absolute fission cross section using ^{235}U fission cross section of ENDF/B-VI.[3]

Fission cross section was measured by Hage et al.[24] in the energy range from 10 keV to 1030 keV, using ^{235}U as a standard. Continuous spectrum neutrons were produced via the ^{7}Li(p,n) (10-140 keV) and quasi-monoenergetic spectra neutrons also via the ^{7}Li(p,n) (120-1030 keV) reaction with the Van de Graaff accelerator. In other respects the experimental setup is similar to that of Wisshak and Käppeler.[23] The resulted fission cross section agrees quite good with the data of Wisshak and Käppeler[23], while both data sets lay about 2 times lower than the data of Knitter and Budtz-Jorgensen[25] below 250 keV. At higher energies the data of Knitter and Budtz-Jorgensen[25], Hage et al.[24], Shpack et al.[21] and Kupriyanov et al.[30] agree with each other.

The fission cross section ratios were measured by Behrens and Browne[33] from 0.2 MeV to 30 MeV using ionization fission chambers and a threshold cross section method. To avoid alpha pileup problems ^{241}Am sample of 4 mg was used. The most severe discrepancy is observed in the first plateau region with previous data of Knitter and Budtz-Jorgensen[25] and Kupriyanov et al.[30], which are up to ~10% lower.

The widest energy range covered in one measurement is from 0.02 eV

to 20 MeV by Dabbs et al.[12] They have measured cross sections ratio of ^{241}Am and ^{235}U above 101 keV, while at lower energies ^{6}Li(n,α) cross section, normalized to ^{235}U fission cross section in the 7.8-eV to 11-eV interval served as a standard. The reduction of the effects of intense alpha-particle background was achieved with the "honeycomb" fission ionization chamber. Below 101 keV the data of Dabbs et al.[12] are the lowest in the cross section level (14± 0.6 mbarns at 52 to 58 keV.) In the threshold region the data of Dabbs et al.[12] agree with data of Hage et al.[25], the data of Knitter and Budtz-Jorgensen[26] being higher than both data sets up to 600 keV. At higher energies, especially in the first plateau region, the data of Dabbs et al.[12] appear to be consistent with data of Knitter and Budtz-Jorgensen[25], but remain systematically lower than data of Behrens and Browne.[33] Above the emissive fission threshold the shapes of the data by Dabbs et al.[12] and Behrens and Browne[33] are drastically different.

A number of measurements exists around 14 MeV energy point, which are rather discrepant. Protopopov et al.[34], Kazarinova et al.[35]and Fomushkin et al.[36], have measured fission cross section at 14.6 MeV. The sample weight was defined using $T_{\alpha_{1/2}}$ =458.1 years, so their results should be renormalized to new value of $T_{\alpha_{1/2}}$ =432 years. The absolute fission cross section measurement was made at 14.6 MeV with a gaseous scintillator using associated particle method by Cance and Grenier.[37] Prindle et al.[38] have obtained an estimate of fission cross section 2.32±0.09 barn at 14.8 MeV by comparative analysis of mass-yields of ^{241}Am and ^{238}U neutron-induced fission. They have observed a 13% discrepancy of absolute yields defined using ^{241}Am and ^{238}U fission cross section ratio and summing mass-yield curve, when the fission cross section of ^{241}Am is obtained using data of Behrens and Browne.[33]

The problem of consistency of ^{241}Am fission cross section looks like that. In the plateau region the data of Knitter and Budtz-Jorgensen[25], Kuprivanov et al.[30] and Dabbs et al.[12] practically coincide, while the data of Behrens and Browne[33] are lying systematically higher(~6 %).

The severe discrepancies again occur below ~0.250 keV up. The data of Dabbs et al.[12] define the lowest cross section level, while the data of Knitter and Budtz-Jorgensen[25] define the highest level. The data of Wisshak and Kappeler[23] and Hage et al.[24] tend to support the data of Dabbs et al.[12] tendency to lower cross section values.

4.2.2 Statistical model calculation of fission cross section

We choose to fit primarily data of Dabbs et al.[12] describing measured data base. That means the lowest cross section level from 10 keV up to 250 keV. From 250 keV up to 2 MeV the measured data are virtually consistent. From 2 MeV up to emissive fission threshold the data of Dabbs et al.[12], Knitter and Budtz-Jorgensen[26] exhibit a distinct slope with incident neutron energy

($d\sigma_f/dE \sim 0.06$ barn/MeV). This is at variance with the trend of data by Kupriyanov et al.[30] which exhibit perfect "plateau" shape. The most peculiar feature of data by Dabbs et al.[12] is the broad bump around the threshold of (n,2nf) reaction, while there is a wild scatter of available data around 14.6 MeV. This bump can not be reproduced within the current statistical model calculations, mostly due to adopted reaction cross section (see fig. 4.1). To predict the fission cross section above 14 MeV, we choose to fit the ^{241}Am(n,2n) reaction cross section.[39] The comparison of calculated fission cross section with measured data is shown in figs. 4.4, 4.5, 4.6 and 4.7. The statistical theory calculation of fission cross section was accomplished within the double-humped fission barrier model. The approach employed in code STAT for fission cross section calculation is described in more details elsewhere.[40,41] The procedure of calculating fission transmission coefficients is briefly described below.

4.2.3 Fission transmission coefficient, level density and transition state spectrum

The intrinsic two-quasiparticle state spectrum of odd-odd nuclide ^{242}Am at equilibrium deformation are modelled by Sood and Singh.[42] The expected location of still unobserved two-quasiparticle states was predicted. Using these intrinsic states as the bandhead energies we have built the rotational bands, i.e. transition state spectra of fissioning nuclide ^{242}Am. The discrete transition spectra, as well as continuous level contribution to the fission transmission coefficient are dependent upon the order of symmetry for ^{242}Am fissioning nucleus at inner and outer saddles. Due to the axial asymmetry at the inner saddle[42] we additionally assume $(2J+1)$ rotational levels for each J value. The rotational band levels at outer saddle are assumed to be doubly degenerate due to mass asymmetry.[42] With transition state spectra defined in the first 0.2 MeV excitation energy range (see Table 4.1) the fission barrier parameters (see Table 4.2) are obtained by fitting fission data (see figs. 4.4, 4.5). The fission width for $s-$wave neutrons $\langle\Gamma_f\rangle$, calculated at incident neutron energy of 0.15 keV is consistent with average fission width value, obtained in unresolved resonance region.

The discrete character of few-quasiparticle excitations is virtually unimportant for level density modelling in case of odd-odd ^{242}Am fissioning nuclide. We will model the level density above 0.2 MeV in the following approximate way. The level density of axially symmetric fissioning nucleus is calculated in constant temperature approximation, i.e. $\rho(U) = T_f^{-1}\exp((U-U_o)/T_f)$. The respective parameters, nuclear temperature T_f and excitation energy shift U_o are defined at the matching energy U_c =2.4 MeV. At excitation energies above U_c the continuum part of the transition state spectrum is represented with the phenomenological model[19], which

takes into account pairing, shell and collective effects at saddle deformations. The asymptotic value of the main parameter of the level density for fissioning nucleus ^{242}Am is assumed to be the same, as that of ^{242}Am compound nuclide. After that the effects of non-axiality and mass asymmetry are included. The detailed procedure of calculating fission transmission coefficient is described elsewhere.[40] The respective parameters: shell correction at saddles δW, pairing correlation function Δ, quadrupole deformation ε, and momentum of inertia at zero temperature $F_0/\hbar^2$ are given in Table 4.3.

Table 4.1

Transition spectra band-heads of ^{242}Am

inner saddle		outer saddle	
K^{π}	$E_{K^{\pi}}$, MeV	K^{π}	$E_{K^{\pi}}$, MeV
1^-	0.0	1^-	0.0
0^-	0.044	0^-	0.044
5^-	0.049	5^-	0.049
6^-	0.170	6^-	0.170
1^-	0.220	1^-	0.220
3^-	0.242	$3-$	0.242
2^-	0.288	2^-	0.288

Table 4.2

Fission barrier parameters

Nucleus	Barrier	Barrier height, MeV	Curvature, MeV
^{242}Am	inner	6.315	0.6
^{242}Am	outer	5.775	0.4
^{241}Am	inner	6.000	0.8
^{241}Am	outer	5.350	0.5
^{240}Am	inner	6.100	0.6
^{240}Am	outer	6.000	0.4
^{239}Am	inner	6.000	0.8
^{239}Am	outer	5.400	0.6

Table 4.3

Level density parameters of ^{242}Am fissioning nucleus and residual nucleus ^{241}Am

Parameter	inner saddle	outer saddle	neutron channel
δW, MeV	2.5	0.6	-2.402
$\triangle$, MeV	$\triangle_0$ +0.11	$\triangle_0$ +0.11	$\triangle_0$
ε	0.6	0.8	0.24
$F_0/\hbar^2$, MeV^{-1}	100	200	73

Above ~2 MeV incident neutron energy fission cross section data were fitted (see fig. 4.6) by slight increase of pairing correlation function value. The parameters used for calculation of residual nuclide ^{241}Am level density for neutron emission competition are described below. Below incident neutron energy of 0.312 MeV the neutron cross sections are calculated within Hauser-Feshbach approach with a width fluctuation correction taken into account. For width fluctuation correction calculation only Porter-Thomas fluctuations are taken into account. Effective number of degrees of freedom for fission channel is defined at the higher (inner) saddle as $\nu_f^{J\pi} = T_f^{J\pi}/T_{f\,max}^{J\pi}$, where $T_{f\,max}^{J\pi}$ is the maximum value of the fission transmission coefficient $T_f^{J\pi}$. Above incident neutron energy of 0.312 MeV the Tepel et al.[44] approach is employed. The calculations are made with code STAT.[45]

4.2.4 Fission cross section above emissive fission threshold

The first chance fission cross section of ^{241}Am(n,f) reaction above the emissive fission threshold is fixed with the level density and fission barrier parameters systematics[40,41] (see Tables 4.2, 4.3) and secondary neutron spectra parameterization (see fig. 4.7). A consistent description of a complete set of measured data on (n,f), (n,2n) and (n,3n) for ^{238}U and ^{235}U targets was accomplished with the secondary neutron spectra parameterization[46], which is used here. The fission cross section is calculated with the statistical code STAPRE.[47] The fission barrier parameters of ^{241}Am and ^{240}Am are defined by fitting ^{241}Am(n,f) reaction data above emissive fission threshold. The neutron resonance spacing values for target nuclei ^{240}Am and ^{239}Am were taken from evaluation of Fort et al.[48] The calculated fission cross section is drastically different from JENDL-3 evaluated curve above (n,2nf) reaction threshold (see figs. 4.7, 4.8). The calculated fission cross section at 14.8 MeV neutron energy virtually coincides with the data by Prindle et al.[38] and Fomushkin et al.[36] The discrepancy with Dabbs et al.[12] is unavoidable,

since the measured data by Dabbs et al.[12] appear to be just as high as reaction cross section at 14.8 MeV. They are incompatible with the calculated fission cross section.

4.3 Inelastic scattering cross section

The inelastic scattering cross section is calculated with the statistical codes STAT[45] and STAPRE.[47] The discrete level excitation (compound and direct), continuum excitation and pre-equilibrium emission contribute to the inelastic scattering cross section.

4.3.1 Levels of ^{241}Am

The low-lying levels of scheme of Nuclear Data Sheets[49] appears incomplete at rather low excitation energy (see fig. 4.9). In JENDL-3 evaluation there are 16 discrete excited levels up to 0.682 MeV, i.e. the missing of levels above ~0.682 MeV is ignored (see fig. 4.9). Only one level with J^{π} =13/2$^-$ of the ground state band was added to the adopted level scheme of latest edition of ENSDF.[49]

4.3.2 ^{241}Am level density

The continuum level density below excitation energy U_c = 3.6 MeV is calculated with the constant temperature model

$$\rho(U) = T^{-1} \exp((U - U_o)/T),$$

here, energy shift U_0 = -0.96455 MeV, nuclear temperature T = 0.40723 MeV are the constant temperature model parameters. The cumulative number of observed levels is compared with constant temperature approximation on fig.4.9. At higher excitation energies the phenomenological model[19] is used. The main model parameter $\tilde{a}$ for ^{241}Am residual nucleus is obtained by fitting the predicted neutron resonance spacing[48] of ^{240}Am target nuclide $\langle D_{obs} \rangle$ = 0.372 eV.

4.3.3 Compound inelastic scattering

The residual nucleus ^{241}Am level density modelling, adopted in present work changes the inelastic scattering cross section below 5 MeV as compared with JENDL-3 evaluation (see fig. 4.10). Above ~1 MeV incident neutron energy the discrepancy is due to direct excitation of the ground state band levels. The discrete level excitation cross sections (see figs. 4.11 - 4.16) show that adopted optical potential influences appreciably on the shape of inelastic

cross sections. Above 0.3~ MeV incident neutron energy inelastic scattering to the continuum gives a major contribution to the total inelastic scattering cross section. Above 5 MeV incident neutron energy pre-equilibrium emission and direct inelastic scattering are the two reaction mechanisms which define inelastic scattering cross section (see fig. 4.13). The pre-equilibrium model parameters were tested by the statistical model description of ^{238}U+n interaction secondary neutron spectra and consistent description of fission and (n,xn) reaction data for major actinides.[46] Steep decrease of inelastic scattering cross section of JENDL-3 above ~5 MeV (see fig. 4.10) is due to missing of pre-equilibrium emission of neutrons.

4.3.4 Direct inelastic scattering

The direct inelastic scattering changes the shape of ground band levels excitation cross sections above 1 MeV incident neutron energy (see figs. 4.11 - 4.16). This mechanism defines partly the hard-energy tail in total inelastic scattering cross section (see fig. 4.10). The calculations were accomplished with the code COUPLE.[28]

Table 4.4

Level scheme of ^{241}Am

$E^J_{K^\pi}$, MeV	J^π	K	band	
0.000	$5/2^-$	5/2	A	
0.0418	$7/2^-$	5/2	A	
0.0936	$9/2^-$	5/2	A	
0.1580	$11/2^-$	5/2	A	
0.2059	$5/2^+$	5/2	B	
0.2340	$13/2^-$	5/2	A	*
0.2350	$7/2^+$	7/2	B	
0.2390	$3/2^-$	3/2	C	
0.2720	$9/2^+$	7/2	B	
0.2730	$5/2^-$	5/2	B	
0.3120	$15/2^-$	5/2	A	

*) added

4.3.5 ^{242}Am level density

The level density of odd-odd compound nuclide ^{242}Am one needs to calculate radiative capture width and (n,γn') reaction contribution to the compound

inelastic scattering cross section. The continuum level density below excitation energy U_c = 2.4 MeV is calculated with the constant temperature model, the constant temperature model parameters are: energy shift U_0 = -1.6452 MeV, nuclear temperature T = 0.39241 MeV. The cumulative number of observed levels is compared with constant temperature approximation on fig.4.12. At higher excitation energies the phenomenological model[19] is used. The main model parameter $\tilde{a}$ for ^{242}Am residual nucleus is obtained by fitting the evaluated neutron resonance spacing of ^{241}Am target nuclide $\langle D_{obs} \rangle$ = 0.505 eV.

4.4 Radiative capture cross section

Gayther and Thomas[22] have measured average neutron absorption cross section in the range of incident neutron energy from 100 eV to 500 keV using large liquid scintillator. The shape of incident neutron spectrum was determined by comparison with the ^{6}Li(n,α) cross section below 30 keV and the ^{235}U (n,f) cross section at the higher energies. The cross section was normalized in the 1 keV to 2 keV energy range to the value of 9.48 barns of Weston and Todd.[7] There is a systematic difference between data shapes of Gayther and Thomas[22] and Weston and Todd[7] of up to 20% between 10 and 100 keV.

Capture cross section was measured by Wisshak and Käppeler[23] in the energy range from 10 to 250 keV, using ^{197}Au as a standard. Capture events were detected by Moxon-Rae system. The data have been converted to absolute values using the ^{197}Au(n,γ) cross section of ENDF/B-VI. Capture cross section data agree well with absorption data of Gayther and Thomas[22], while Weston and Todd[7] data are systematically lower than both data sets. We will fit the capture cross section data of Wisshak and Käppeler.[23]

The radiative capture cross section is calculated within a statistical approach up to 5 MeV. Radiative capture strength function equals $S_{\gamma 0}$ = 958.42. At higher incident neutron energies we assume radiative capture cross section to be 1 mbarn. The radiative capture width was calculated with (n,γf) and (n,γn') reactions competition against "true" capture reaction (n,$\gamma\gamma$). Notwithstanding rather high fission threshold for ^{242}Am compound nuclide the competition of (n,γf) reaction is stronger than that of (n,γn') reaction. The influence of (n,γn') and (n,γf) reaction competition on radiative capture cross section is illustrated on fig.4.18 by sharp decrease of capture cross section above 1 MeV incident neutron energy, as compared with (n,γx) reaction cross section. The capture cross section of ENDF/B-VI is systematically higher than present evaluation above 200 keV.

4.5 Cross sections of (n,2n) and (n,3n) reactions

The current and JENDL-3 evaluated (n,2n) and (n,3n) cross sections are rather different. The magnitude of (n,2n) cross section below the (n,2nf) reaction threshold is defined by (n,nf) and (n,2n) reaction competition. We described in our approach the (n,2n) reaction data of Filatenkov et al.[39] around 14 MeV incident neutron energy. To calculate the (n,2n) reaction cross section we use an approach, developed for description of the ^{238}U(n,2n) reaction cross section.[46] The present and JENDL-3 evaluated fission cross sections are rather different, as well as reaction cross sections above 10 MeV incident neutron energy (see fig. 4.1). The present and JENDL-3 evaluations are compared in fig. 4.19. There is no hard-energy tail in (n,2n) reaction cross sections both in JENDL-3 and ENDF/B-VI evaluations. In case of (n,3n) reaction the difference in reaction cross section above 11 MeV (see fig. 4.1) contributes essentially to the discrepancy, shown on fig. 4.20.

5 Energy distributions of secondary neutrons

There is no measured data on secondary neutron spectra. To calculate neutron energy distributions of (n,xnγ) and (n,xnf), x=1, 2, 3 reactions we use a simple Weisscopf-Ewing evaporation model[50] taking into account fission and gamma competition to neutron emission. The pre-equilibrium emission of first neutron is included.

5.1 Model calculations of (n,nx) reaction spectra

The first neutron spectra for the (n,nx) reaction is the sum of evaporated and pre-equilibrium emitted neutron contributions. The pre-equilibrium emission contribution is calculated with a parameter systematics tested in case of n+^{238}U and n+^{235}U interactions.[46] We have calculated the 1st, 2nd and 3d neutron spectra for the (n,nγ), (n,2n) and (n,3n), where applicable. According to the ENDF/B-VI format we included the secondary neutron spectra in the following way. The calculated spectra were summed up and tabular spectra for the (n,nγ), (n,2n) and (n,3n) reactions were obtained. To clarify the competition of neutron, γ-emission emission and fission in case of (n,nx) and (n,2nx) reactions we have chosen the following presentation of spectra. Figure 5.1 shows the spectrum of 1st neutron of the reaction (n,nx) and its partial contributions for (n,nγ), (n,2n), (n,nf) (n,2nf) and (n,3n) reactions. Figure 5.2 shows the spectrum of 2nd neutron of the reaction (n,2nx) and its partial contributions for (n,2n), (n,3n) and (n,2nf) reactions. The spectra of 1st and 2nd neutrons are normalized to unity. The partial neutron spectra shown on figs. 5.1, 5.2 are normalized to the contributions of

appropriate cross sections to the (n,nx) and (n,2nx) reaction cross sections, respectively.

Table 5.1 Average energies of secondary neutron spectra

E_n , MeV	1st neutron average energy, MeV								
	(n, n')			(n, 2n)		(n, n'f)	(n, 3n)		(n, 2n'f)
	pres.	B - 6	J - 3	pres.	J - 3	pres.	pres.	J - 3	pres.
2.0	0.54	0.52	0.60						
8.0	3.55	3.59	1.12	0.68	0.69	1.02			
15.0	10.79	9.65	1.53	3.85	1.53	3.44	1.02	1.19	0.91
20.0	15.78	15.64	1.77	9.06	1.77	4.75	3.11	1.77	2.80

E_n , MeV	2nd neutron average energy, MeV					3d neutron	
	(n, 2n)		(n, 3n)		(n, 2n'f)		
	pres.	J - 3	pres.	J - 3	pres.	pres.	J - 3
8.0	0.23	0.65					
15.0	0.86	1.07	0.73	0.98	0.66	0.22	0.77
20.0	0.85	1.38	1.14	1.39	1.12	0.64	0.80

The inclusion of pre-equilibrium emission changes significantly the average energies of emitted neutron spectra. That is shown in Table 5.1, where the average secondary neutron energies for current and JENDL-3 and ENDF/B-VI evaluations are compared. The most significant is the change of neutron spectra of (n,nγ) reaction. Figs 5.3-5.7 demonstrate the discrepancies of secondary neutron spectra in current, JENDL-3 and ENDF/B-VI evaluations. Spectra of our and ENDF/B-VI evaluations are in qualitative agreement, while those of JENDL-3 are much softer.

The 1st neutron spectra of (n,nf) reaction also becomes harder and that influences prompt fission neutron spectra. On the other hand, the spectra of 2nd and 3d neutrons become softer.

5.2 Prompt fission neutron spectra

Prompt fission neutron spectra were calculated within the framework of Madland-Nix model.[51]

5.2.1 Model calculations of prompt fission neutron spectra

The model parameters, which should be defined are the following.

5.2.1.1 Fragment masses. The fragment masses are defined as $A_L = 102$ and $A_H = 140$, in accordance with the data of Asghar et al.[52] Fragment charges are defined using the ratios of

$$\langle A_{L,H} \rangle / (Z_{L,H} \mp 0.5) = A_F / Z_F.$$

The average fragments adopted are ^{102}Nb and ^{140}Xe.

5.2.1.2 Energy parameters. Average total fission energies $\langle E_R \rangle$ and average fission-fragment separation energies are calculated as in Madland-Nix model using mass tables of Audi and Wapstra.[53] Measured total fragment kinetic energy $\langle TKE \rangle$ for ^{242}Am fissioning nucleus differs significantly in limits 179-185 MeV in various measurements. Therefore the value of $\langle TKE \rangle$ for this nuclei had been defined to fit $\nu_p(E)$ from thermal to 5 MeV energy. The resulted $\langle TKE \rangle = 183.02 - 0.08E_n$, for other fissioning nuclei $\langle TKE \rangle$ had been defined as $\langle TKE \rangle(A-1) = \langle TKE \rangle(A) + 0.24E_n$ in accordance with Viola et al.[54] systematics.

5.2.2 Other parameters.

The level density parameter of the fermi-gas model is calculated as $a = A_{L,H}/10.2$, MeV.$^{-1}$ Becchetti-Greenlees[55] spherical optical potential parameters are employed to calculate compound cross section.

5.2.3 Prompt fission neutron spectra evaluation

Below emissive fission threshold prompt fission neutron spectra are calculated with the parameters given in Table 5.2. Figure 5.8 shows the comparison of calculated thermal prompt fission neutron spectrum with maxwellian spectra of JENDL-3 (T =1.389 MeV) and ENDF/B-VI (T = 1.3906 MeV). Average energy of fission spectrum is 2.14 MeV, it is compatible with evaluated values of JENDL-3 and ENDF/B-VI, however the spectra shapes are significantly different. Figures 5.9, 5.10 demonstrate the discrepancy of our calculation and JENDL-3 and ENDF/B-VI evaluations. The discrepancies are due to emissive fission contribution in present evaluation as well as maxwellian fission spectrum presentation in JENDL-3 independent from incident neutron energy.

Above emissive fission threshold the fission neutron spectra $N(E)$ is the superposition of emissive fission spectra, i.e.

$$N(E) = (\frac{\sigma_{nf}}{\sigma_{nF}} \nu_1 N_1(E) + \frac{\sigma_{nn'f}}{\sigma_{nF}} [\Phi_{nn'f}(E) + \nu_2 N_2(E)]$$

$$+\frac{\sigma_{n2nf}}{\sigma_{nF}}\left[\Phi^1_{n2nf}(E)+\Phi^2_{n2nf}(E)+\nu_3 N_3(E)\right])/$$
$$\left[\frac{\sigma_{nf}}{\sigma_{nF}}\nu_1+\frac{\sigma_{nn'f}}{\sigma_{nF}}(1+\nu_2)+\frac{\sigma_{n2nf}}{\sigma_{nF}}(2+\nu_3)\right],$$

where σ_{nF}, σ_{nf}, $\sigma_{nn'f}$, σ_{n2nf} are the total and i-th chance fission cross sections (i = 1,2,3); $\Phi_{nn'f}$, Φ^1_{n2nf}, and Φ^2_{n2nf} are emitted neutron spectra: for (n,nf) reaction, 1st and 2nd neutrons of (n,2nf) reaction, respectively; ν_i and N_i are multiplicity and prompt neutron spectra for the i-th fissioning nucleus. The pre-equilibrium emission of the first neutron is included, the $\Phi^i_{n,xnf}$ spectra for the emissive fission are calculated with Weisscopf-Ewing evaporation model.[50]

Table 5.2

Parameters of the Madland-Nix model

Fissioning nucleus	A_L fragm.	A_H fragm.	$\langle E_R \rangle$, MeV	$\langle TKE \rangle$, MeV	B_n, MeV
^{242}Am	^{102}Nb	^{140}Xe	204.963	183.020	5.538
^{241}Am	^{101}Nb	^{140}Xe	204.353	183.260	6.641
^{240}Am	^{100}Nb	^{140}Xe	204.845	183.500	5.957

Table 5.3 Comparison of Madland-Nix and present approach

	E_n = 8 MeV		E_n = 15 MeV	
Quantity	M-N model[50]	Present	M-N model[50]	Present
$\langle E_1 \rangle$	2.333	2.333	2.485	2.485
ν_1	4.241	4.241	5.220	5.220
$\langle E_{n'f} \rangle$	1.179	1.021	1.600	3.436
$\langle E_2 \rangle$	2.158	2.162	2.310	2.269
ν_2	3.117	3.139	4.000	3.757
$\langle E_{2nf} \rangle^1$	-	-	1.600	0.906
$\langle E_{2nf} \rangle^2$	-	-	1.088	0.658
$\langle E_3 \rangle$	-	-	2.147	2.173
ν_3	-	-	2.967	3.105
$\langle E \rangle$	2.230	2.221	2.367	2.475
ν	4.210	4.215	5.140	5.062

Table 5.3 (continued)

E_n = 20 MeV	
M-N model[50]	Present
2.586	2.586
5.900	5.900
1.839	4.753
2.412	2.351
4.620	4.242
1.839	2.804
1.412	1.124
2.254	2.238
3.560	3.470
2.436	2.625
5.764	5.614

The influence of pre-equilibrium pre-fission neutrons on prompt fission neutron multiplicity ν_i and prompt neutron spectra N_i predictions as well as $N(E)$ and $\nu(E)$, is illustrated in Table 5.3 and Fig. 5.11. In Table 5.3 $\langle E_i \rangle$ denotes average prompt fission neutron energy of i-th fissioning nucleus, $\langle E \rangle$ is the average fission neutron energy, $\langle E_{n'f} \rangle$, $\langle E_{2nf} \rangle^1$and $\langle E_{2nf} \rangle^2$are the average energies of neutrons, emitted in (n,nf) and 1st and 2nd neutrons emitted in (n,2nf) reactions, respectively. The Figs. 5.12-5.14 show the partial contributions of i-th chance fission to the total fission neutron spectrum at incident neutron energies of 8, 15 and 20 MeV.

6 Number of neutrons per fission

The number of prompt fission neutrons at thermal energies was measured by Lebedev and Kalashnikova[56] in 1958 (ν_p=3.066±0.05) and Jaffey and Lerner[57] in 1970 (ν_p=3.219±0.021). At higher energies the $\nu_p(E)$ was measured by Khokhlov et al.[58,59], but the the data are unaccessible and only linear energy dependence $\nu_p(E)$=(3.055±0.023)+(0.139± 0.007)E_n fitted to experimental data is provided. Note, that the data points on the figures of refs.[58,59] lie systematically higher than proposed energy dependence. That may be due to different weights for data points while producing the energy dependence estimate. Therefore the present evaluation of $\nu_p(E)$ is based on calculation within Madland-Nix model, fitted in the energy range up to 5 MeV to the energy dependence of Khokhlov et al.[59]: $\nu_p(E)$=3.078+0.146E_n. The calculated number of prompt fission neutrons is consistent with both the data points and the energy dependence of Khokhlov et al.[59] up to $\sim$ 10 MeV incident neutron energy. The comparison of $\nu_p(E)$ with measured data,

JENDL-3 and ENDF/B-VI evaluations is shown on fig. 6.1. The Madland-Nix model calculations predict non-linear increase of $\nu_p(E)$ above emissive threshold. The influence of pre-equilibrium pre-fission neutrons manifests in additional appreciable decrease of $d\nu/dE$ above 12 MeV. The delayed number of neutrons per fission ν_d and the decay constants for six groups of delayed neutrons are taken from Brady et al.[60] Specifically, $\nu_d = 0.00427$ for incident neutron energies up to 4 MeV and $\nu_d = 0.002418$ for $E_n \geq 7$ MeV.

7 Angular distributions of secondary neutrons

The angular distributions of elastically scattered neutrons and those for neutrons, scattered on three levels of ground state band are calculated with the coupled channel method. The isotropic compound scattering contribution is taken into account by renormalizing l-th Legendre polynomial coefficients A_l^{cc}, calculated with coupled channels:

$$A_l = A_l^{cc}\sigma_{dir}/(\sigma_{dir}+\sigma_{comp}),$$

where σ_{dir} and σ_{comp} are the scattering cross section direct and compound contributions, respectively. For the other contributing reactions angular distributions of secondary neutrons are assumed isotropic.

8 Conclusions

The evaluated neutron data file for ^{241}Am is compiled in ENDF/B-VI format and sent to the International Science and Technology Center (Moscow) and Japan Nuclear Data Center at Japan Atomic Energy Research Institute.

Numerous discrepancies of experimental data coupled with possibility of some new data becoming available (for example, ^{241}Am(n,f) data of Kobayashi et al.[5] (Kyoto University, Japan) may urge some revision of data file. Present version of ^{241}Am data file may be revised before 1 March of 1998, the expiration date of Project CIS-03-95.

9 References

1. Nakagawa T., Kikuchi Y., Proc. of the Int. Conf. on Nuclear Data and Technology, Gatlinburg, Tenn., USA, 9-13 May, 1994, Dickens J.K. (Editor), 709, ANS Inc., 1994.
2. Japanese Evaluated Data Library, Version 3, JAERI 1319, 1990.
3. C.L. Dunford, Nuclear Data for Science and Technology, Proc. Int. Conf. Julich, 1991,788.Springer-Verlag,1992, Berlin
4. Seeger P.A., Hemmendinger A., Diven B.C. Nucl. Phys. A96, 605 (1967)
5. Kobayashi K., Yamamoto S., Fujita Y., et al. Nuclear Data for Science and Technology, Proc. Int. Conf., Gatlinburg, 1994, 242, ANS.
6. Derrien H., Lucas B. Nuclear Cross Sections and Technology, Proc. Conf., Washington DC, March 3-7, 1975, p.637, NBS Special Publication 425 (1975).
7. Weston L.W. and Todd J.H. Nucl. Sci. Eng., 61, 356 (1976).
8. Kalebin S. Sov. J. At. Energy, 40, 373, (1976)
9. Lynn J.E., Patrick B.H., Sowerby M.G. and Bowey E.M. AERE-R8528, 1979
10. Adamchuk Yu.V. et al. Conf. on Peaceful Uses of Atomic Energy, Geneva, vol. 4, p. 216, 1955.
11.Belanova T.S., Zamyatnin Yu.S., Kolesov A.G., et al. Preprint NIIAR-307, 1977.
12. Dabbs J.W.T., Johnson C.H., Bemis Jr. C.E. Nucl. Sci. Engng. 83, 22 (1983).
13. Bowman C.D., Coops M.S., Auchampaugh G.F., Fultz S.C. Phys. Rev. B326, 137 (1965)
14. Gerasimov V.F. Yadernaya Fyzika 4, 985 (1966).
15. Vanpraet G., Cornelis E., Raman S., Rohr G. Nuclear Data for Basic and Applied Science, Proc. Int. Conf., Santa Fe, 1985, vol. 1, 493.
16. Maslov V.M., Porodzinskij Yu.V., Sukhovitskij E.Sh., Klepatskij A.B., Morogovskij G.B. INDC(BLR)-3, 1996.
17. Dunford C.L.: "ENDF Utility Codes Release 6.9", IAEA-NDS-29 (1993)
18. Porodzinskij Yu.V., Sukhovitskij E.Sh., Nuclear Constants, 4, p.27, 1987 (in Russian)
19. Ignatjuk A.V., Istekov K.K., Smirenkin G.N. Sov. J. Nucl. Phys. 29, 450 (1979). 1984.
20. Bowman J.C., Auchampaugh G.F., Fultz S.C., Hoff R.W. Phys. Rev. 166, 1216 (1968)
21. Shpack D.L., Ostapenko Yu.B., Smirenkin G.N. JETP Lett. 10, 175 (1969)
22. Gayther D.B. and Thomas B.W. Proc. 4th All-Union Conf. Neutron Physics, Kiev, Soviet Union, April 18-22, 1977, III, 3, Atomizdat (1977).

23. Wisshak K., Kappeler Nucl. Sci. Eng. 76, 148 (1980)
24. Hage W., Wisshak K., Kappeler Nucl. Sci. Eng. 78, 248 (1981)
25. Knitter H.-H., Budtz-Jorgensen C. Atomkernenergie. Kerntechnik, 3, 205 (1979).
26. Phillips T.W., Howe R.E. Nucl. Sci. Engng. 69, 375 (1979)
27. Haouat G., Lachkar J., Lagrange Ch., et al., Nucl.Sci. Engng. 81, 491 (1982)
28. Klepatskij A.B., Sukhovitskij E.Sh., private communication.
29. Fomushkin E.F., Gutnikova Sov. J. Nucl. Phys. 10, 529 (1970).
30. Kupriyanov V.M., Fursov B.I., Ivanov V.I., Smirenkin G.N. Sov. J. At. Energy 45, 176 (1979)
31. Fursov B.I., Kupriyanov V.M., Ivanov V.I., Smirenkin G.N. Sov. J. At. Energy 43, 894 (1978).
32. Aleksandrov B.M., Nemilov Yu. A., Selitskii Yu.A., et al. Sov. J. At. Energy 46, 475 (1979).
33. Behrens J.W., Browne J.C. Nucl. Sci. Engng. 77, 444 (1981)
34. Protopopov A.N., Selitskij Yu.A., Solov'ev S.M. Sov. J. At. Energy 6, 36 (1959)
35. Kazarinova M.I., Zamyatnin Yu.S., Gorbachev V.M. Sov. J. At. Energy 8, 125 (1960)
36. Fomushkin E.F., Gutnikova E.K., Zamyatnin Yu.S., Maslennikov B.K., et al. Sov. J. Nucl.Phys. 5, 689,(1967).
37. Cance M., Grenier G., CEA-N-2194, 1981
38. Prindle A.L., Sisson D.H., Nethaway D.R., Kantelo M.V., Sigg R.A. Phys. Rev. C20, 1824 (1979).
39. Filatenkov A.A, Ikeda Y., Smith D.L. Private communication.
40. Ignatjuk A.V., Maslov V.M., Proc. Int. Symp. Nuclear Data Evaluation Methodology, Brookhaven,USA, October 12-16, 1992, p.440, World Scientific, 1993.
41. Maslov V.M. Sov. J. At. Energy 64, 478 (1988).
42. Sood P.C., Singh R.N. Nucl. Phys. A373, 519 (1982).
43. Howard W.M., Moller P. Atomic Data and Nuclear Data Tables,25, 219 (1980)
44. Tepel J.W., Hoffman H.M., Weidenmuller H.A. Phys. Lett. 49, 1 (1974).
45. Klepatskij A.B., Maslov V.M., Sukhovitskij E.Sh., private communication.
46. Ignatjuk A.V., Maslov V.M., Pashchenko A.B. Sov. J. Nucl. Phys. 47, 224 (1988).
47. Uhl M. and Strohmaier B., Report IRK - 76/10 (Vienna,1976).
48. Fort E., Darrouzet M., Derrien H., et al. Proc. Int. Conf. Nucl. Cross Sections for Technology, Knoxville, 22-26 Oct. 1979, NBS Special Publ., p.862, 1980.

49. ENSDF, 1995.
50. Maslov V.M., Porodzinskij Yu.V.,Sukhovitskij E.Sh., Proc. Int. Conf. on Neutron Physics, 14-18 Sept., Kiev, USSR, V.1, p.413, 1988.
51. Madland D.G., Nix J.R., Nucl. Sci. Engng. 81, 213 (1982).
52. Asghar M. et al., Nuclear Physics A, 334, 327 (1980).
53. Audi G., Wapstra A.H., Nuclear Physics A, 565, 1 (1980).
54. Viola V.E., Kwiatkowski K., Walker M., Phys. Rev., 31, 1550 (1985).
55. Becchetti F.D., Greenlees G.W., Phys. Rev. 182, 1190 (1969).
56. Lebedev V.I., Kalashnikova V.I., Atomnaya Energiya 5, 176 (1958)
57. Jaffey A.H., Lerner J.L., Nuclear Physics A, 145, 1 (1970).
58. Khokhlov Yu.A. et al., Nuclear Data for Science and Technology Proc. of the Int. Conf., Julich, Germany, 13-17 May, 1991 (Springer-Verlag, 1992), p. 51.
59. Khokhlov Yu.A. et al., Nuclear Data for Science and Technology, Proc. of the Int. Conf., Gatlinburg, Tennessee, USA, May 9-13, 1994, v.I, p. 272.
60. Brady M.C., Wright R.Q., England T.R., Report ORNL/CSD/TM-226(1991), IAEA-NDS-102, 1992.

10 Figure captions

Fig. 2.1 Total cross section of ^{241}Am in the energy region below 1 eV.
Fig. 2.2 Total cross section of ^{241}Am in the energy region below 8 eV.
Fig. 2.3 Total cross section of ^{241}Am in the energy region below 0.1 eV.
Fig. 2.4 Absorption cross section of ^{241}Am in the energy region below 0.1 eV.
Fig. 2.5 Fission cross section of ^{241}Am in the energy region below 0.1 eV.
Fig. 2.6 Distribution of radiative capture widths for ^{241}Am.
Fig. 3.1 Cumulative sum of neutron resonance levels of ^{241}Am.
Fig. 3.2 Cumulative sum of reduced neutron widths of ^{241}Am.
Fig. 3.3 Distribution of reduced neutron widths for ^{241}Am.
Fig. 3.4 Neutron resonance spacing distribution for ^{241}Am.
Fig. 3.5 Fission cross section of ^{241}Am in unresolved resonance region.
Fig. 3.6 Radiative capture cross section of ^{241}Am in unresolved resonance region.
Fig. 4.1 Compound reaction cross section of ^{241}Am.
Fig. 4.2 Total cross section of ^{241}Am.
Fig. 4.3 Elastic scattering cross section of ^{241}Am.
Fig. 4.4 Fission cross section of ^{241}Am.
Fig. 4.5 Fission cross section of ^{241}Am.
Fig. 4.6 Fission cross section of ^{241}Am.
Fig. 4.7 Fission cross section of ^{241}Am.
Fig. 4.8 Fission cross section of ^{241}Am.
Fig. 4.9 Cumulative number of levels of ^{241}Am.
Fig. 4.10 Inelastic scattering cross section of ^{241}Am.
Fig. 4.11 Cross section of ^{241}Am: 0.0418 MeV, $7/2^-$ level excitation.
Fig. 4.12 Cross section of ^{241}Am: 0.0936 MeV, $9/2^-$ level excitation.
Fig. 4.13 Cross section of ^{241}Am: 0.158 MeV, $11/2^-$ level excitation.
Fig. 4.14 Cross section of ^{241}Am: 0.2085 MeV, $5/2^+$ level excitation.
Fig. 4.15 Cross section of ^{241}Am: 0.235 MeV, $7/2^+$ level excitation.
Fig. 4.16 Cross section of ^{241}Am: 0.272 MeV, $9/2^+$ level excitation.
Fig. 4.17 Cumulative number of levels of ^{242}Am.
Fig. 4.18 Radiative capture cross section of ^{241}Am.
Fig. 4.19 ^{241}Am(n,2n) reaction cross section.
Fig. 4.20 ^{241}Am(n,3n) reaction cross section.
Fig. 5.1 Components of first neutron spectrum of ^{241}Am for incident neutron energy 15 MeV.
Fig. 5.2 Components of second neutron spectrum of ^{241}Am for incident neutron energy 15 MeV.

Fig. 5.3 Comparison of (n,n'γ) reaction neutron spectra of ^{241}Am for incident neutron energy 8 MeV.
Fig. 5.4 Comparison of (n,2n) reaction neutron spectra of ^{241}Am for incident neutron energy 8 MeV.
Fig. 5.5 Comparison of (n,n'γ) reaction neutron spectra of ^{246}Cm for incident neutron energy 15 MeV.
Fig. 5.6 Comparison of (n,2n) reaction neutron spectra of ^{241}Am for incident neutron energy 15 MeV.
Fig. 5.7 Comparison of (n,3n) reaction neutron spectra of ^{241}Am for incident neutron energy 15 MeV.
Fig. 5.8 Thermal prompt fission neutron spectrum of ^{241}Am.
Fig. 5.9 Calculated fission neutron spectra of ^{241}Am ratio to JENDL-3 evaluation ($T_{maxw} = 1.389$).
Fig. 5.10 Calculated fission neutron spectra of ^{241}Am ratio to ENDF/B-VI evaluation.
Fig. 5.11 Fission neutron spectra of ^{241}Am ratio to standard Madland-Nix model calculation for incident neutron energies 8, 15 and 20 MeV.
Fig. 5.12 Fission neutron spectra of ^{241}Am for incident neutron energy 8 MeV.
Fig. 5.13 Fission neutron spectra of ^{241}Am for incident neutron energy 15 MeV.
Fig. 5.14 Fission neutron spectra of ^{241}Am for incident neutron energy 20 MeV.
Fig. 6.1 Prompt fission neutron multiplicity for ^{241}Am.

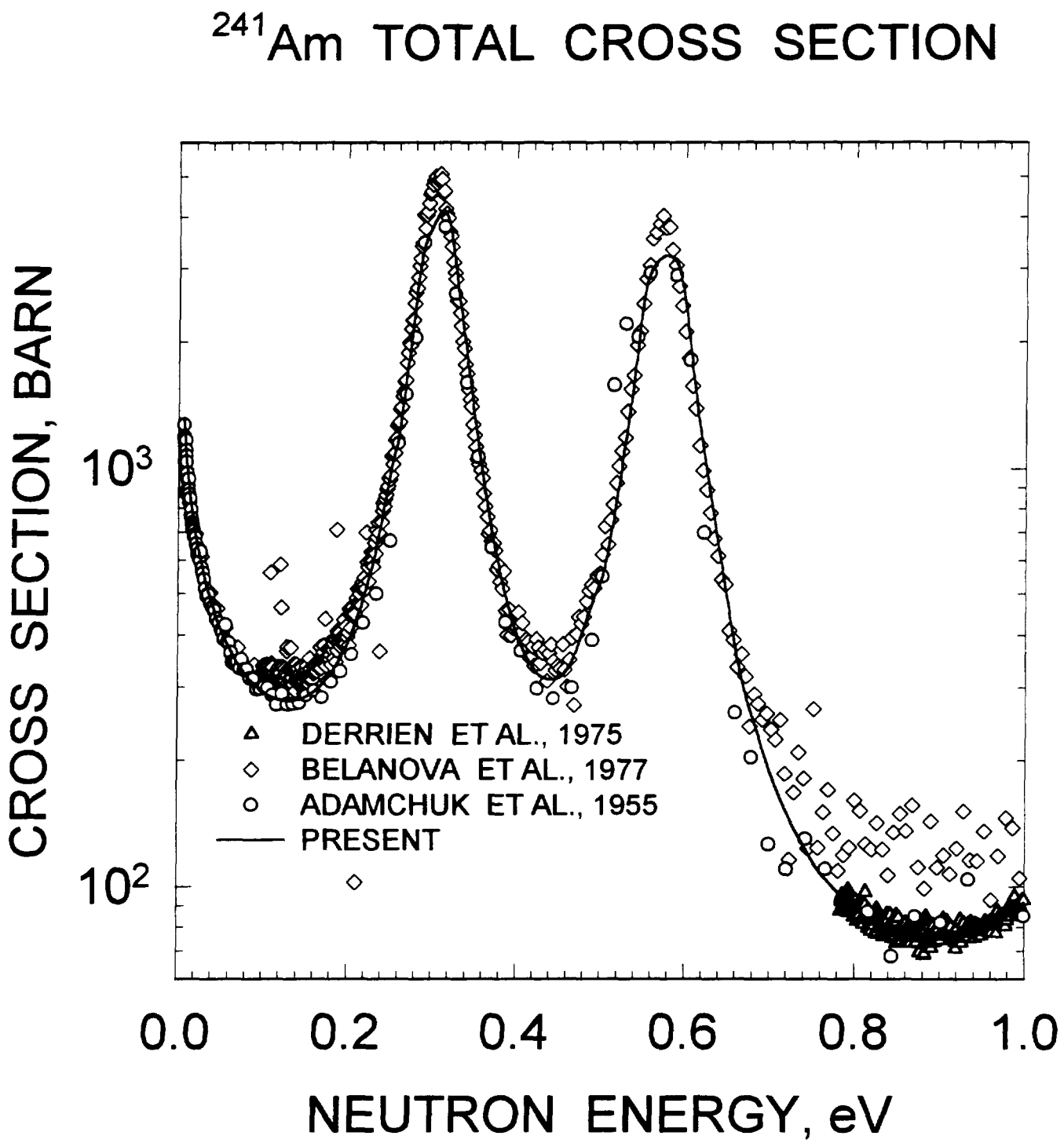
^{241}Am TOTAL CROSS SECTION
CROSS SECTION, BARN
10^3
10^2
DERRIEN ET AL., 1975
BELANOVA ET AL., 1977
ADAMCHUK ET AL., 1955
PRESENT
0.0
0.2
0.4
0.6
0.8
1.0
NEUTRON ENERGY, eV

FIG.2.1

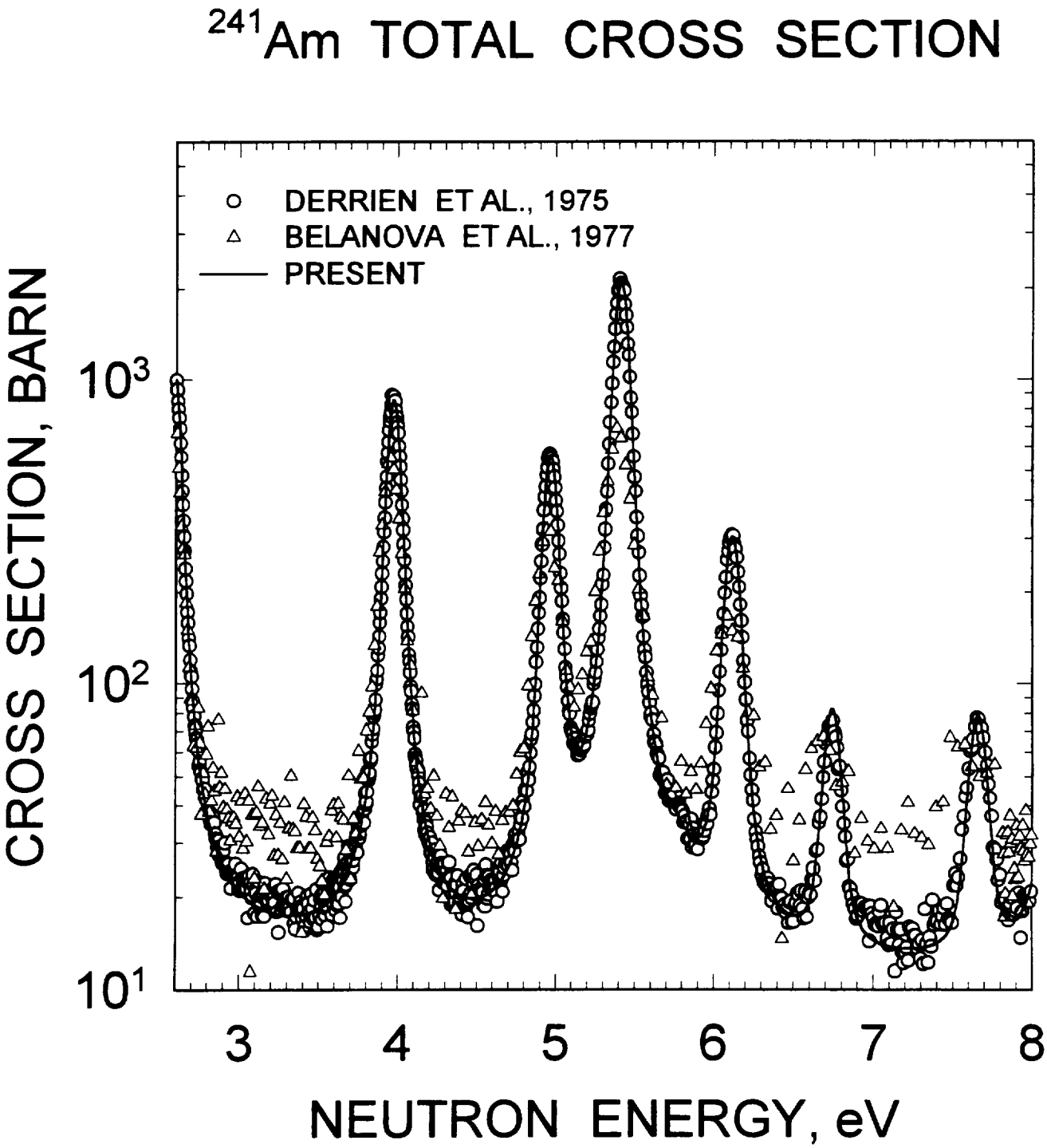
^{241}Am TOTAL CROSS SECTION
DERRIEN ET AL., 1975
BELANOVA ET AL., 1977
PRESENT
CROSS SECTION, BARN
10^3
10^2
10^1
3
4
5
6
7
8
NEUTRON ENERGY, eV

FIG.2.2

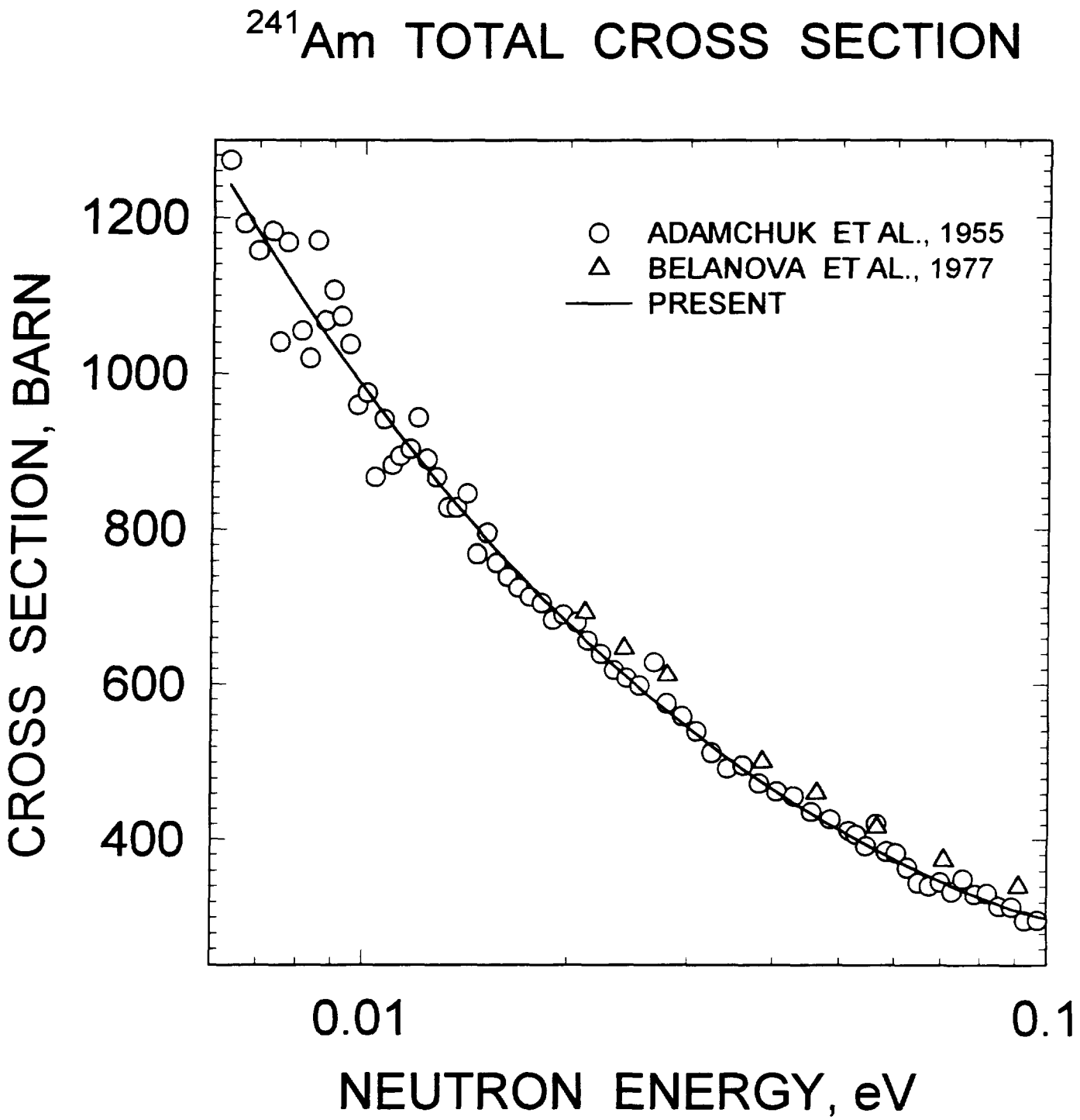
^{241}Am TOTAL CROSS SECTION
CROSS SECTION, BARN
1200
1000
800
600
400
ADAMCHUK ET AL., 1955
BELANOVA ET AL., 1977
PRESENT
0.01
0.1
NEUTRON ENERGY, eV

FIG.2.3

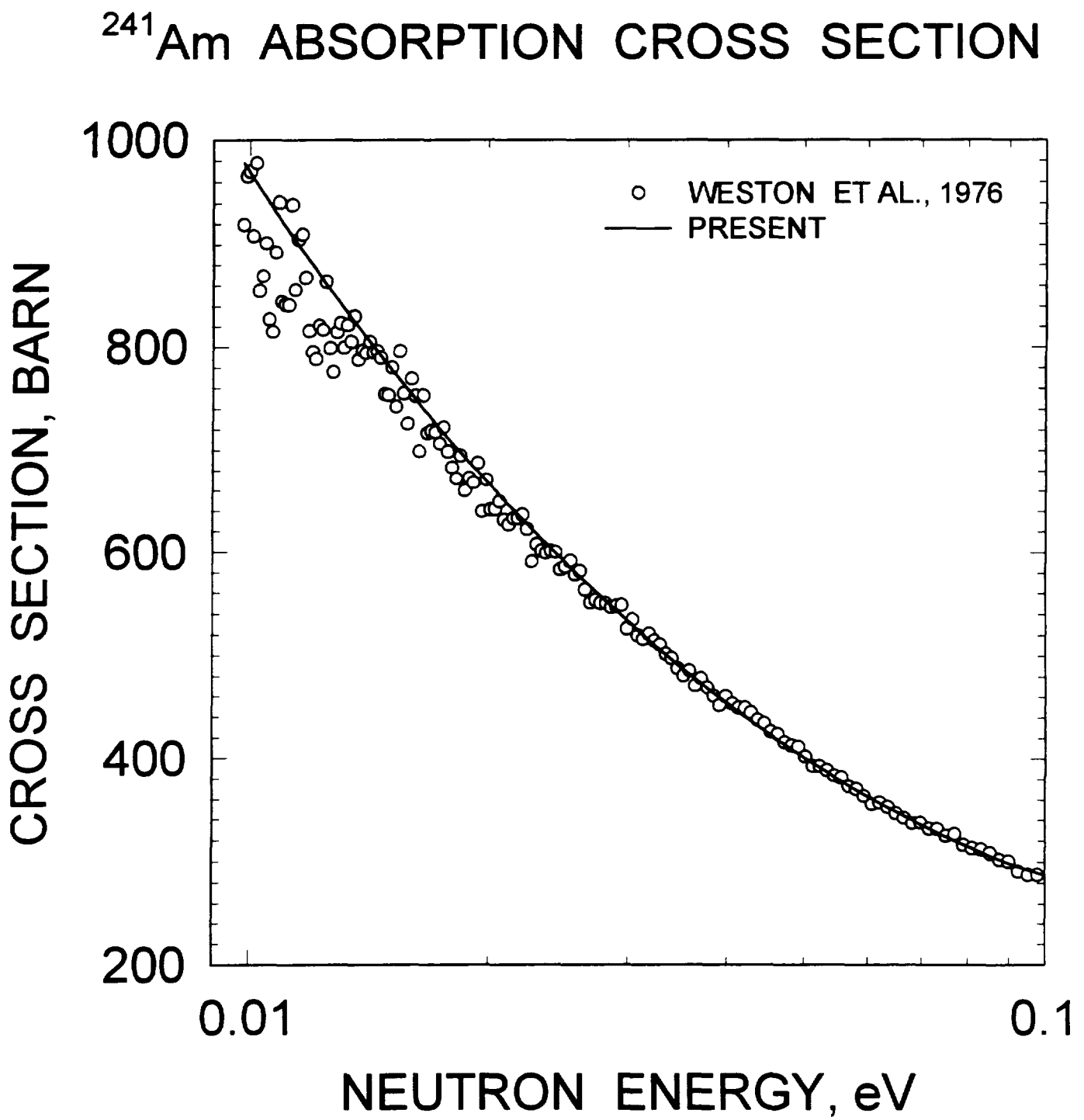
^{241}Am ABSORPTION CROSS SECTION
1000
800
600
400
200
CROSS SECTION, BARN
WESTON ET AL., 1976
PRESENT
0.01
0.1
NEUTRON ENERGY, eV

FIG.2.4

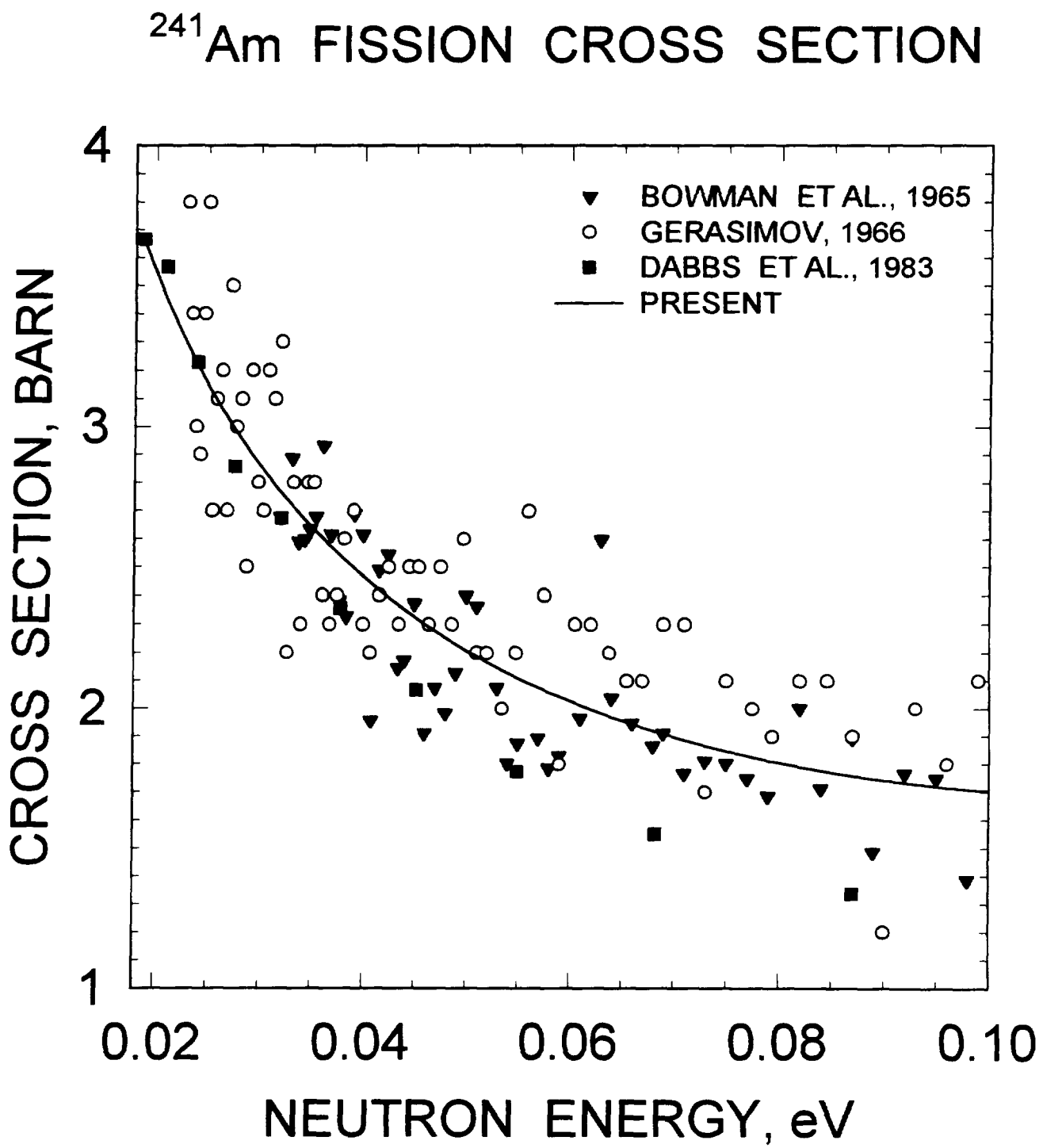
^{241}Am FISSION CROSS SECTION
CROSS SECTION, BARN
4
3
2
1
0.02
0.04
0.06
0.08
0.10
NEUTRON ENERGY, eV
BOWMAN ET AL., 1965
GERASIMOV, 1966
DABBS ET AL., 1983
PRESENT

FIG.2.5

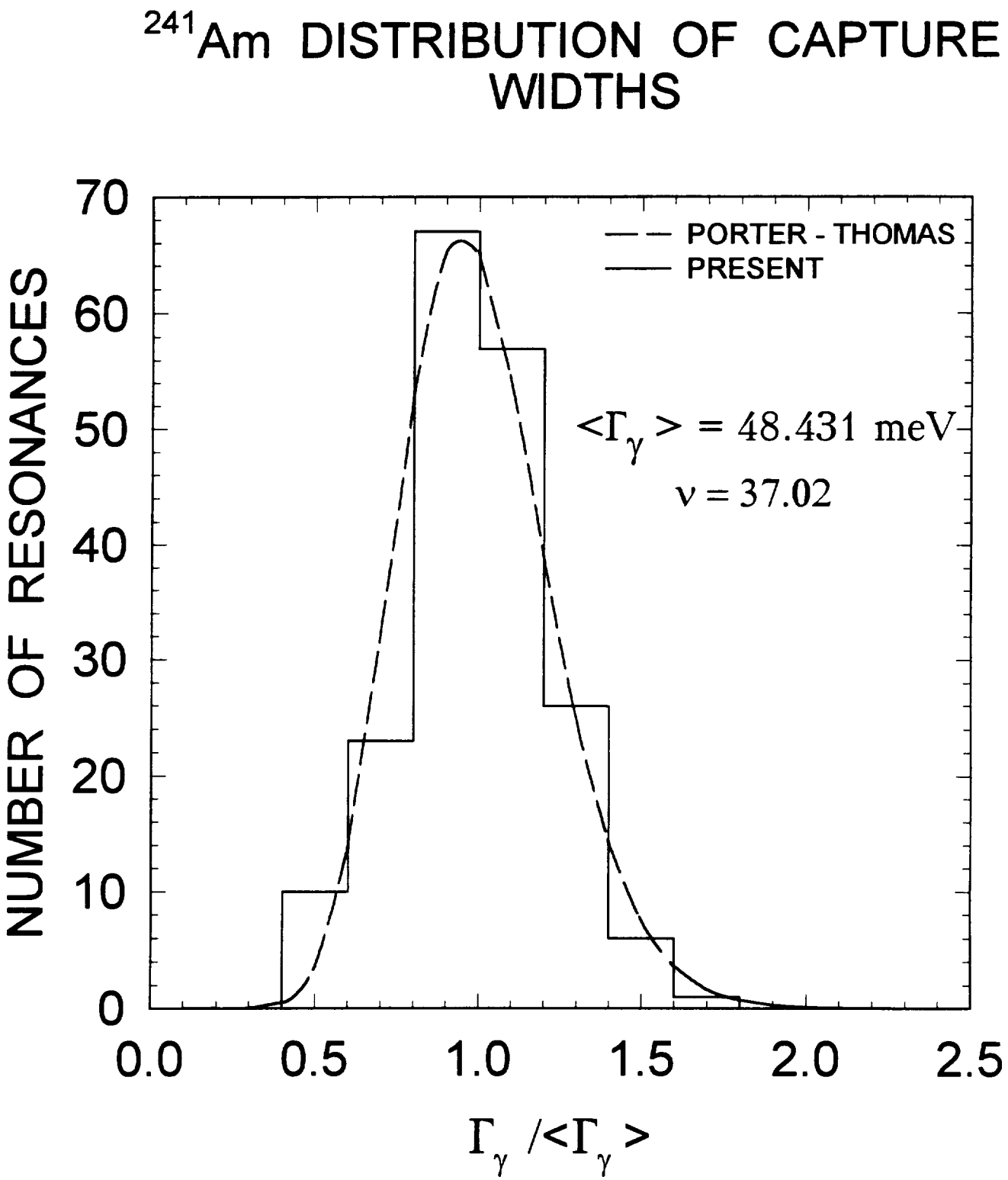
^{241}Am DISTRIBUTION OF CAPTURE WIDTHS
NUMBER OF RESONANCES
70
60
50
40
30
20
10
0
0.0
0.5
1.0
1.5
2.0
2.5
$\Gamma_\gamma / \langle\Gamma_\gamma\rangle$
PORTER - THOMAS
PRESENT
$\langle\Gamma_\gamma\rangle$ = 48.431 meV
ν = 37.02

FIG.2.6

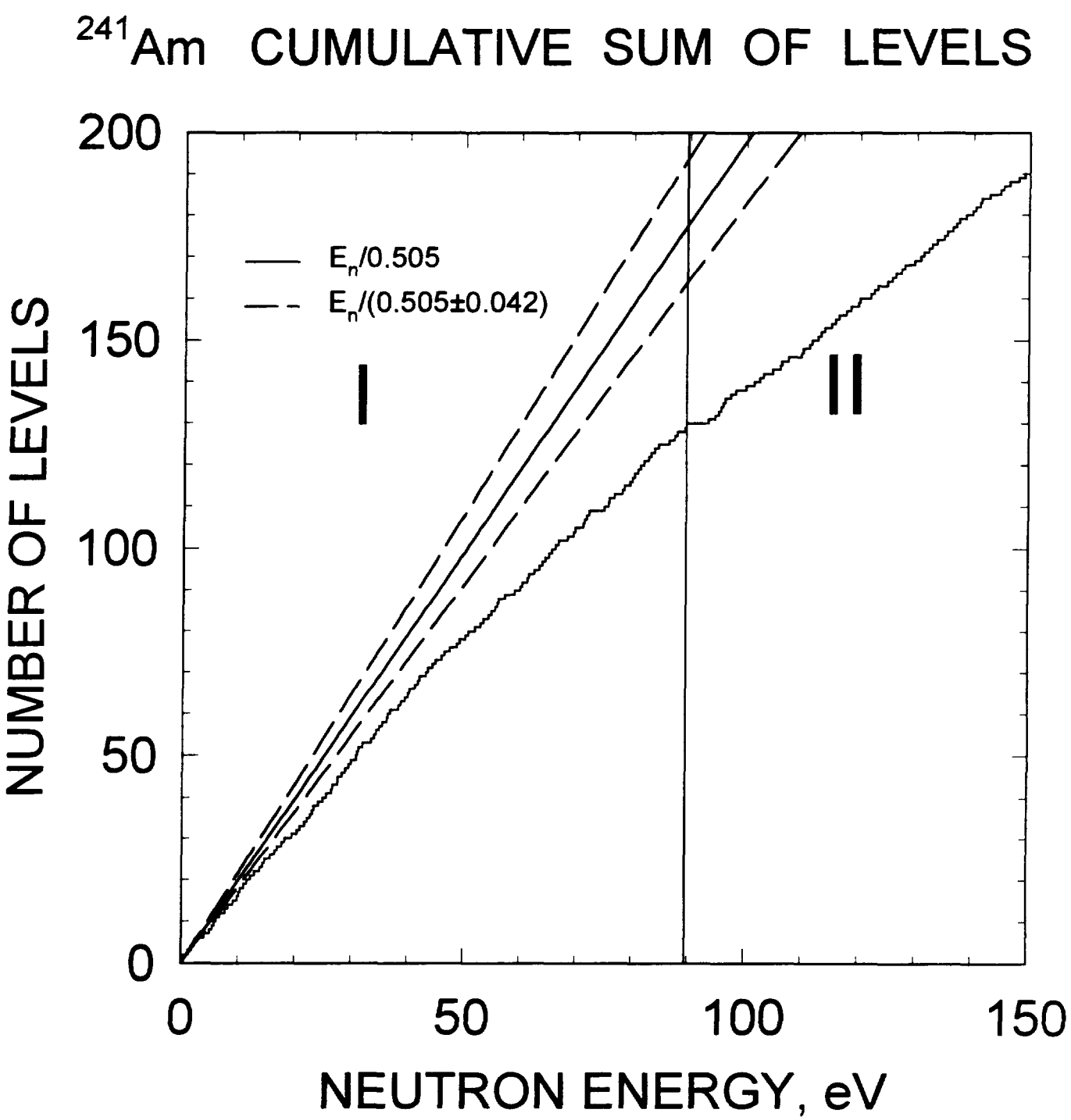
^{241}Am CUMULATIVE SUM OF LEVELS
NUMBER OF LEVELS
200
150
100
50
0
E_n/0.505
E_n/(0.505±0.042)
I
II
0
50
100
150
NEUTRON ENERGY, eV

FIG.3.1

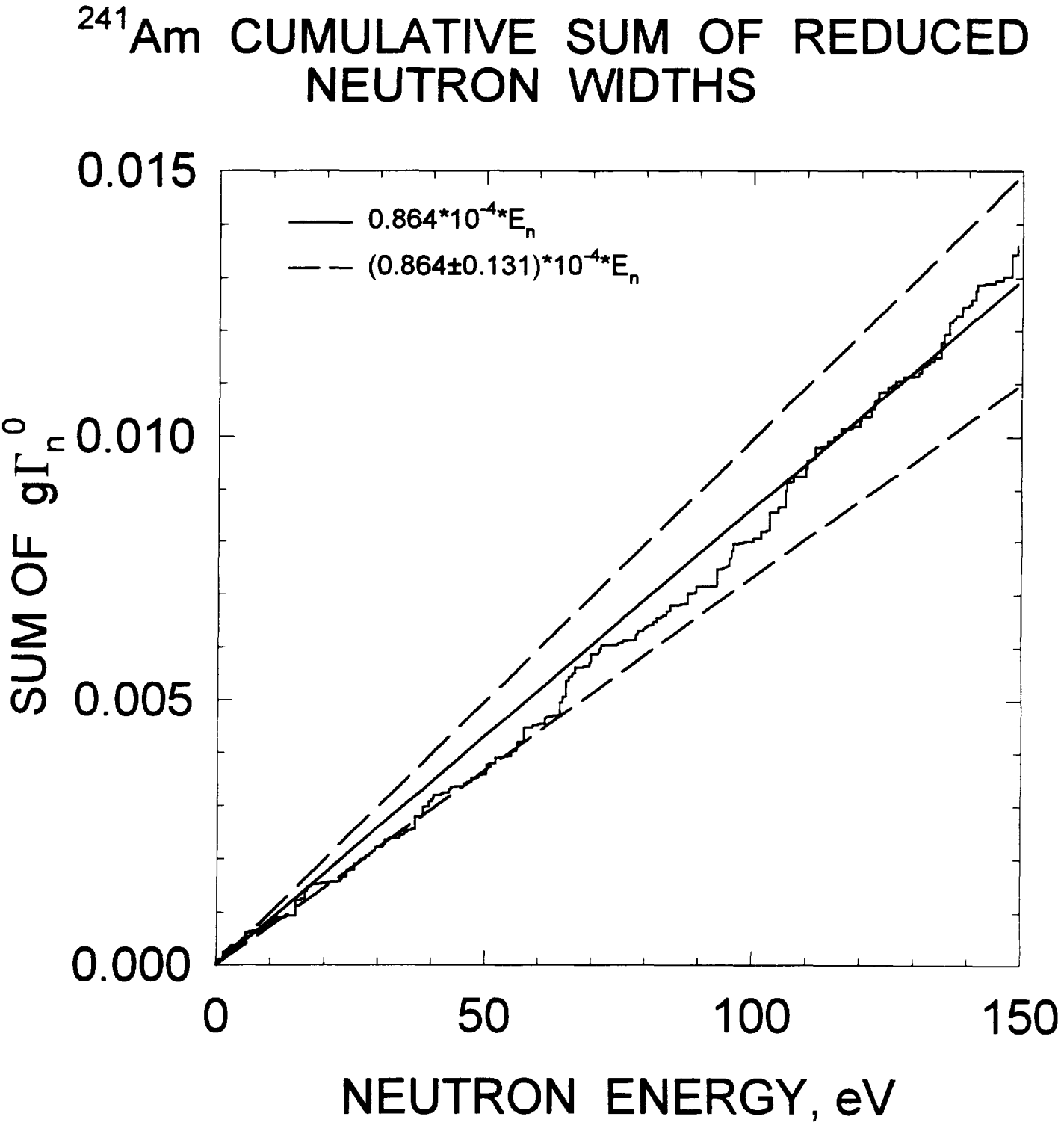
^{241}Am CUMULATIVE SUM OF REDUCED NEUTRON WIDTHS
0.015
0.010
0.005
0.000
SUM OF $g\Gamma_n^0$
$0.864*10^{-4}*E_n$
$(0.864\pm0.131)*10^{-4}*E_n$
0
50
100
150
NEUTRON ENERGY, eV

FIG.3.2

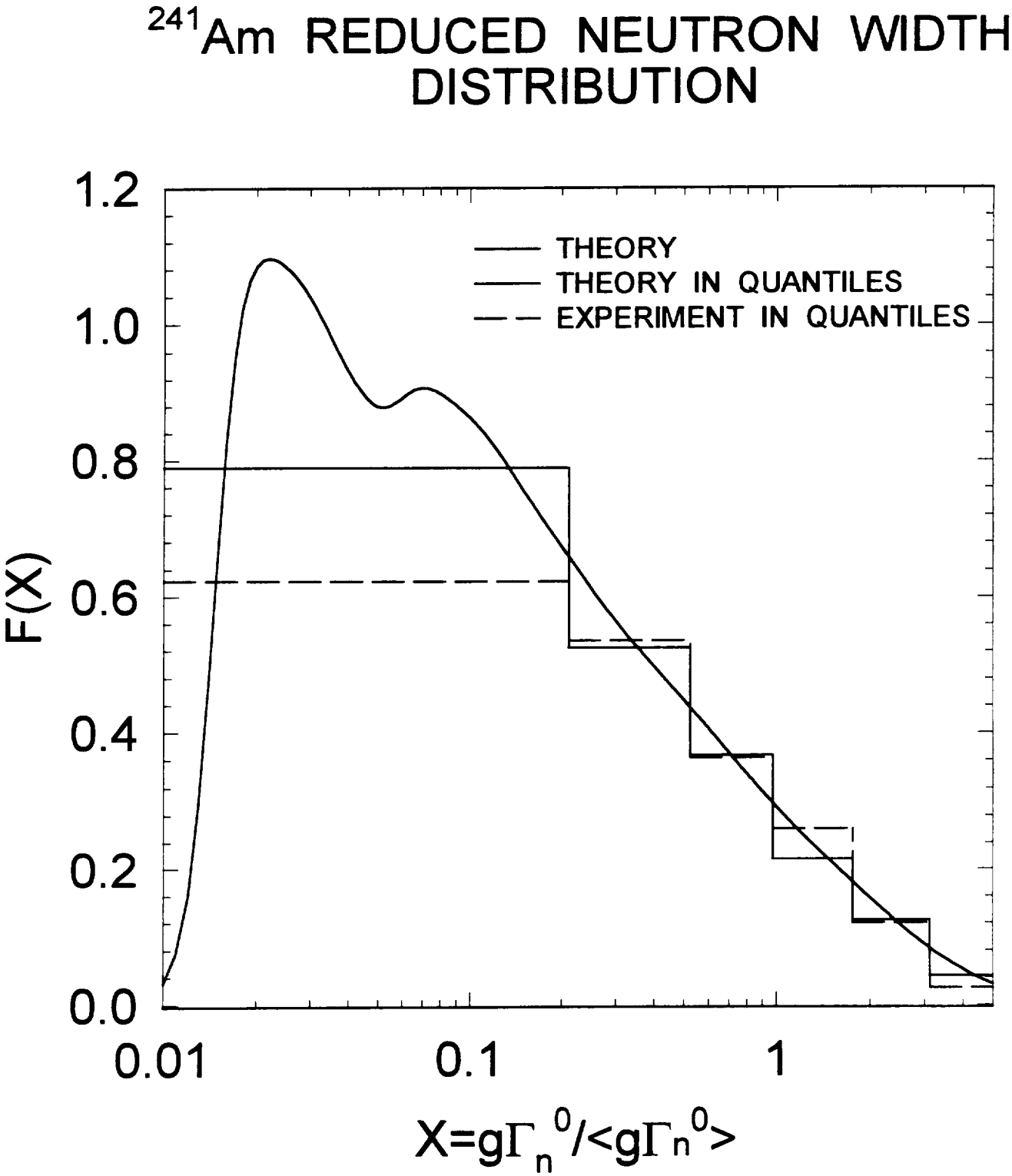
^{241}Am REDUCED NEUTRON WIDTH DISTRIBUTION
THEORY
THEORY IN QUANTILES
EXPERIMENT IN QUANTILES
F(X)
1.2
1.0
0.8
0.6
0.4
0.2
0.0
0.01
0.1
1
X=gΓn0/<gΓn0>

FIG.3.3

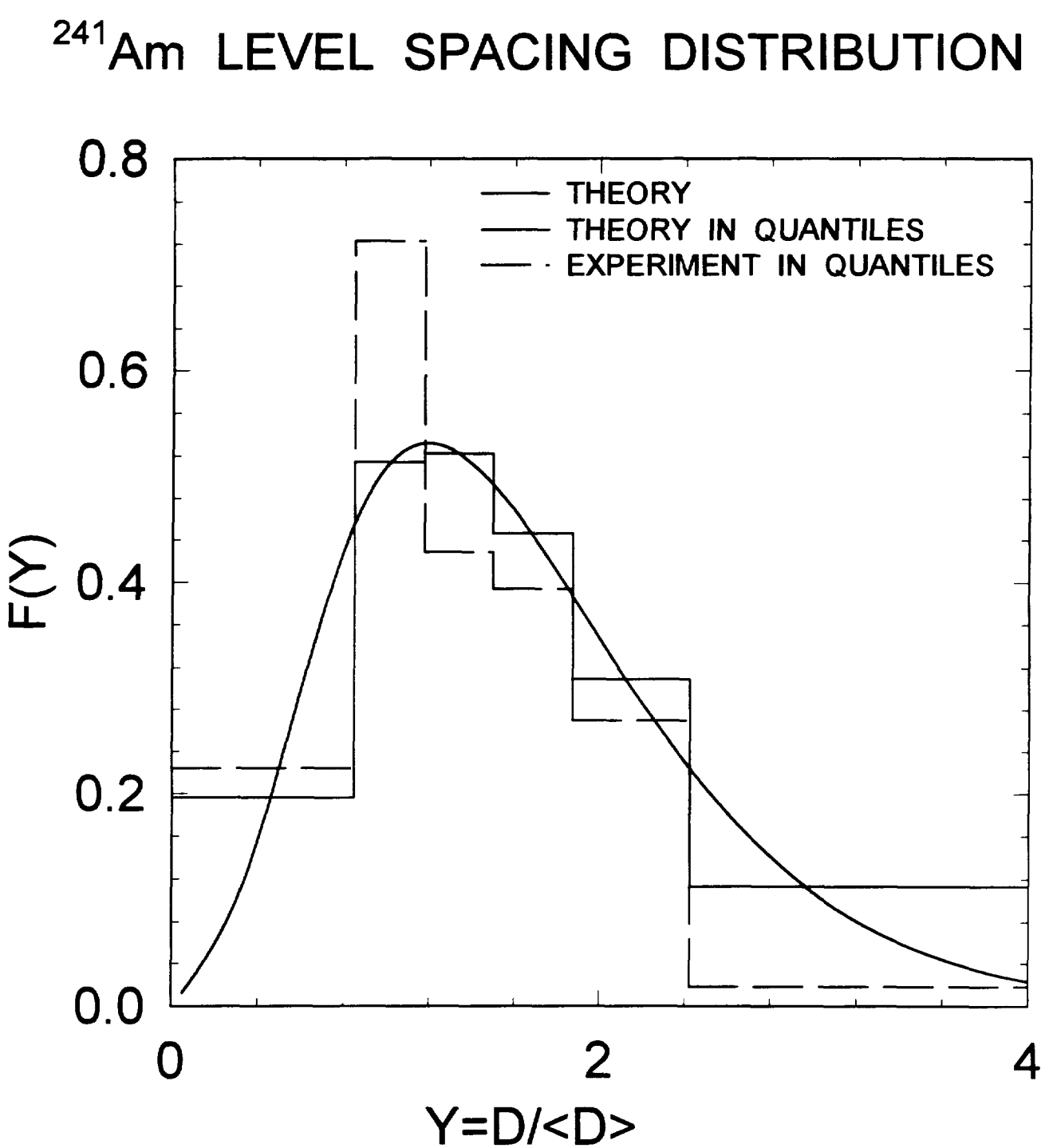
^{241}Am LEVEL SPACING DISTRIBUTION
THEORY
THEORY IN QUANTILES
EXPERIMENT IN QUANTILES
F(Y)
0.0
0.2
0.4
0.6
0.8
0
2
4
Y=D/<D>

FIG.3.4

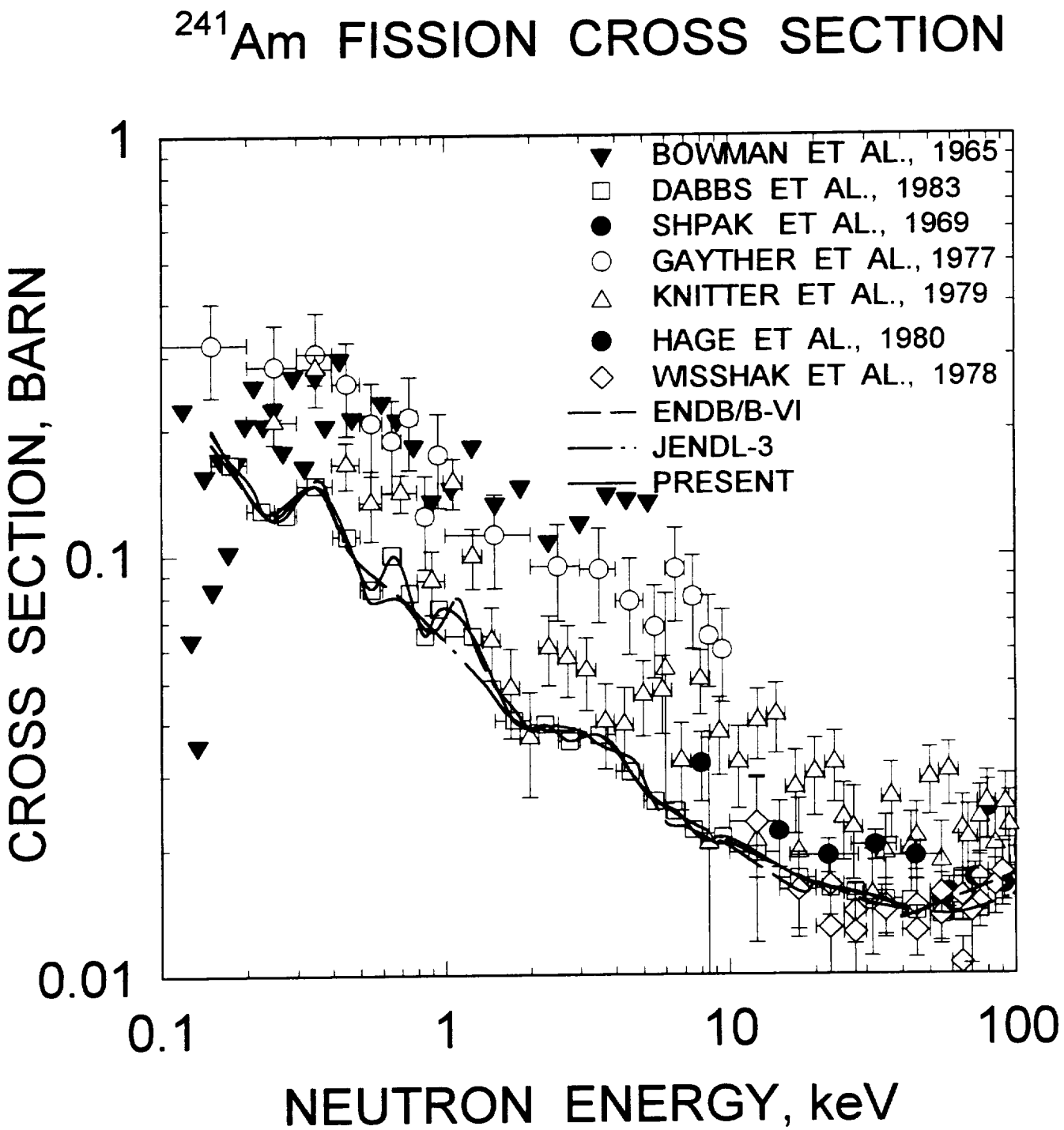
^{241}Am FISSION CROSS SECTION
CROSS SECTION, BARN
NEUTRON ENERGY, keV
1
0.1
0.01
0.1
1
10
100
BOWMAN ET AL., 1965
DABBS ET AL., 1983
SHPAK ET AL., 1969
GAYTHER ET AL., 1977
KNITTER ET AL., 1979
HAGE ET AL., 1980
WISSHAK ET AL., 1978
ENDB/B-VI
JENDL-3
PRESENT

FIG.3.5

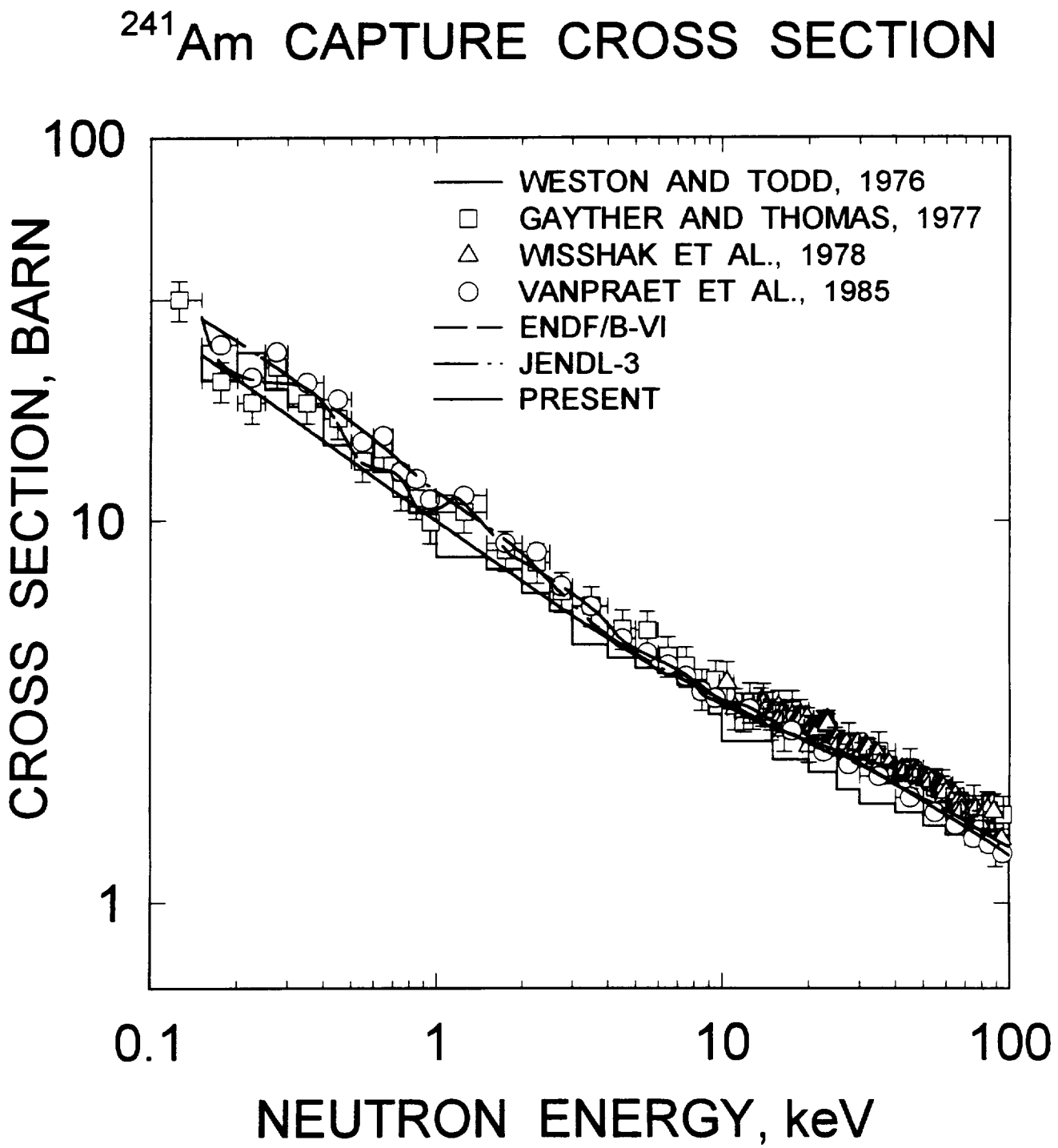
^{241}Am CAPTURE CROSS SECTION
100
10
1
CROSS SECTION, BARN
WESTON AND TODD, 1976
GAYTHER AND THOMAS, 1977
WISSHAK ET AL., 1978
VANPRAET ET AL., 1985
ENDF/B-VI
JENDL-3
PRESENT
0.1
1
10
100
NEUTRON ENERGY, keV

FIG.3.6

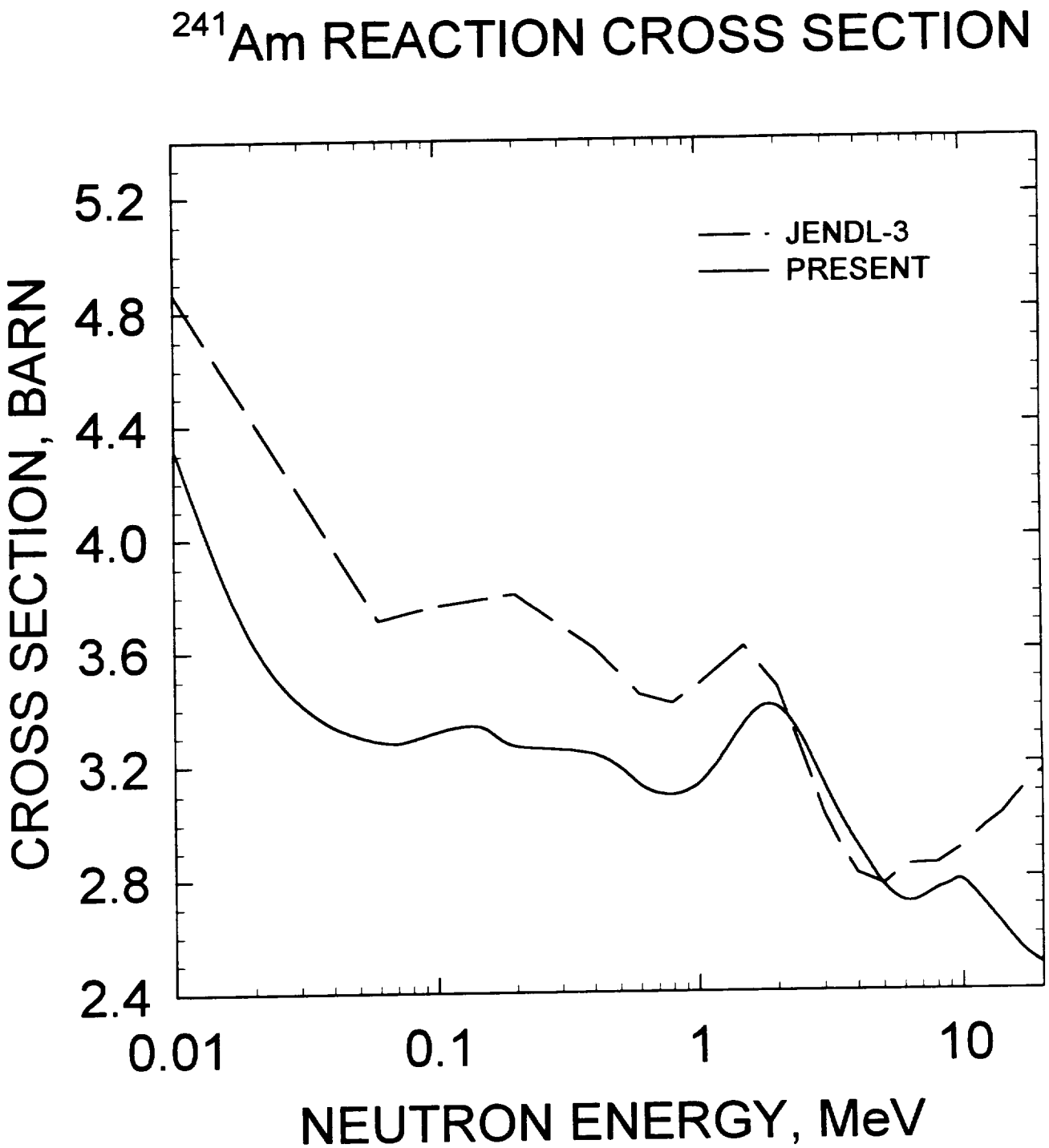
^{241}Am REACTION CROSS SECTION
CROSS SECTION, BARN
5.2
4.8
4.4
4.0
3.6
3.2
2.8
2.4
0.01
0.1
1
10
NEUTRON ENERGY, MeV
JENDL-3
PRESENT

FIG.4.1

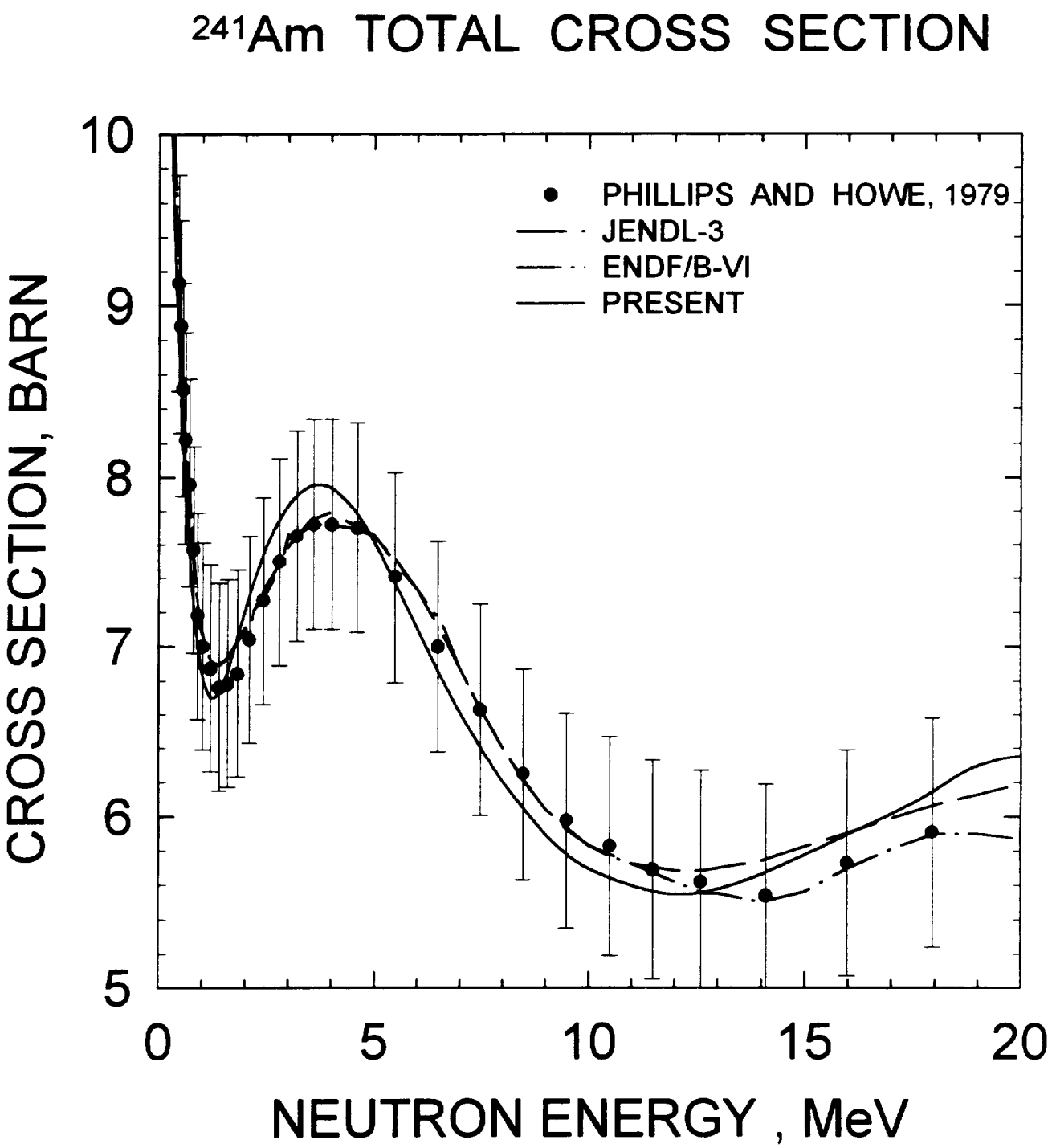
241Am TOTAL CROSS SECTION
PHILLIPS AND HOWE, 1979
JENDL-3
ENDF/B-VI
PRESENT
CROSS SECTION, BARN
NEUTRON ENERGY , MeV
10
9
8
7
6
5
0
5
10
15
20

FIG.4.2

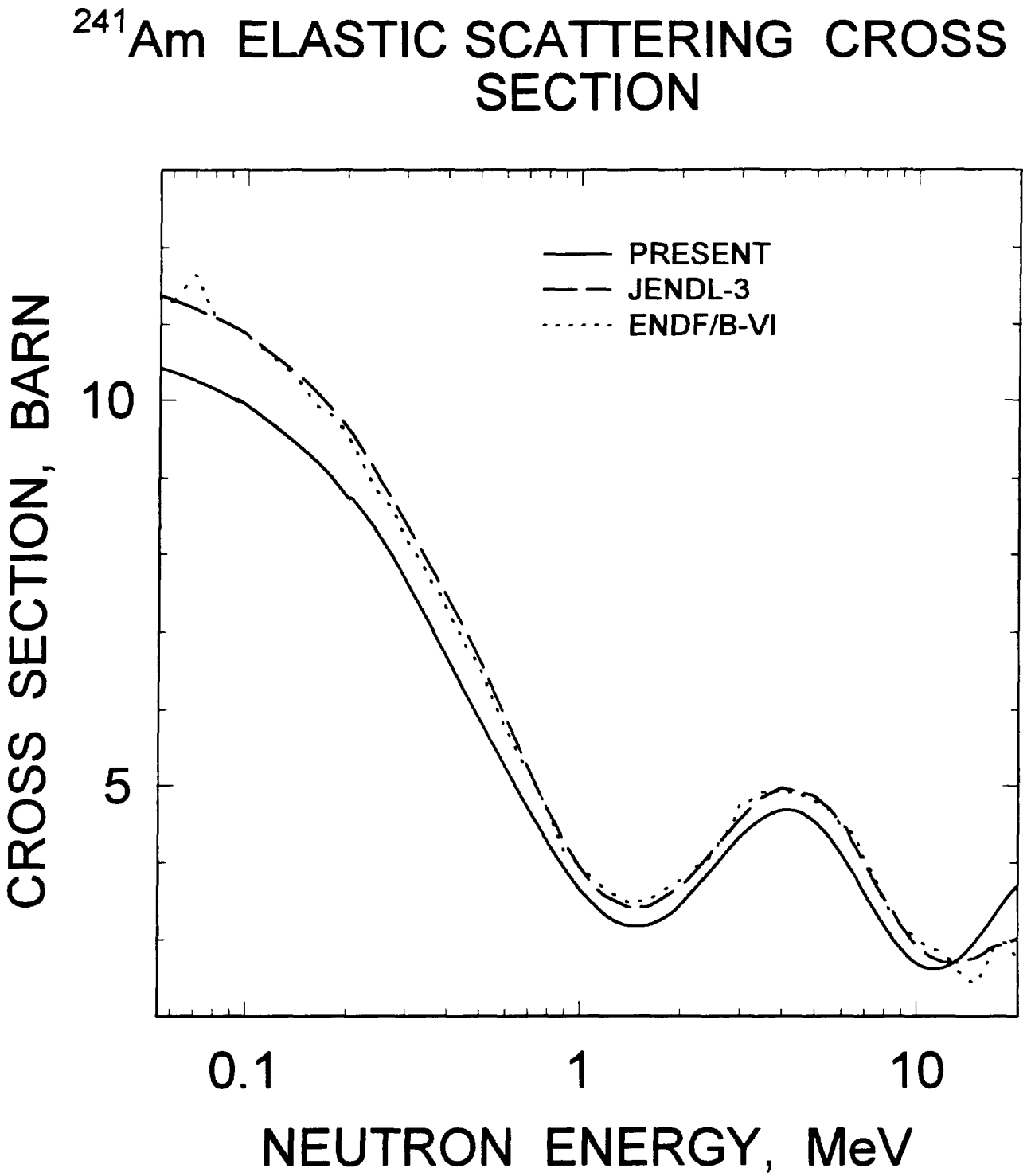
^{241}Am ELASTIC SCATTERING CROSS SECTION
PRESENT
JENDL-3
ENDF/B-VI
CROSS SECTION, BARN
10
5
0.1
1
10
NEUTRON ENERGY, MeV

FIG.4.3

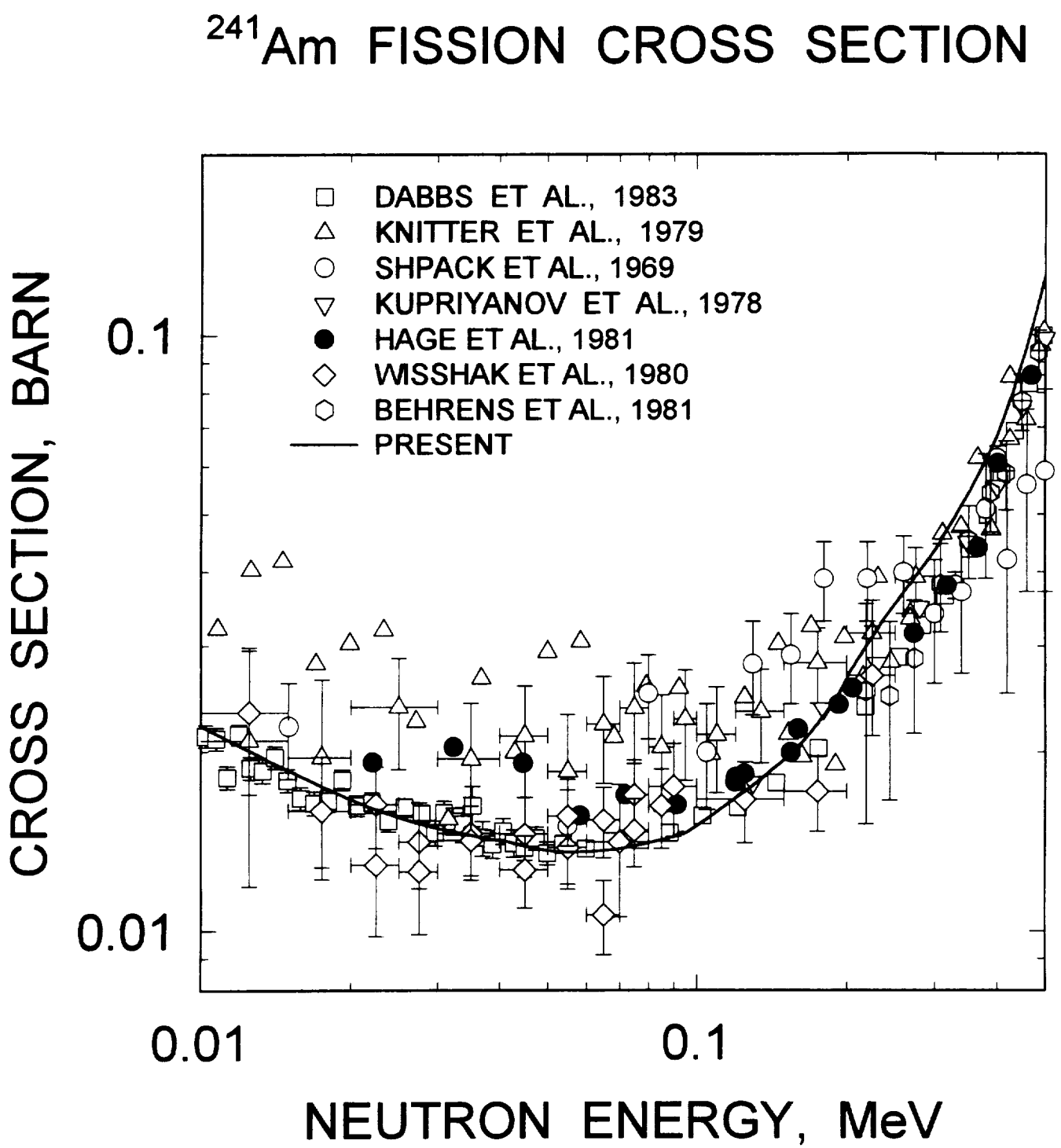
^{241}Am FISSION CROSS SECTION
DABBS ET AL., 1983
KNITTER ET AL., 1979
SHPACK ET AL., 1969
KUPRIYANOV ET AL., 1978
HAGE ET AL., 1981
WISSHAK ET AL., 1980
BEHRENS ET AL., 1981
PRESENT
CROSS SECTION, BARN
0.1
0.01
0.01
0.1
NEUTRON ENERGY, MeV

FIG. 4.4

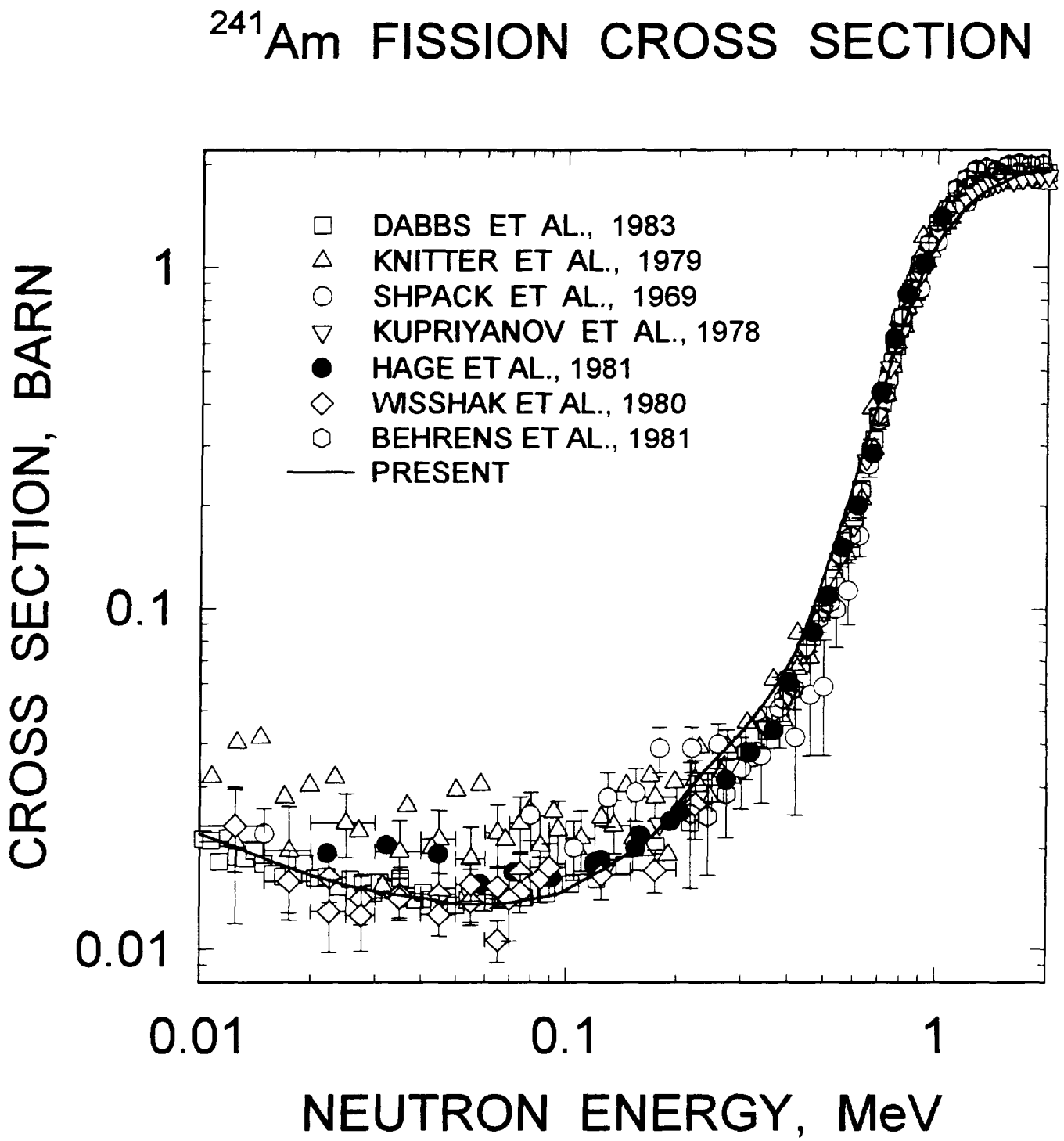
^{241}Am FISSION CROSS SECTION
DABBS ET AL., 1983
KNITTER ET AL., 1979
SHPACK ET AL., 1969
KUPRIYANOV ET AL., 1978
HAGE ET AL., 1981
WISSHAK ET AL., 1980
BEHRENS ET AL., 1981
PRESENT
CROSS SECTION, BARN
1
0.1
0.01
0.01
0.1
1
NEUTRON ENERGY, MeV

FIG. 4.5

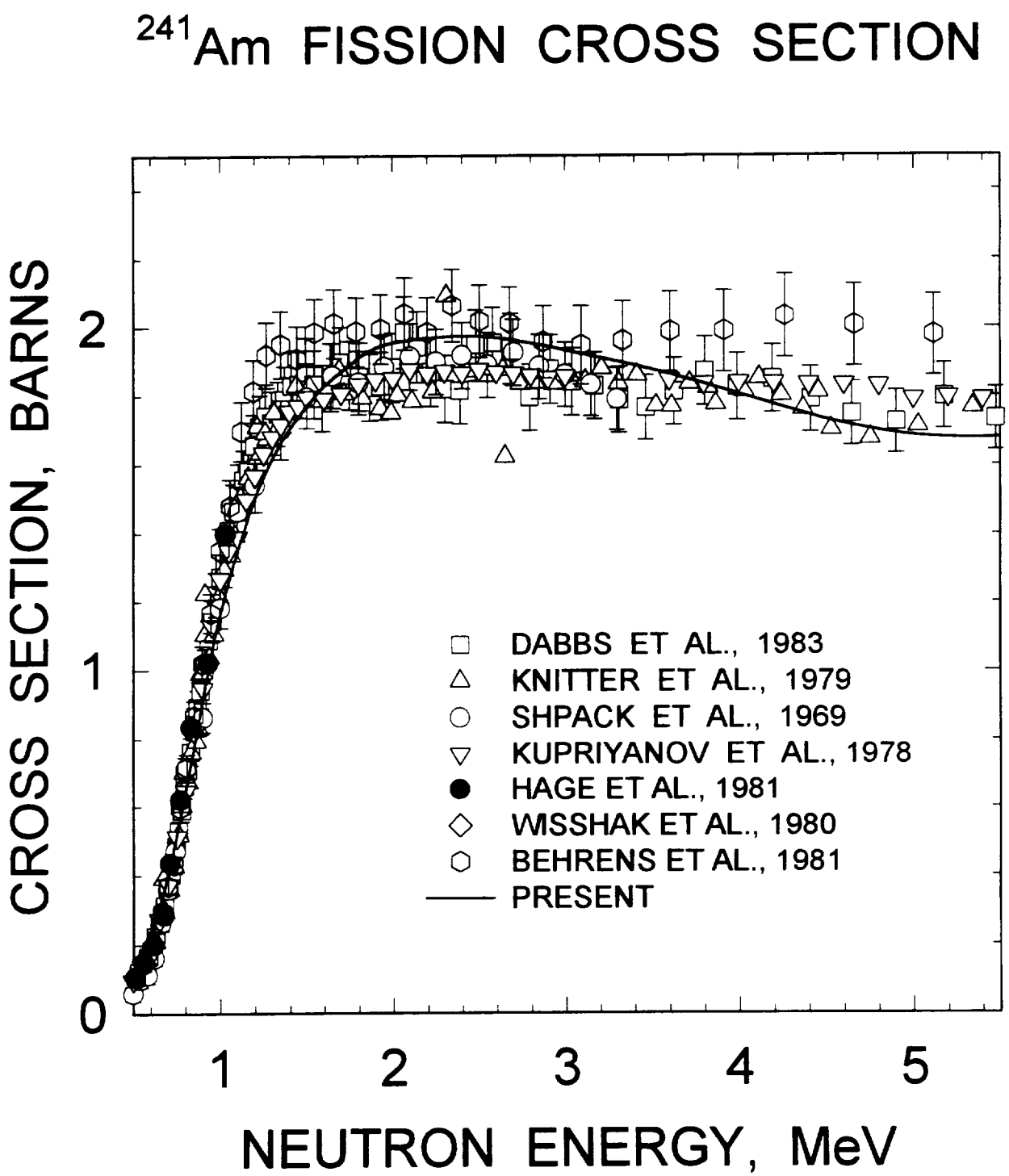
^{241}Am FISSION CROSS SECTION
CROSS SECTION, BARNS
0
1
2
1
2
3
4
5
NEUTRON ENERGY, MeV
DABBS ET AL., 1983
KNITTER ET AL., 1979
SHPACK ET AL., 1969
KUPRIYANOV ET AL., 1978
HAGE ET AL., 1981
WISSHAK ET AL., 1980
BEHRENS ET AL., 1981
PRESENT

FIG. 4.6

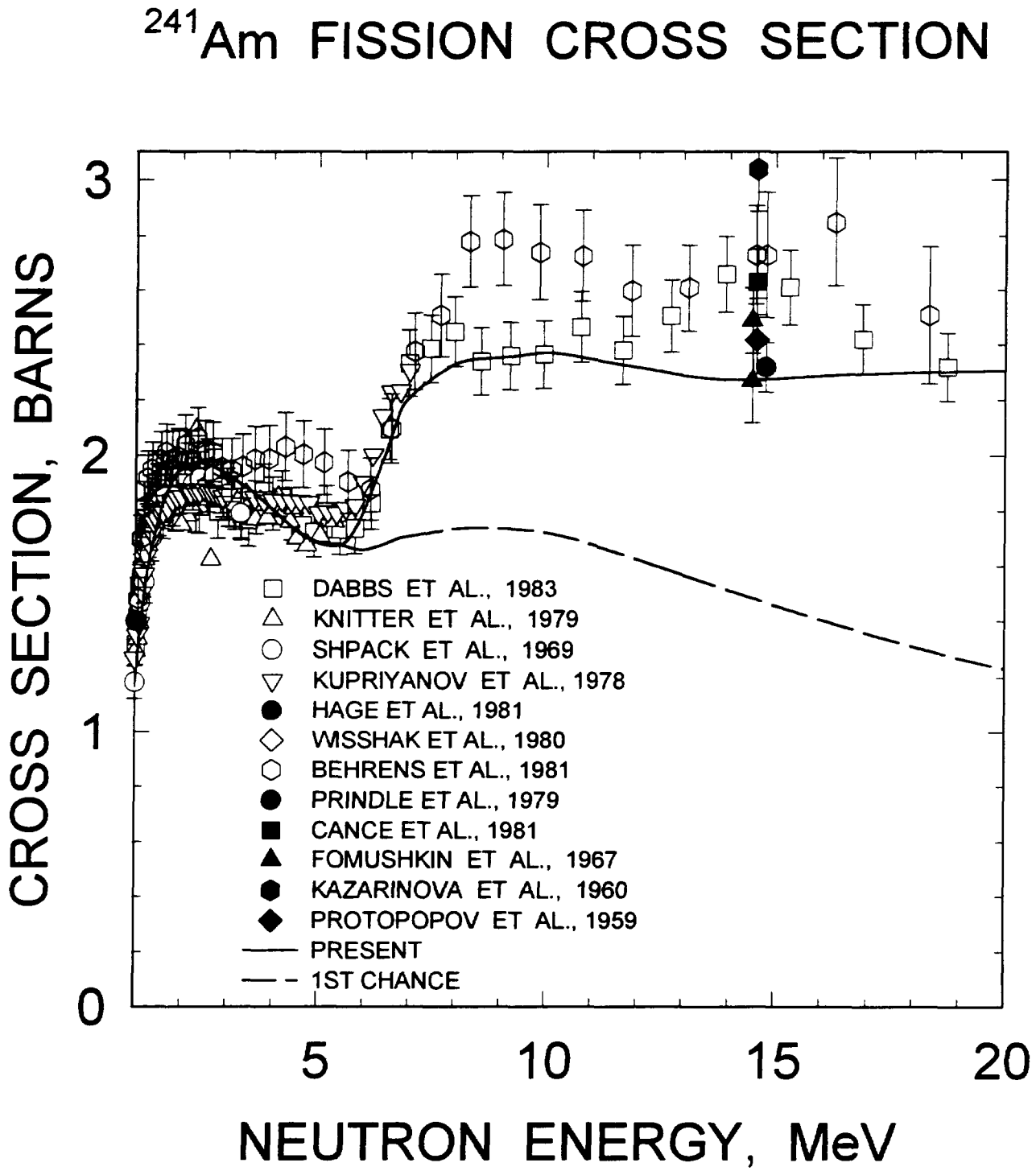
^{241}Am FISSION CROSS SECTION
CROSS SECTION, BARNS
0
1
2
3
5
10
15
20
NEUTRON ENERGY, MeV
DABBS ET AL., 1983
KNITTER ET AL., 1979
SHPACK ET AL., 1969
KUPRIYANOV ET AL., 1978
HAGE ET AL., 1981
WISSHAK ET AL., 1980
BEHRENS ET AL., 1981
PRINDLE ET AL., 1979
CANCE ET AL., 1981
FOMUSHKIN ET AL., 1967
KAZARINOVA ET AL., 1960
PROTOPOPOV ET AL., 1959
PRESENT
1ST CHANCE

FIG. 4.7

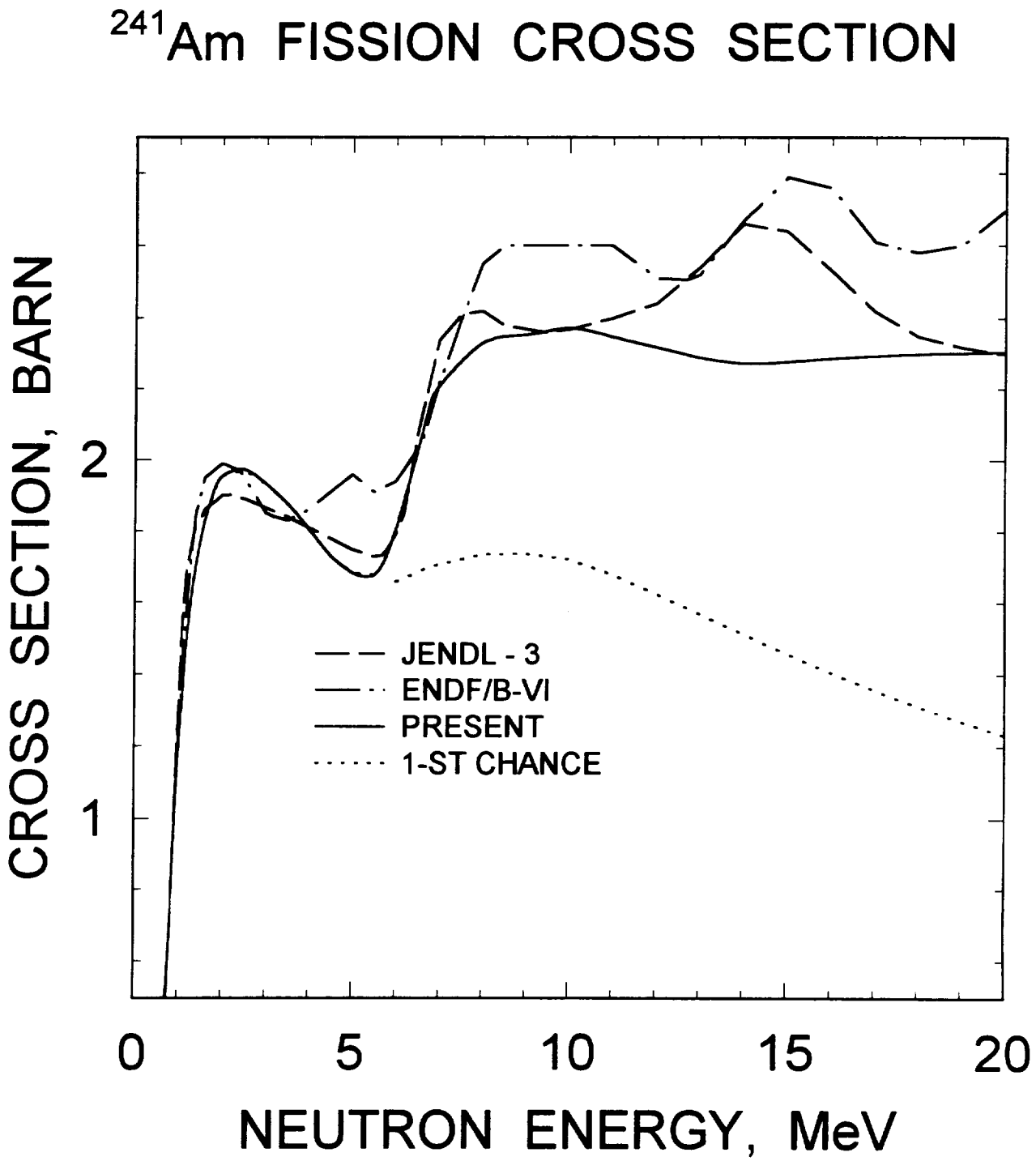
^{241}Am FISSION CROSS SECTION
CROSS SECTION, BARN
1
2
0
5
10
15
20
NEUTRON ENERGY, MeV
JENDL - 3
ENDF/B-VI
PRESENT
1-ST CHANCE

FIG. 4.8

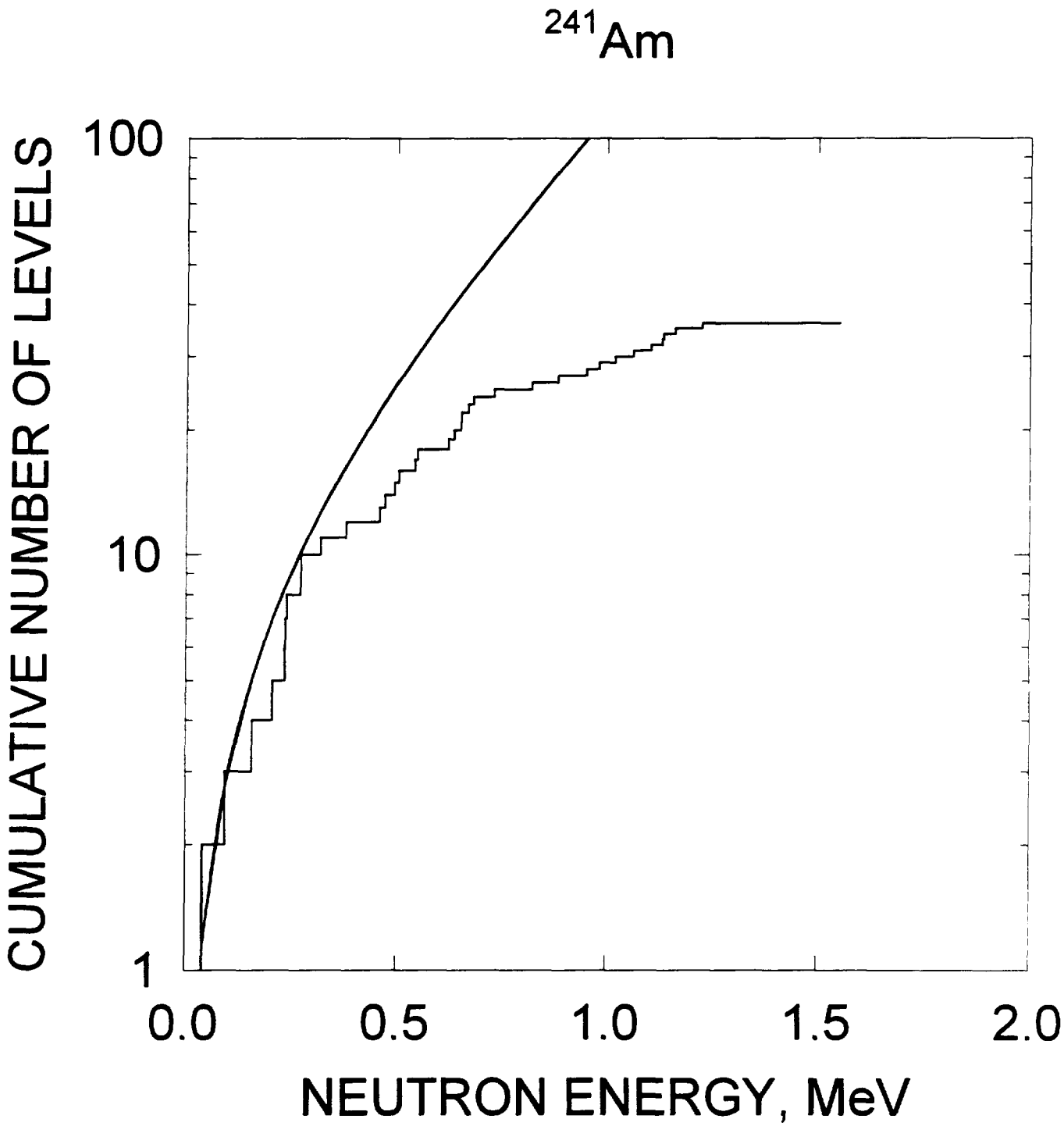
^{241}Am
CUMULATIVE NUMBER OF LEVELS
100
10
1
0.0
0.5
1.0
1.5
2.0
NEUTRON ENERGY, MeV

FIG. 4.9

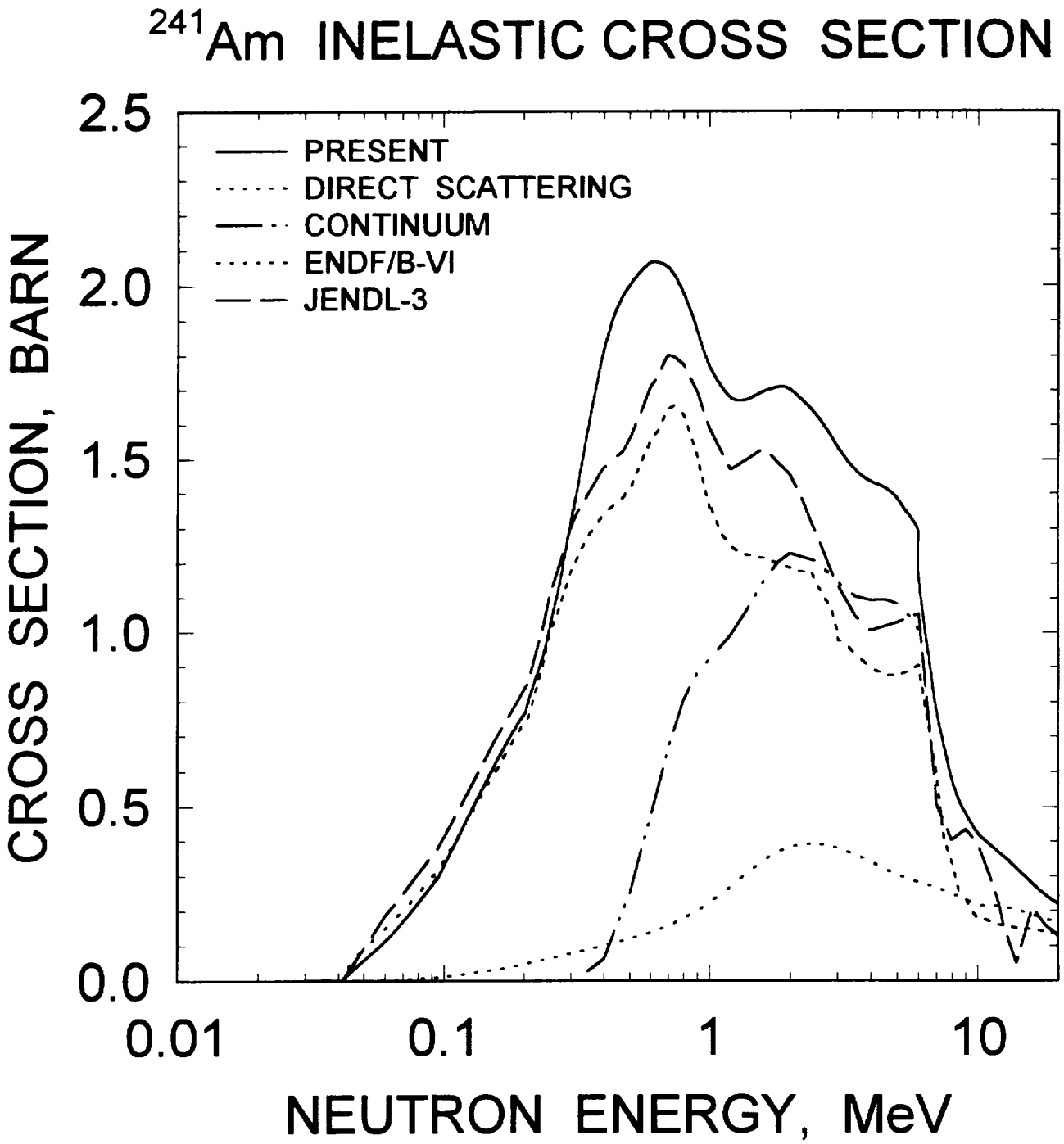
^{241}Am INELASTIC CROSS SECTION
PRESENT
DIRECT SCATTERING
CONTINUUM
ENDF/B-VI
JENDL-3
CROSS SECTION, BARN
2.5
2.0
1.5
1.0
0.5
0.0
0.01
0.1
1
10
NEUTRON ENERGY, MeV

FIG.4.10

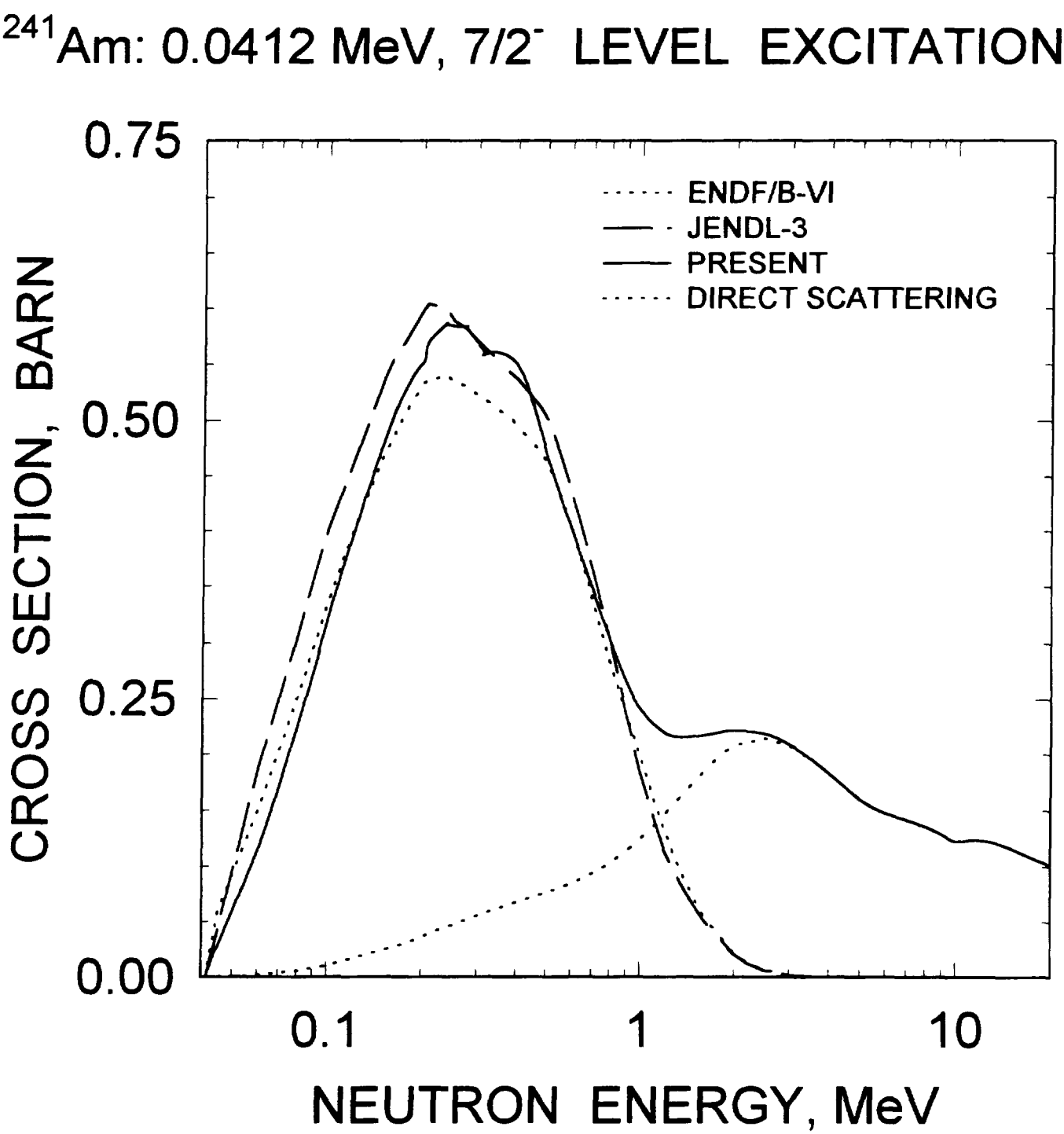
^{241}Am: 0.0412 MeV, 7/2$^-$ LEVEL EXCITATION
0.75
0.50
0.25
0.00
CROSS SECTION, BARN
ENDF/B-VI
JENDL-3
PRESENT
DIRECT SCATTERING
0.1
1
10
NEUTRON ENERGY, MeV

FIG.4.11

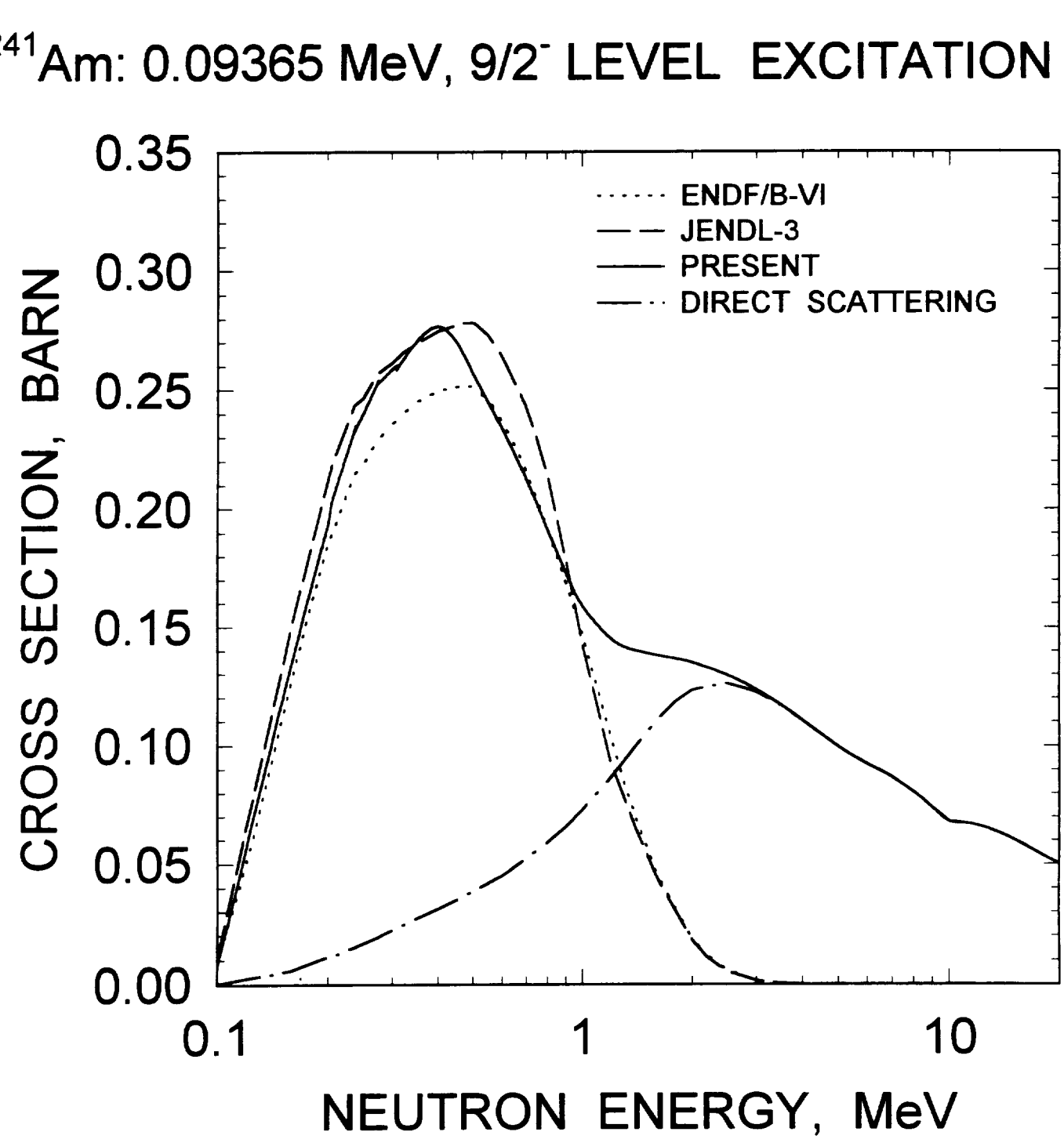
^{241}Am: 0.09365 MeV, 9/2$^-$ LEVEL EXCITATION
ENDF/B-VI
JENDL-3
PRESENT
DIRECT SCATTERING
CROSS SECTION, BARN
0.35
0.30
0.25
0.20
0.15
0.10
0.05
0.00
0.1
1
10
NEUTRON ENERGY, MeV

FIG.4.12

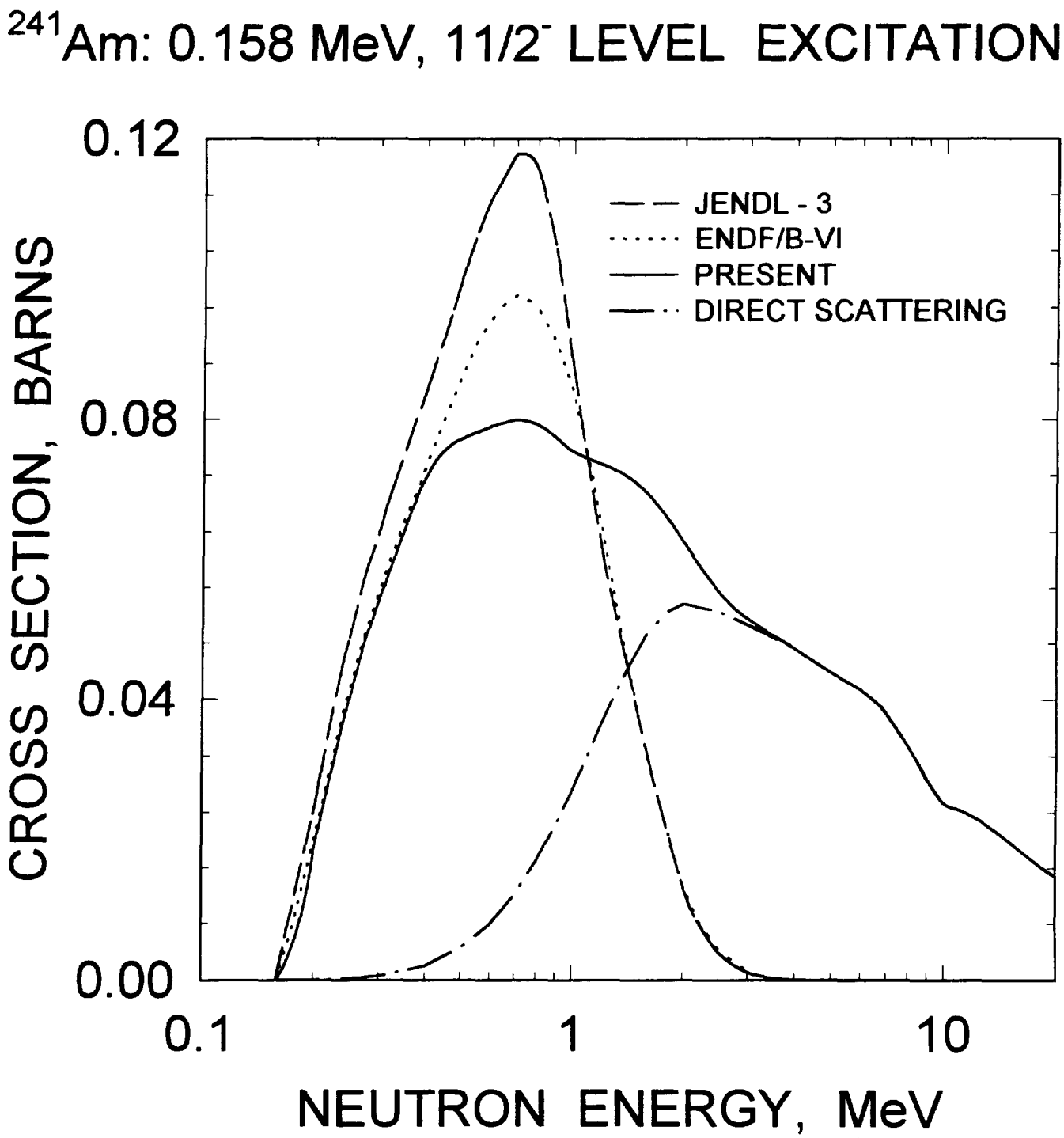
^{241}Am: 0.158 MeV, 11/2$^-$ LEVEL EXCITATION
0.12
0.08
0.04
0.00
CROSS SECTION, BARNS
JENDL - 3
ENDF/B-VI
PRESENT
DIRECT SCATTERING
0.1
1
10
NEUTRON ENERGY, MeV

FIG.4.13

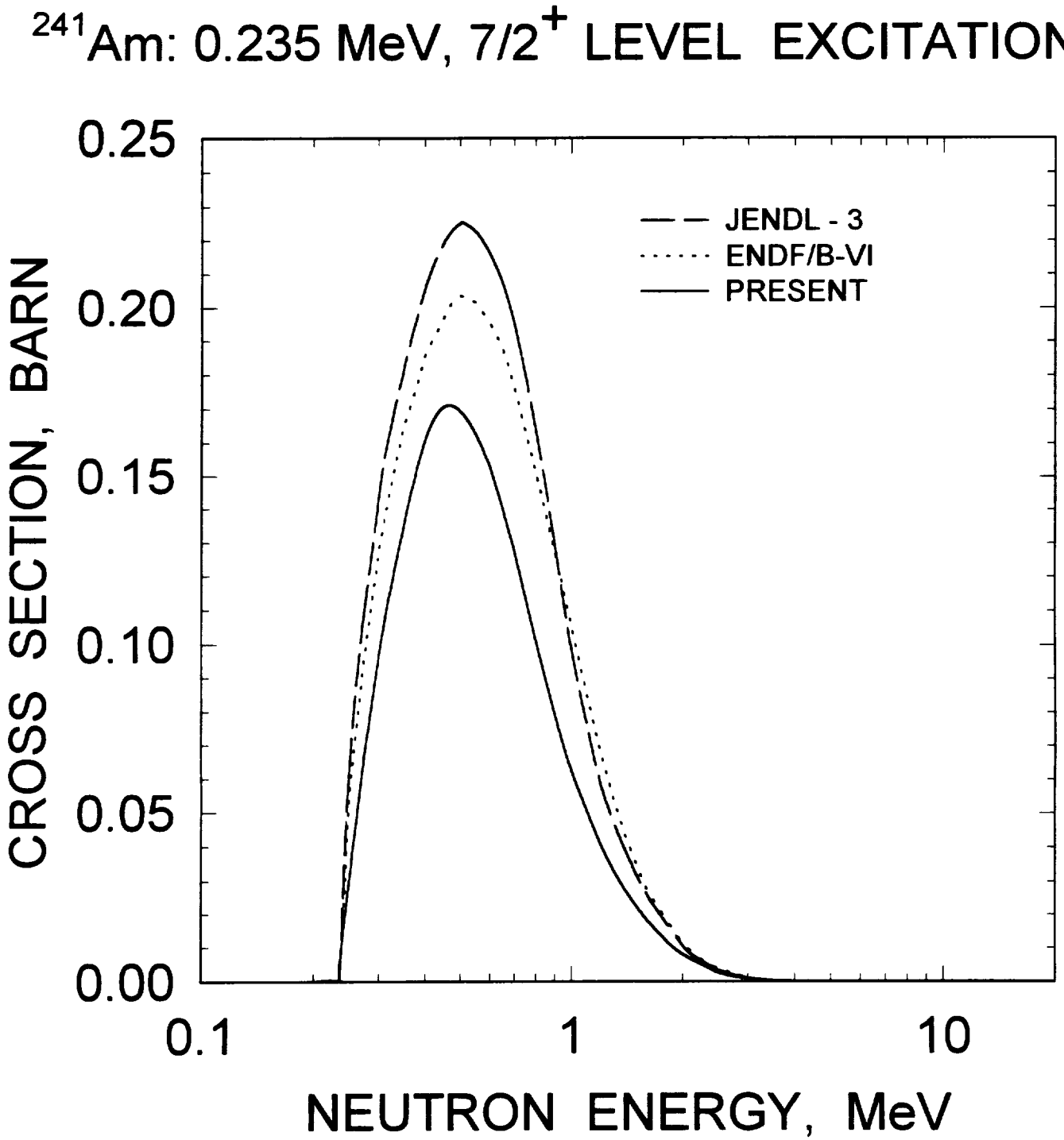
^{241}Am: 0.235 MeV, 7/2^{+} LEVEL EXCITATION
0.25
0.20
0.15
0.10
0.05
0.00
CROSS SECTION, BARN
JENDL - 3
ENDF/B-VI
PRESENT
0.1
1
10
NEUTRON ENERGY, MeV

FIG.4.14

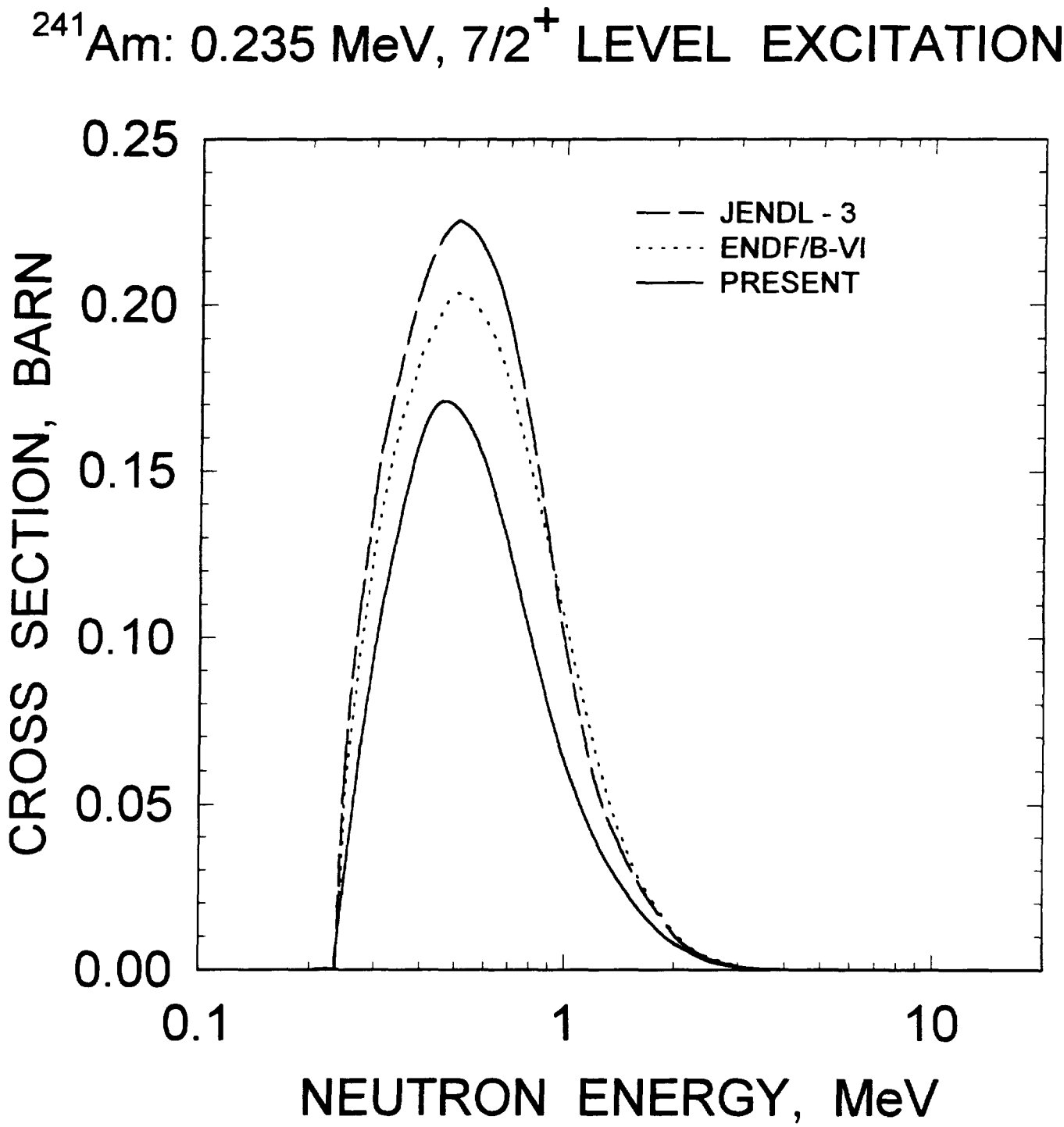
^{241}Am: 0.235 MeV, 7/2^{+} LEVEL EXCITATION
CROSS SECTION, BARN
0.25
0.20
0.15
0.10
0.05
0.00
0.1
1
10
NEUTRON ENERGY, MeV
JENDL - 3
ENDF/B-VI
PRESENT

FIG.4.15

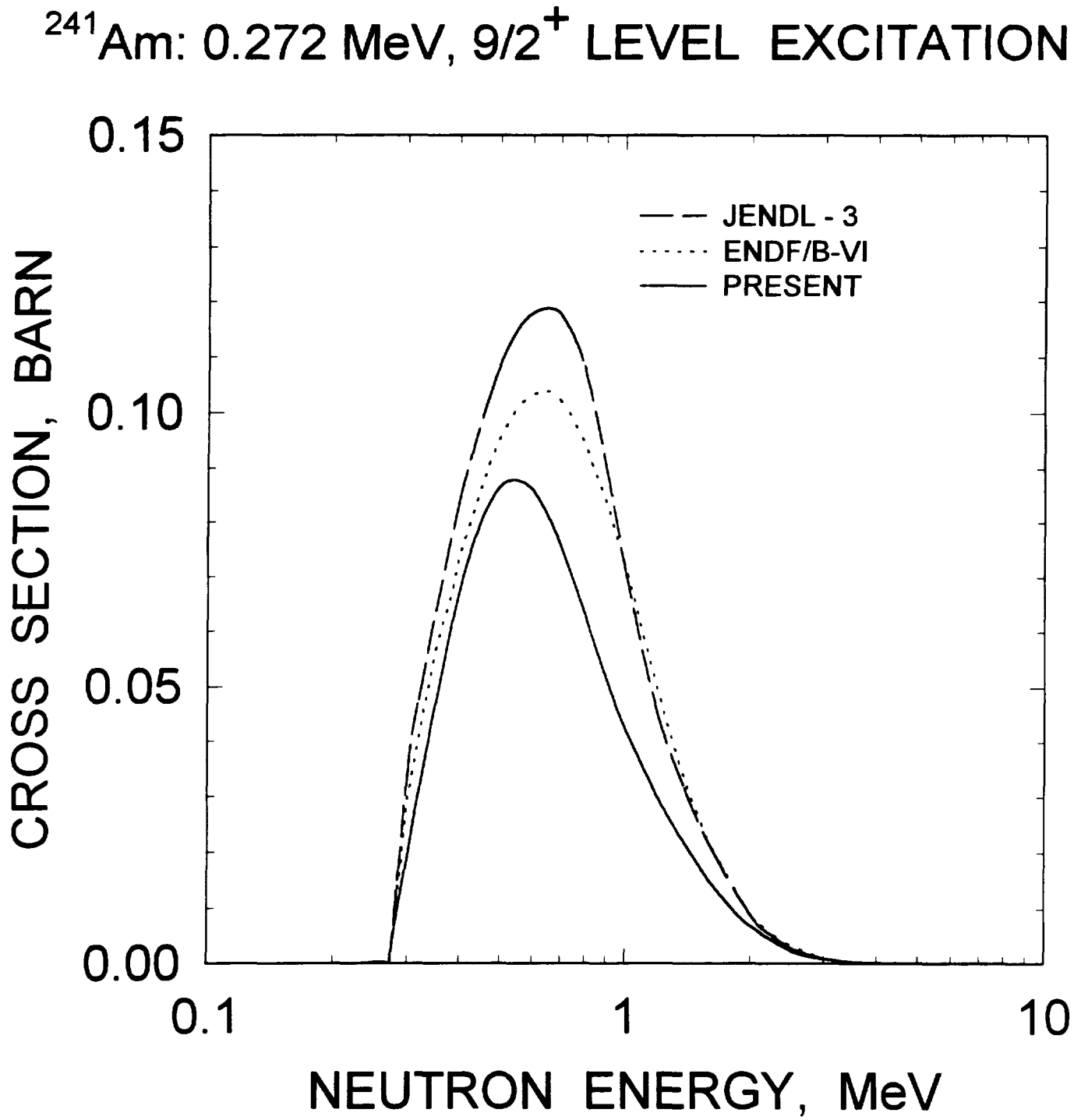
^{241}Am: 0.272 MeV, 9/2^{+} LEVEL EXCITATION
0.15
0.10
0.05
0.00
CROSS SECTION, BARN
JENDL - 3
ENDF/B-VI
PRESENT
0.1
1
10
NEUTRON ENERGY, MeV

FIG.4.16

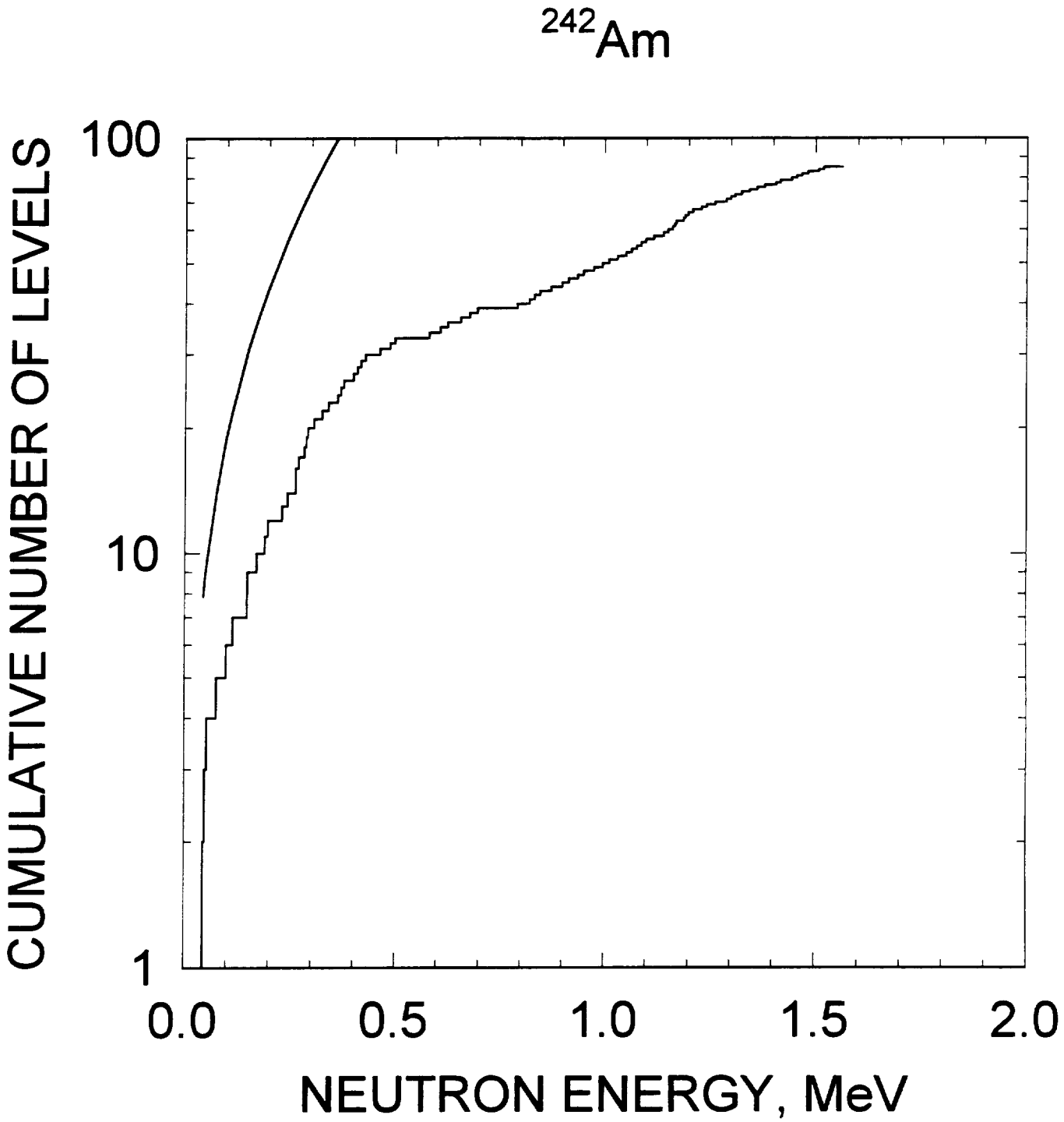
^{242}Am
CUMULATIVE NUMBER OF LEVELS
100
10
1
0.0
0.5
1.0
1.5
2.0
NEUTRON ENERGY, MeV

FIG. 4.17

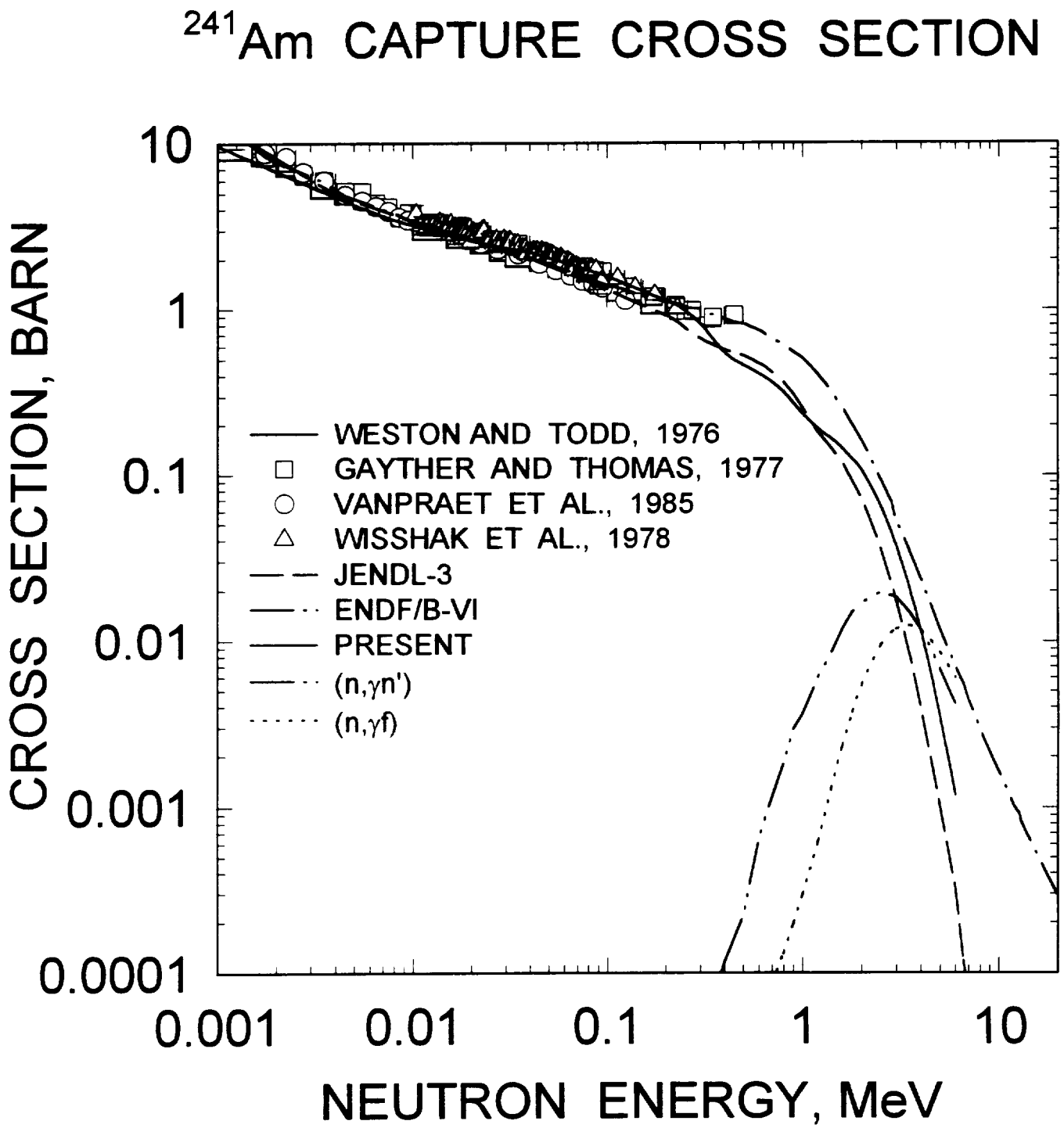
^{241}Am CAPTURE CROSS SECTION
CROSS SECTION, BARN
NEUTRON ENERGY, MeV
10
1
0.1
0.01
0.001
0.0001
0.001
0.01
0.1
1
10
WESTON AND TODD, 1976
GAYTHER AND THOMAS, 1977
VANPRAET ET AL., 1985
WISSHAK ET AL., 1978
JENDL-3
ENDF/B-VI
PRESENT
(n,γn')
(n,γf)

FIG.4.18

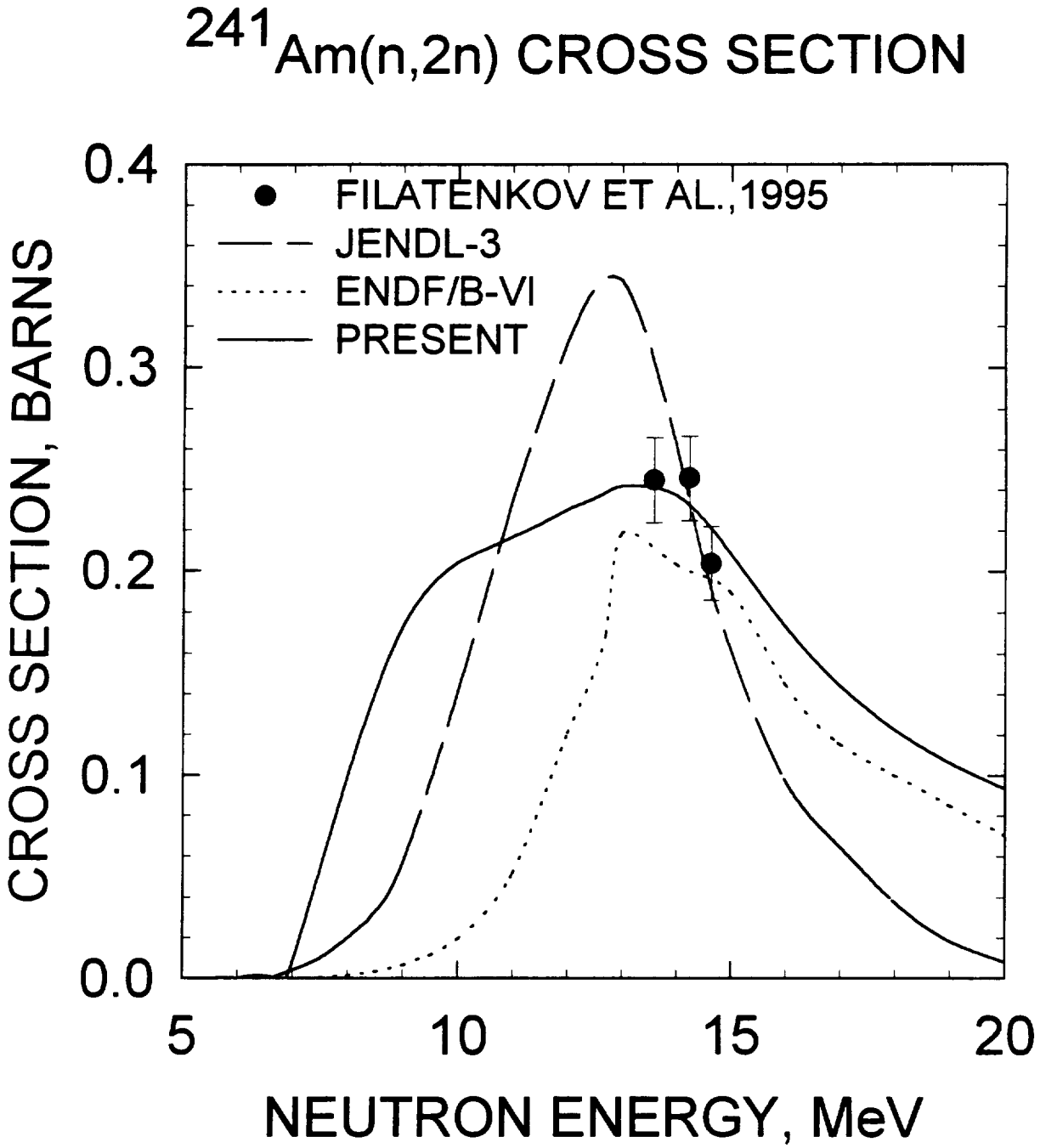
^{241}Am(n,2n) CROSS SECTION
FILATENKOV ET AL.,1995
JENDL-3
ENDF/B-VI
PRESENT
CROSS SECTION, BARNS
0.0
0.1
0.2
0.3
0.4
5
10
15
20
NEUTRON ENERGY, MeV

FIG. 4.19

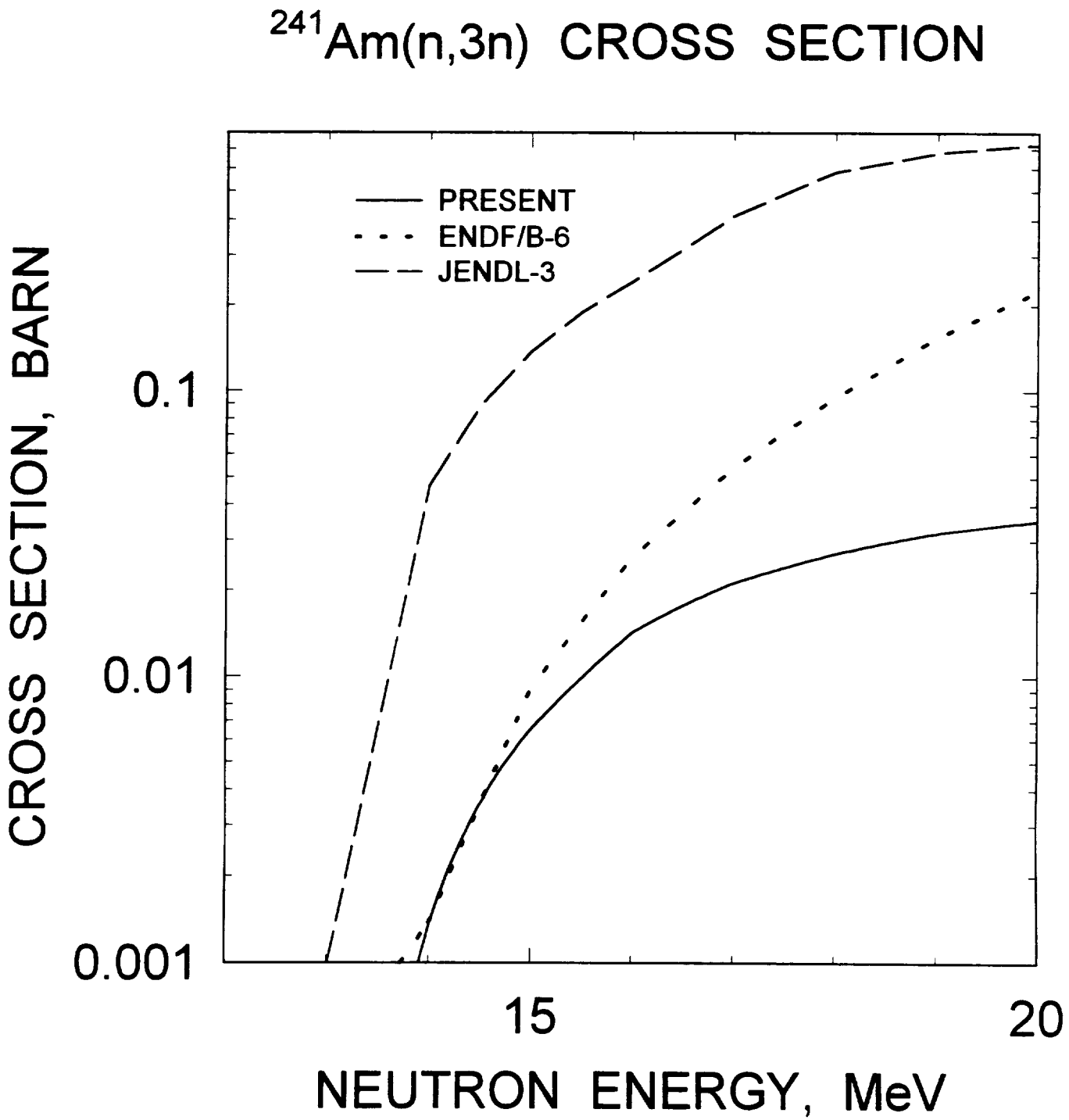
^{241}Am(n,3n) CROSS SECTION
PRESENT
ENDF/B-6
JENDL-3
CROSS SECTION, BARN
0.1
0.01
0.001
15
20
NEUTRON ENERGY, MeV

FIG.4.20

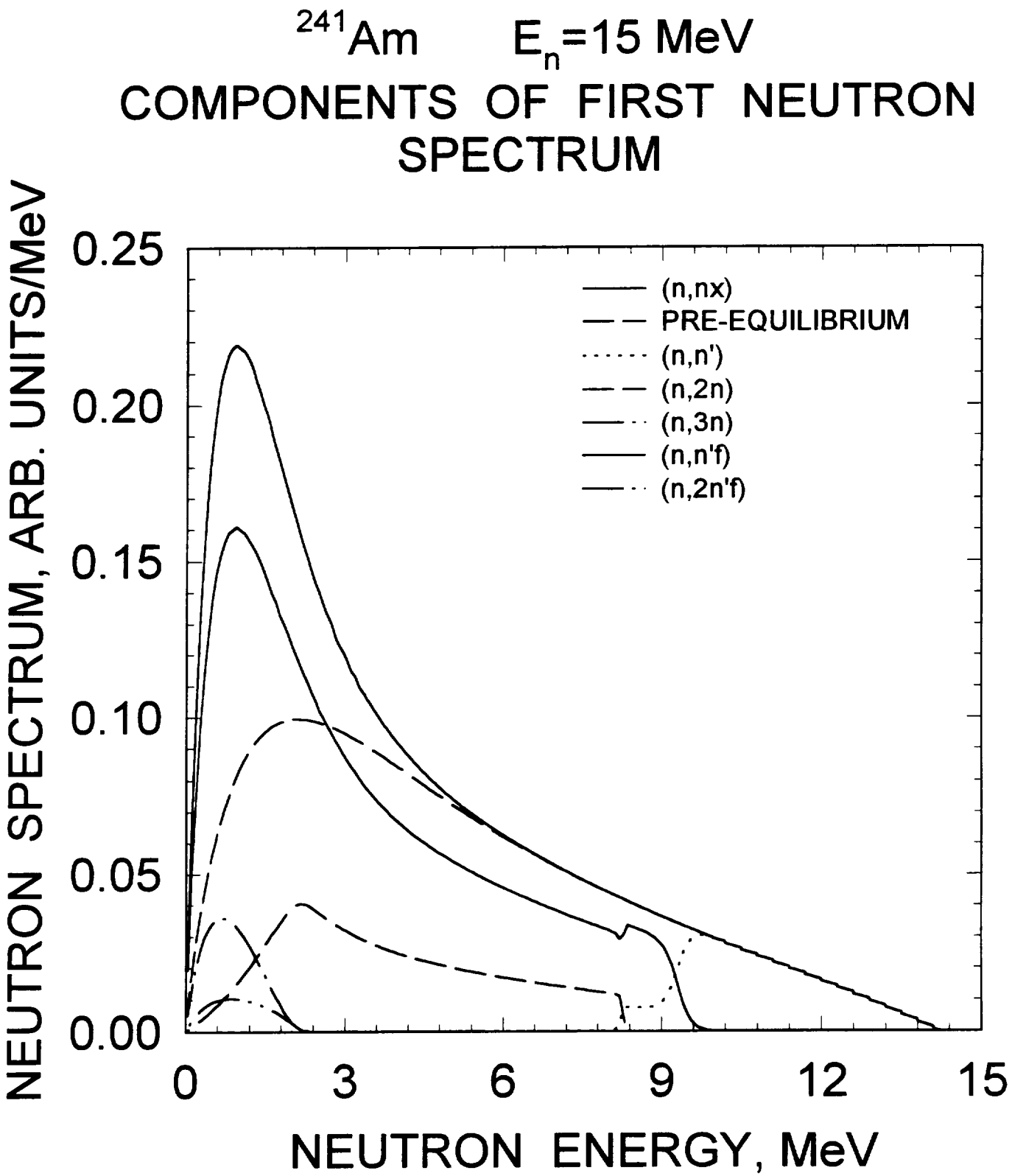
^{241}Am E_n=15 MeV
COMPONENTS OF FIRST NEUTRON SPECTRUM
NEUTRON SPECTRUM, ARB. UNITS/MeV
0.25
0.20
0.15
0.10
0.05
0.00
0
3
6
9
12
15
NEUTRON ENERGY, MeV
(n,nx)
PRE-EQUILIBRIUM
(n,n')
(n,2n)
(n,3n)
(n,n'f)
(n,2n'f)

FIG.5.1

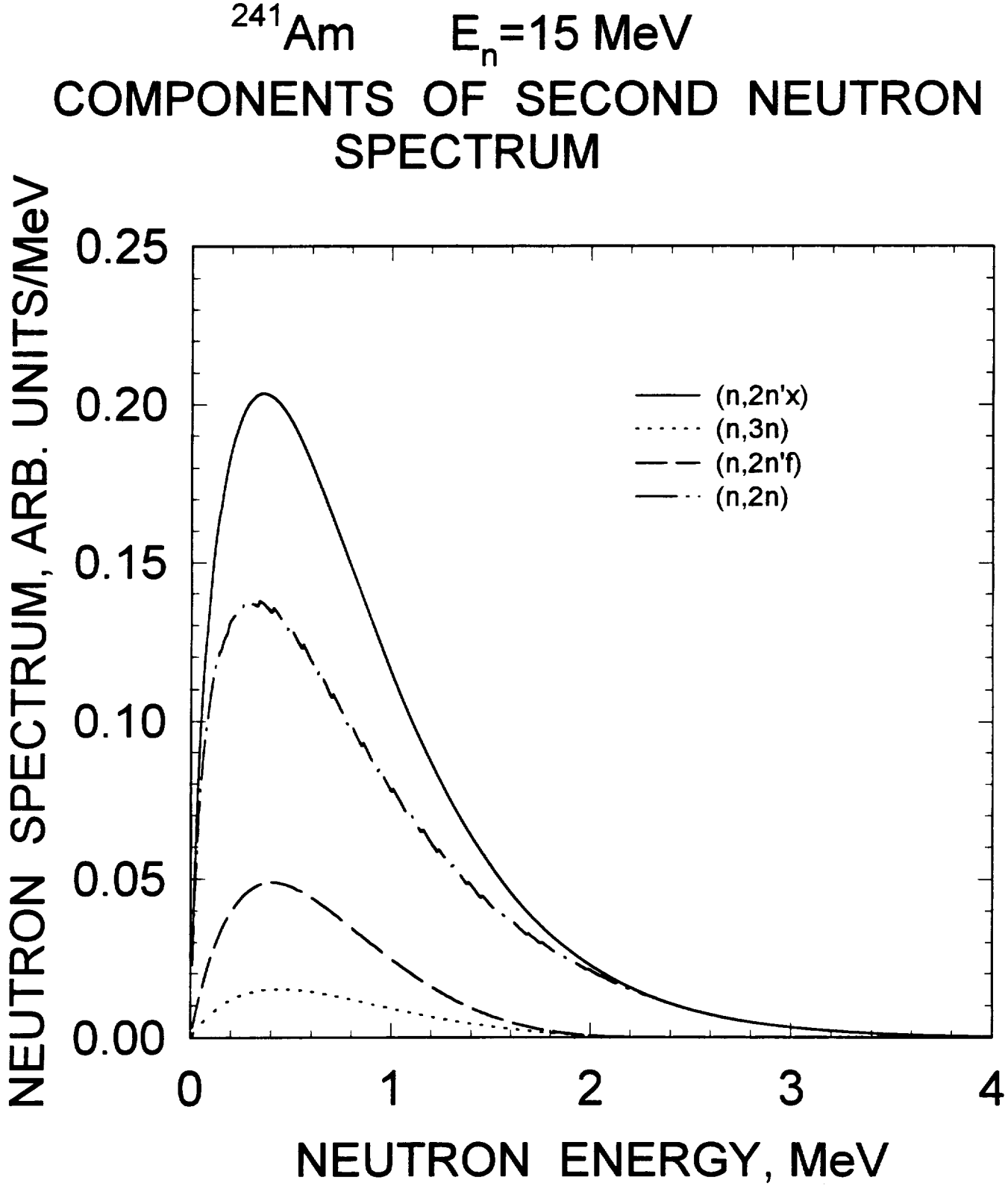
^{241}Am E_n=15 MeV
COMPONENTS OF SECOND NEUTRON SPECTRUM
NEUTRON SPECTRUM, ARB. UNITS/MeV
0.25
0.20
0.15
0.10
0.05
0.00
0
1
2
3
4
NEUTRON ENERGY, MeV
(n,2n'x)
(n,3n)
(n,2n'f)
(n,2n)

FIG.5.2

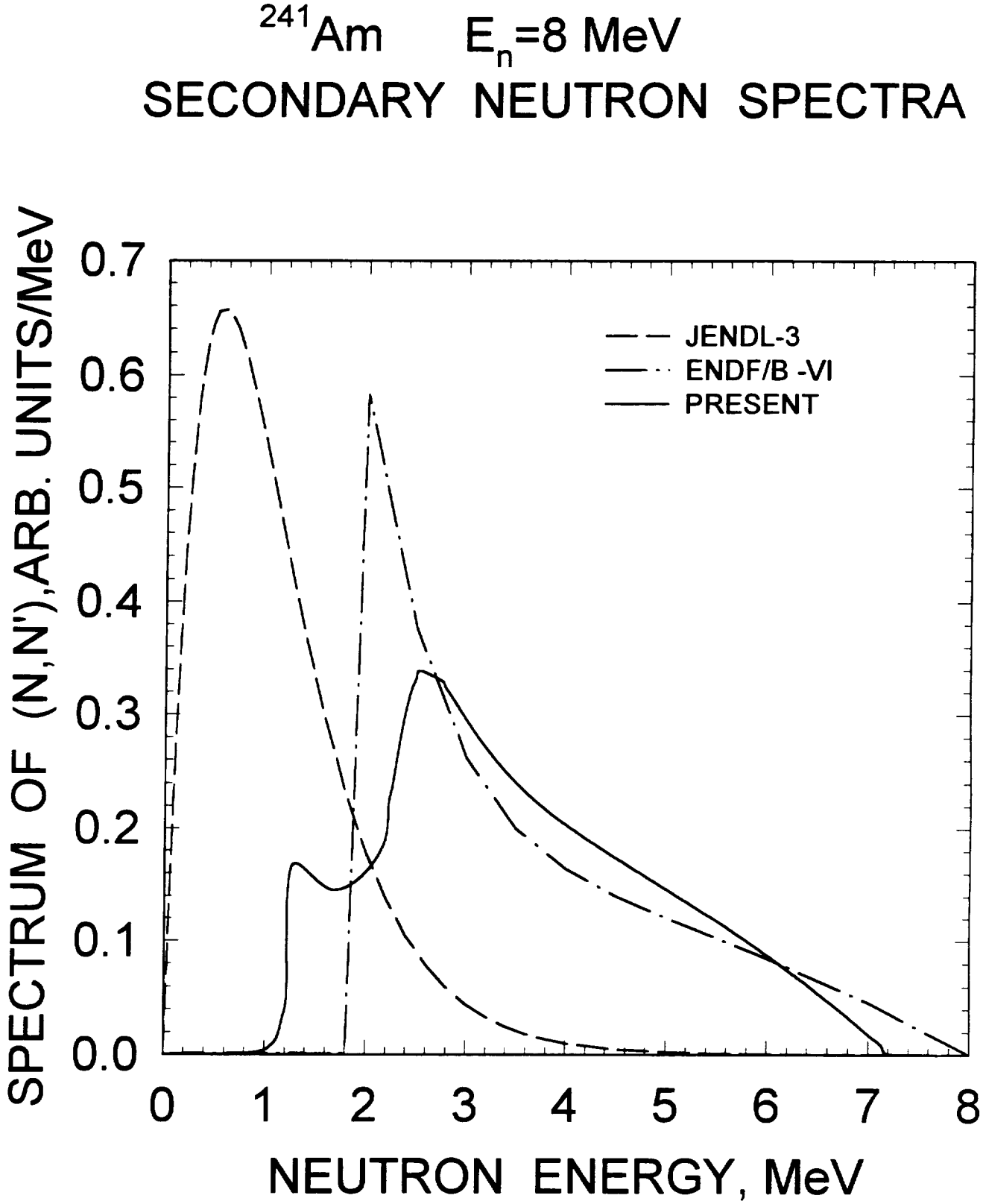
^{241}Am E_n=8 MeV
SECONDARY NEUTRON SPECTRA
SPECTRUM OF (N,N'),ARB. UNITS/MeV
0.0
0.1
0.2
0.3
0.4
0.5
0.6
0.7
0
1
2
3
4
5
6
7
8
NEUTRON ENERGY, MeV
JENDL-3
ENDF/B -VI
PRESENT

FIG.5.3

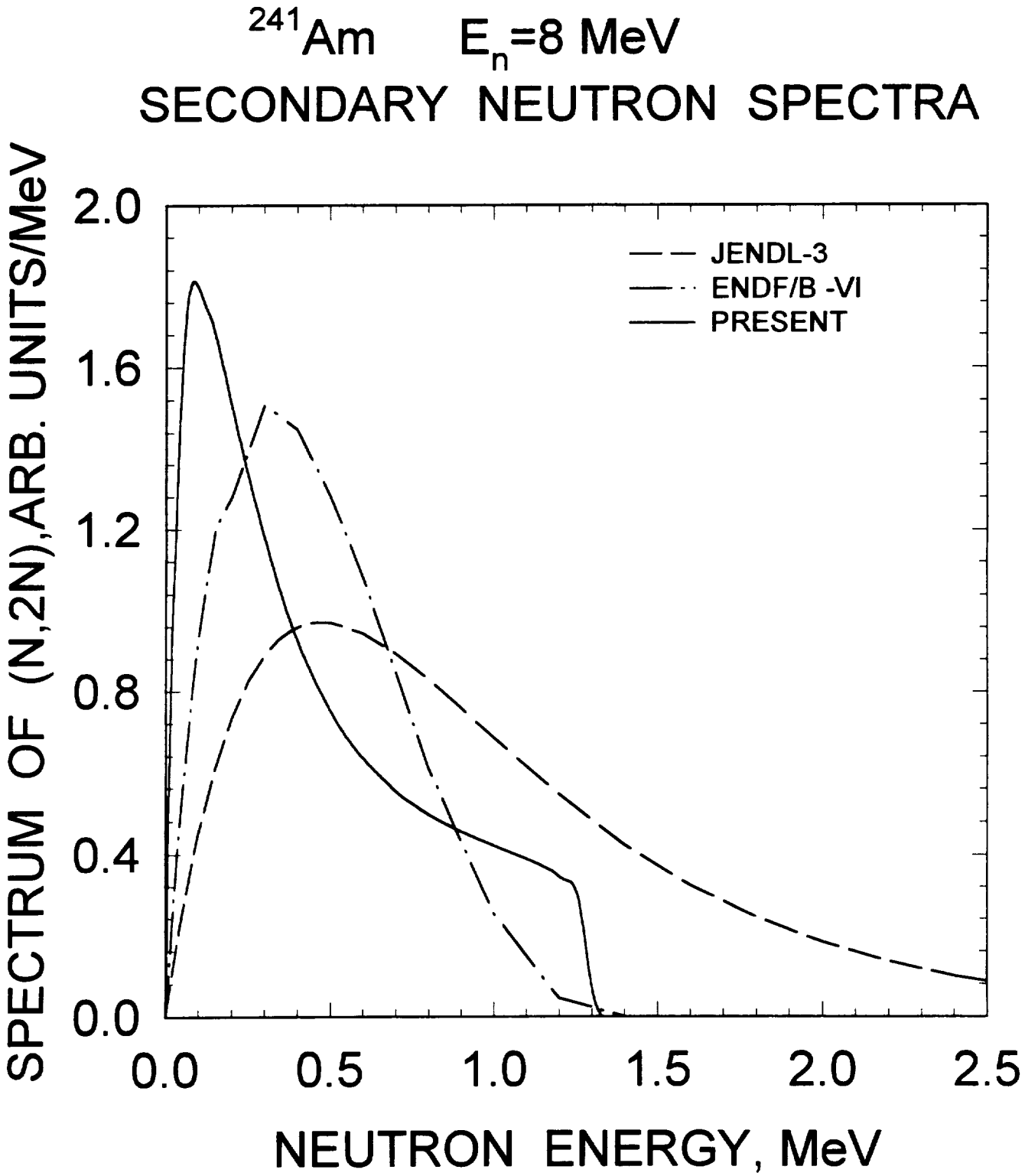
^{241}Am E_n=8 MeV
SECONDARY NEUTRON SPECTRA
SPECTRUM OF (N,2N),ARB. UNITS/MeV
2.0
1.6
1.2
0.8
0.4
0.0
0.0
0.5
1.0
1.5
2.0
2.5
NEUTRON ENERGY, MeV
JENDL-3
ENDF/B -VI
PRESENT

FIG.5.4

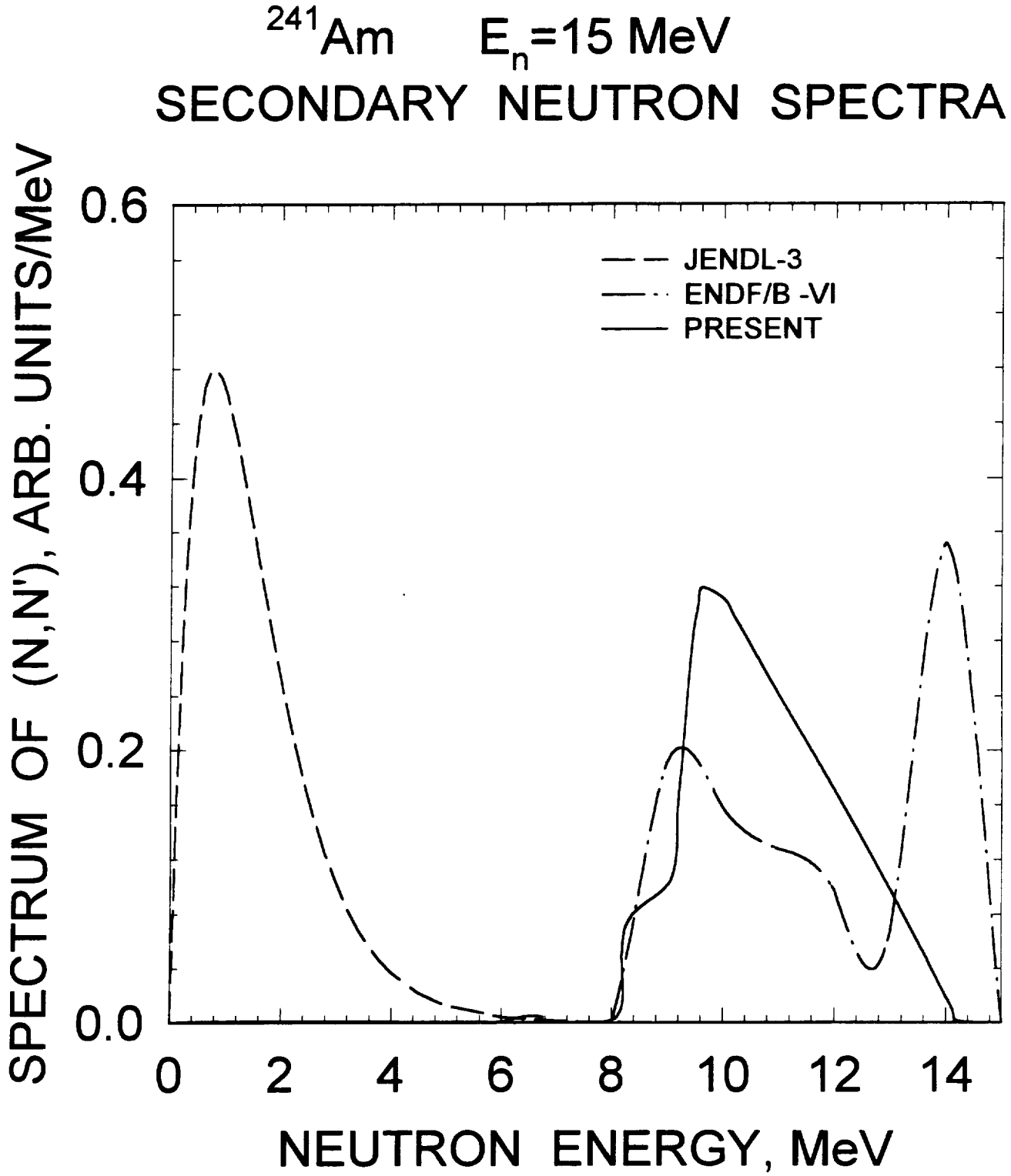
^{241}Am E_n=15 MeV
SECONDARY NEUTRON SPECTRA
SPECTRUM OF (N,N'), ARB. UNITS/MeV
0.6
0.4
0.2
0.0
0
2
4
6
8
10
12
14
NEUTRON ENERGY, MeV
JENDL-3
ENDF/B -VI
PRESENT

FIG.5.5

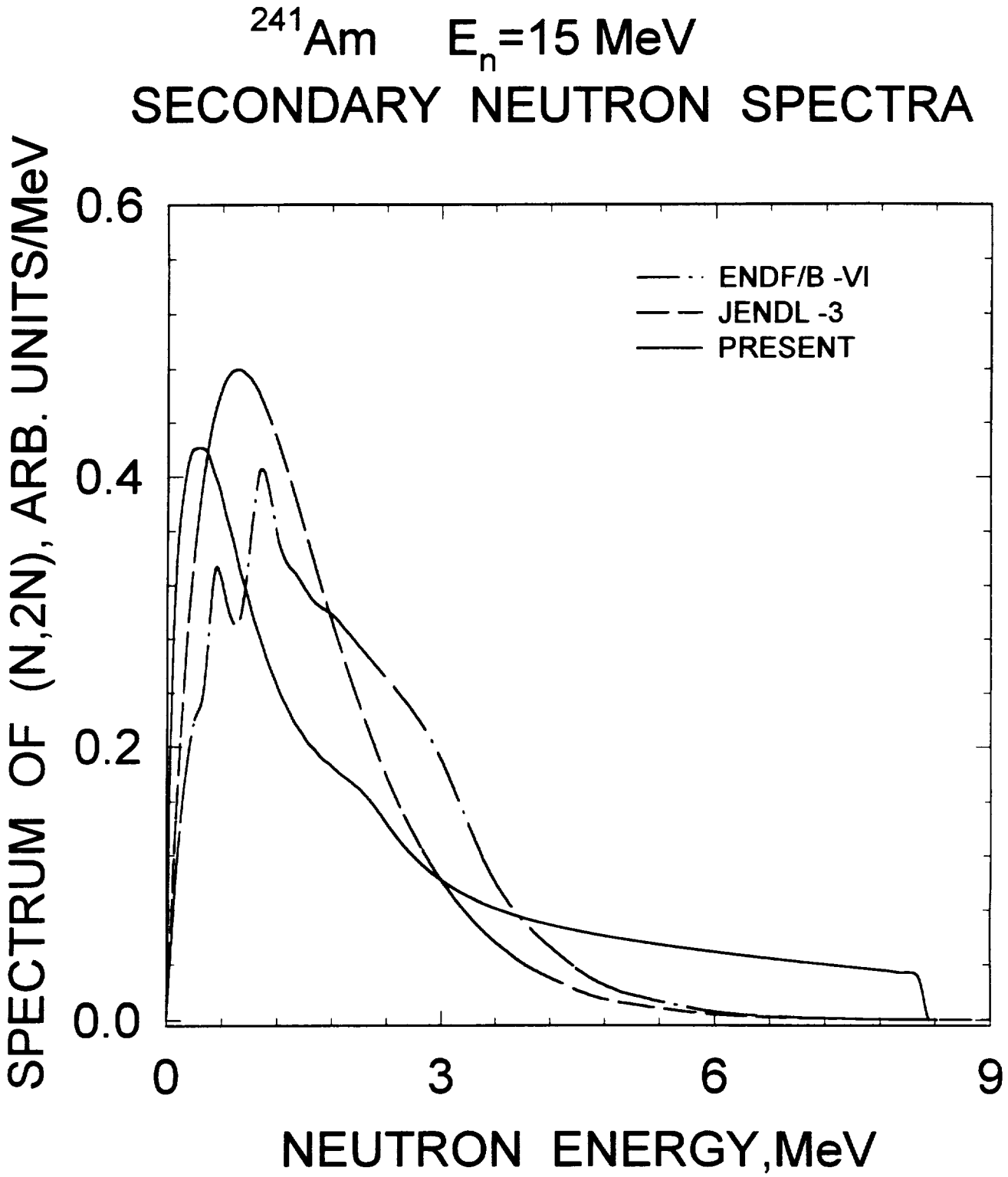
^{241}Am E_n=15 MeV
SECONDARY NEUTRON SPECTRA
SPECTRUM OF (N,2N), ARB. UNITS/MeV
0.6
0.4
0.2
0.0
0
3
6
9
NEUTRON ENERGY,MeV
ENDF/B -VI
JENDL -3
PRESENT

FIG.5.6

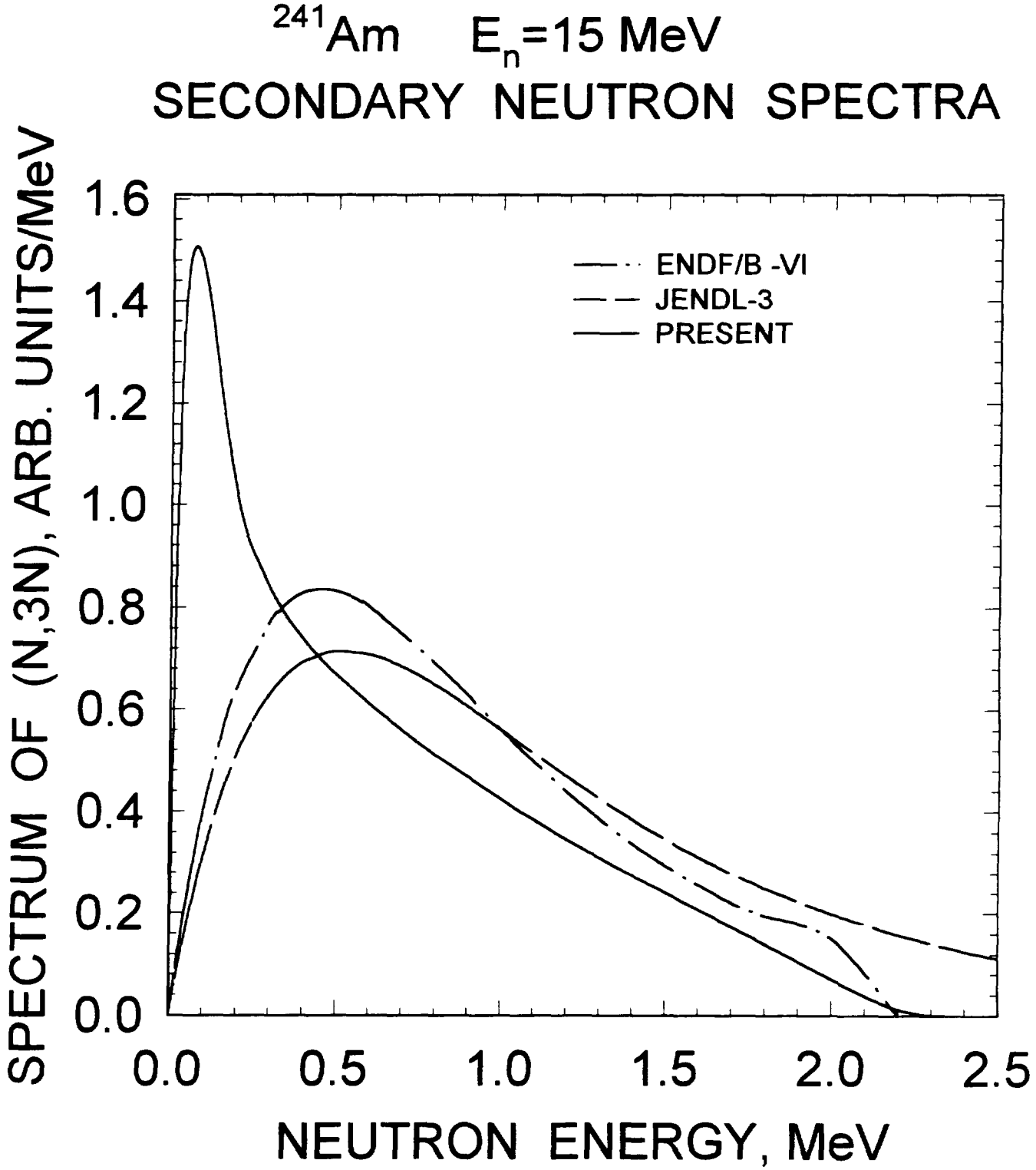
^{241}Am E_n=15 MeV
SECONDARY NEUTRON SPECTRA
SPECTRUM OF (N,3N), ARB. UNITS/MeV
1.6
1.4
1.2
1.0
0.8
0.6
0.4
0.2
0.0
ENDF/B -VI
JENDL-3
PRESENT
0.0
0.5
1.0
1.5
2.0
2.5
NEUTRON ENERGY, MeV

FIG.5.7

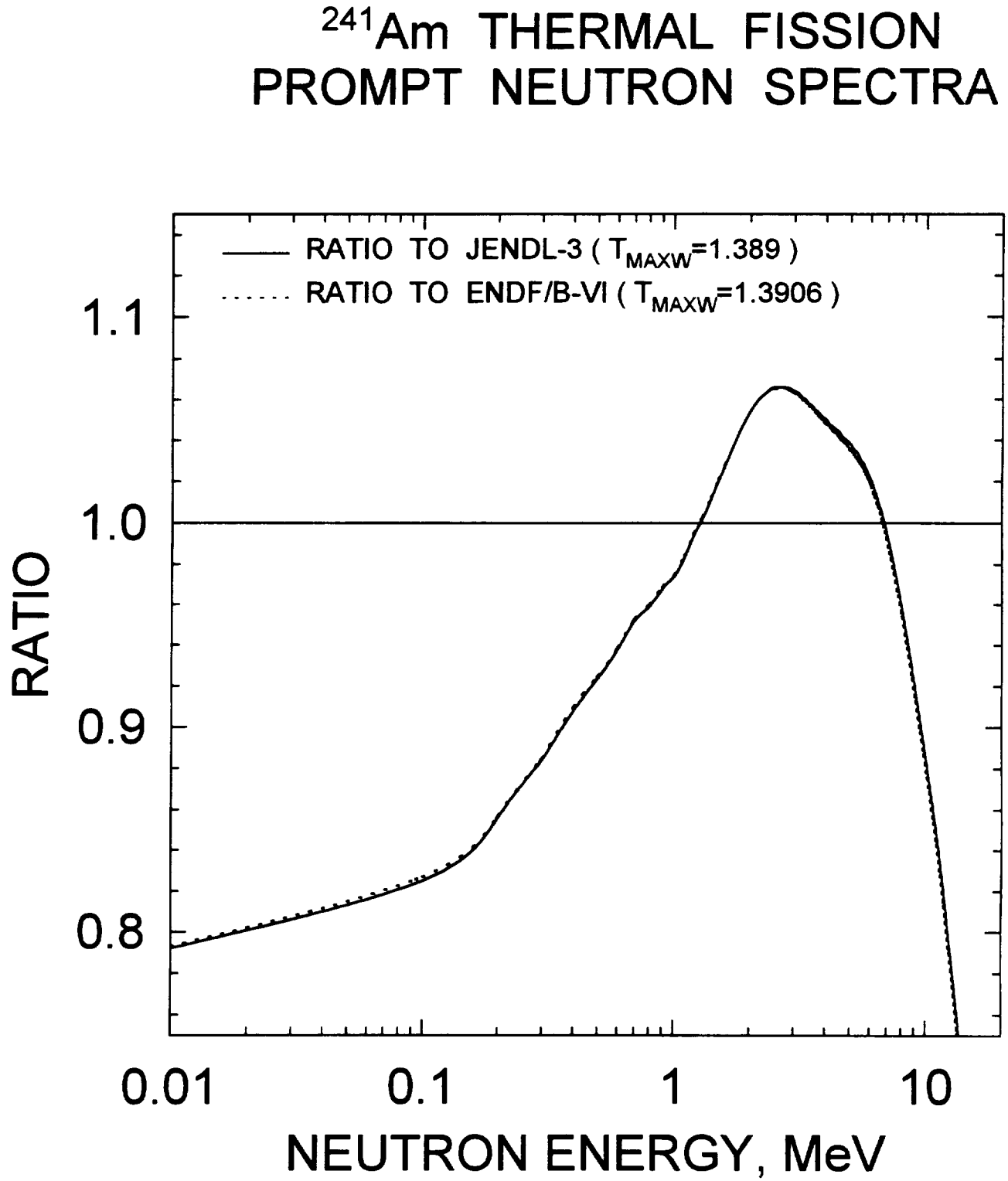
^{241}Am THERMAL FISSION
PROMPT NEUTRON SPECTRA
RATIO TO JENDL-3 (T_{MAXW}=1.389)
RATIO TO ENDF/B-VI (T_{MAXW}=1.3906)
1.1
1.0
0.9
0.8
RATIO
0.01
0.1
1
10
NEUTRON ENERGY, MeV

FIG.5.8

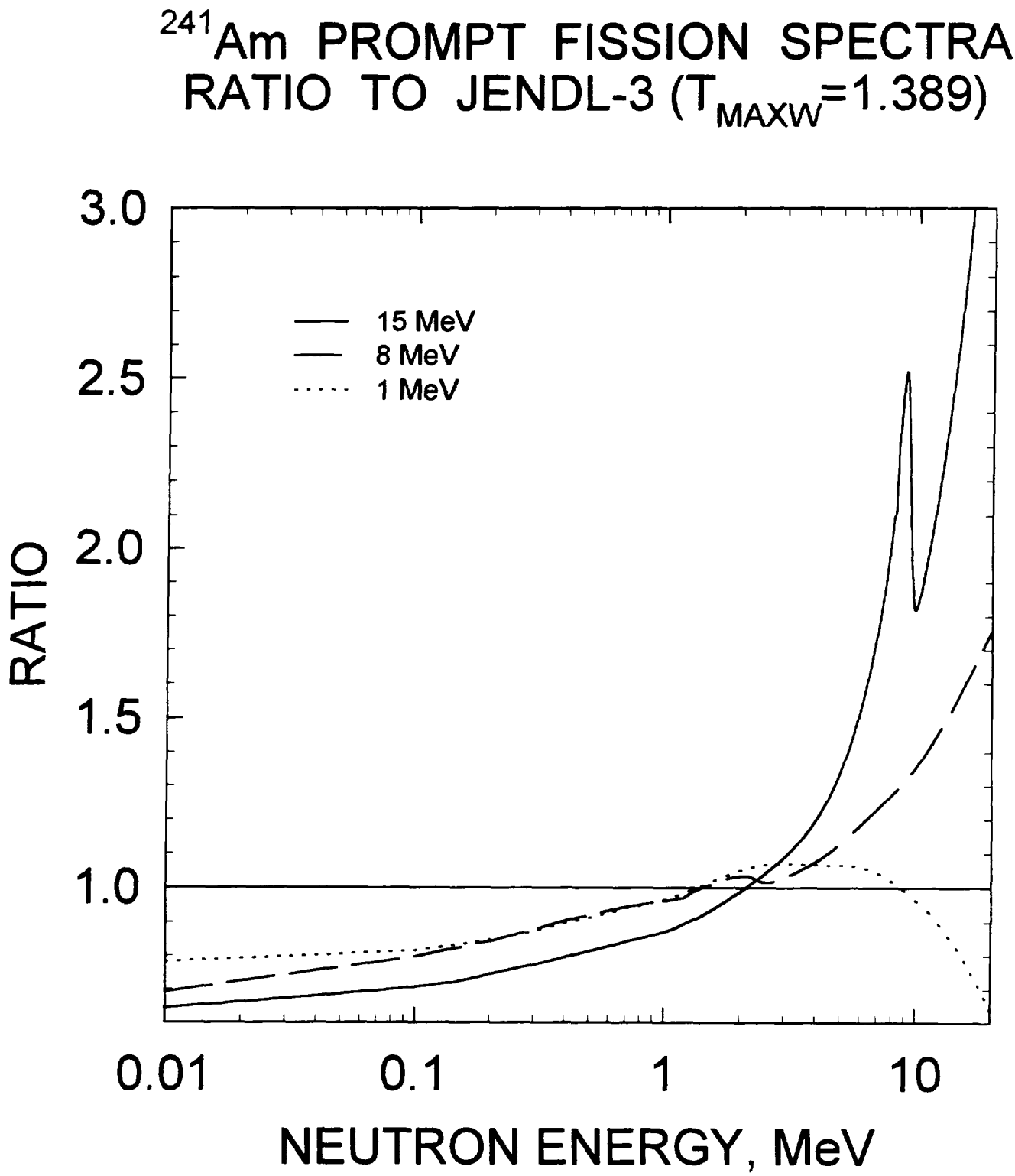
^{241}Am PROMPT FISSION SPECTRA
RATIO TO JENDL-3 (T_{MAXW}=1.389)
3.0
2.5
2.0
1.5
1.0
RATIO
15 MeV
8 MeV
1 MeV
0.01
0.1
1
10
NEUTRON ENERGY, MeV

FIG. 5.9

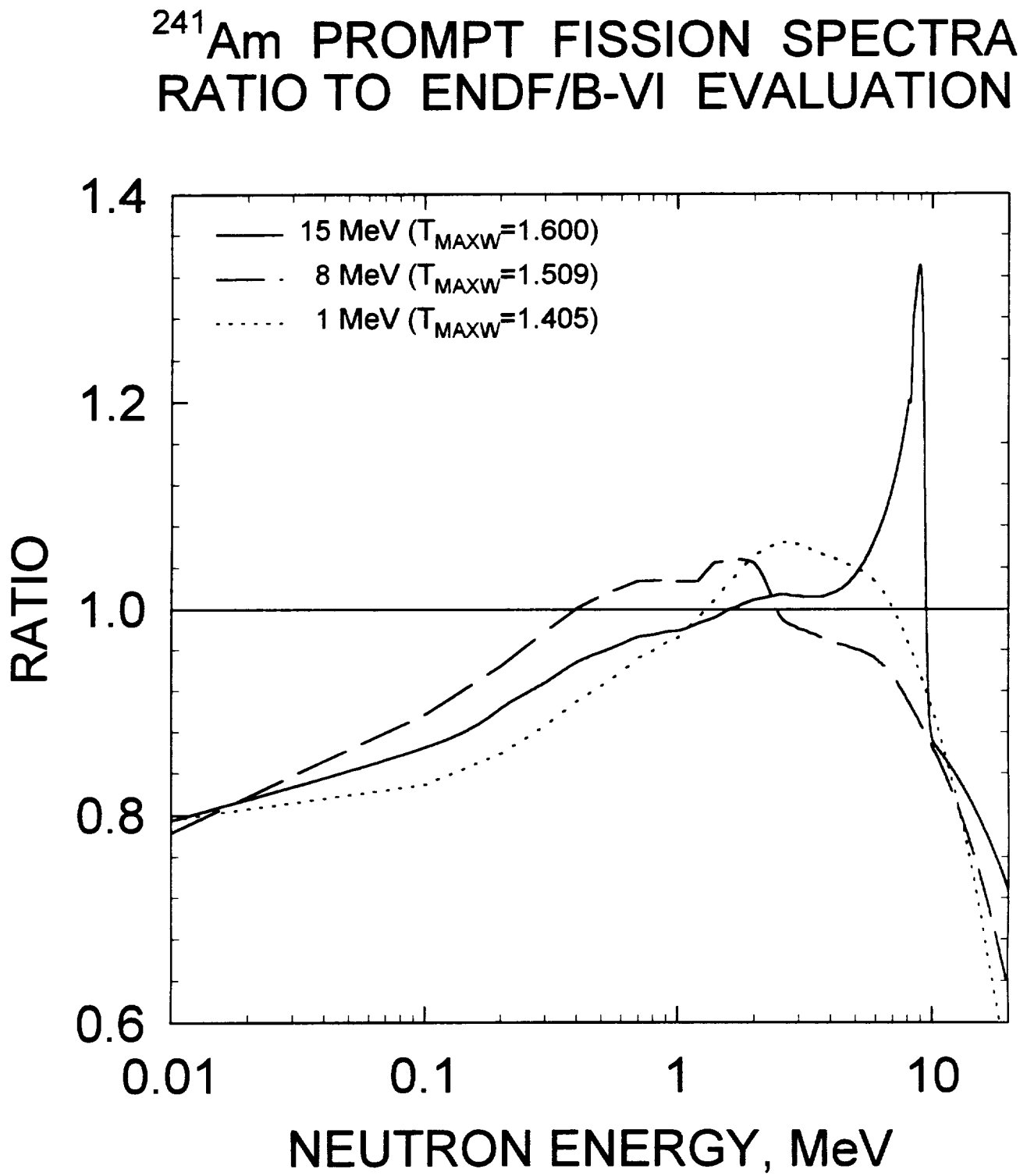
^{241}Am PROMPT FISSION SPECTRA
RATIO TO ENDF/B-VI EVALUATION
15 MeV (T_{MAXW}=1.600)
8 MeV (T_{MAXW}=1.509)
1 MeV (T_{MAXW}=1.405)
RATIO
1.4
1.2
1.0
0.8
0.6
0.01
0.1
1
10
NEUTRON ENERGY, MeV

FIG. 5.10

^{241}Am FISSION NEUTRON SPECTRA RATIO TO MADLAND-NIX MODEL CALCULATION

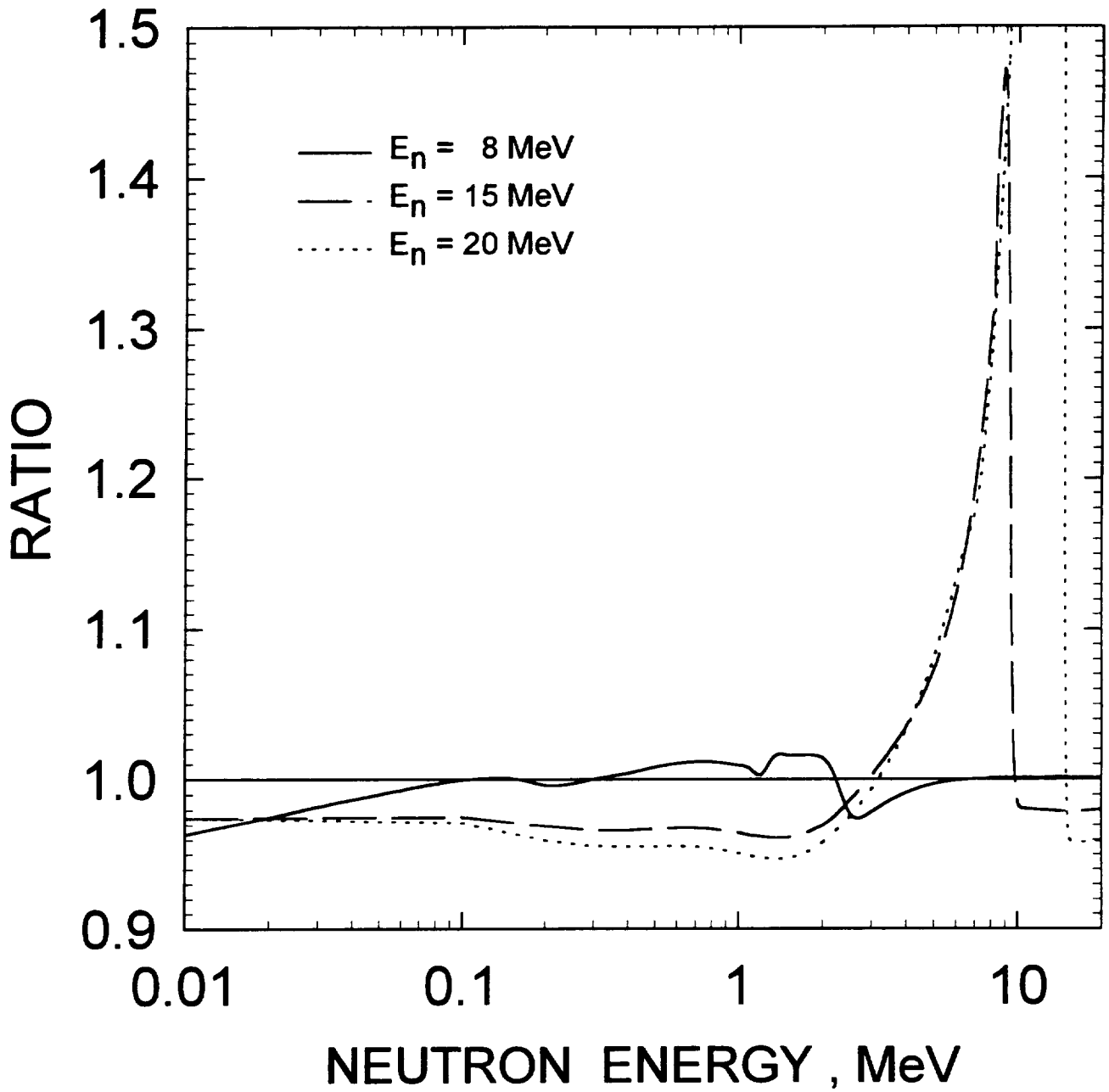

FIG.5.11

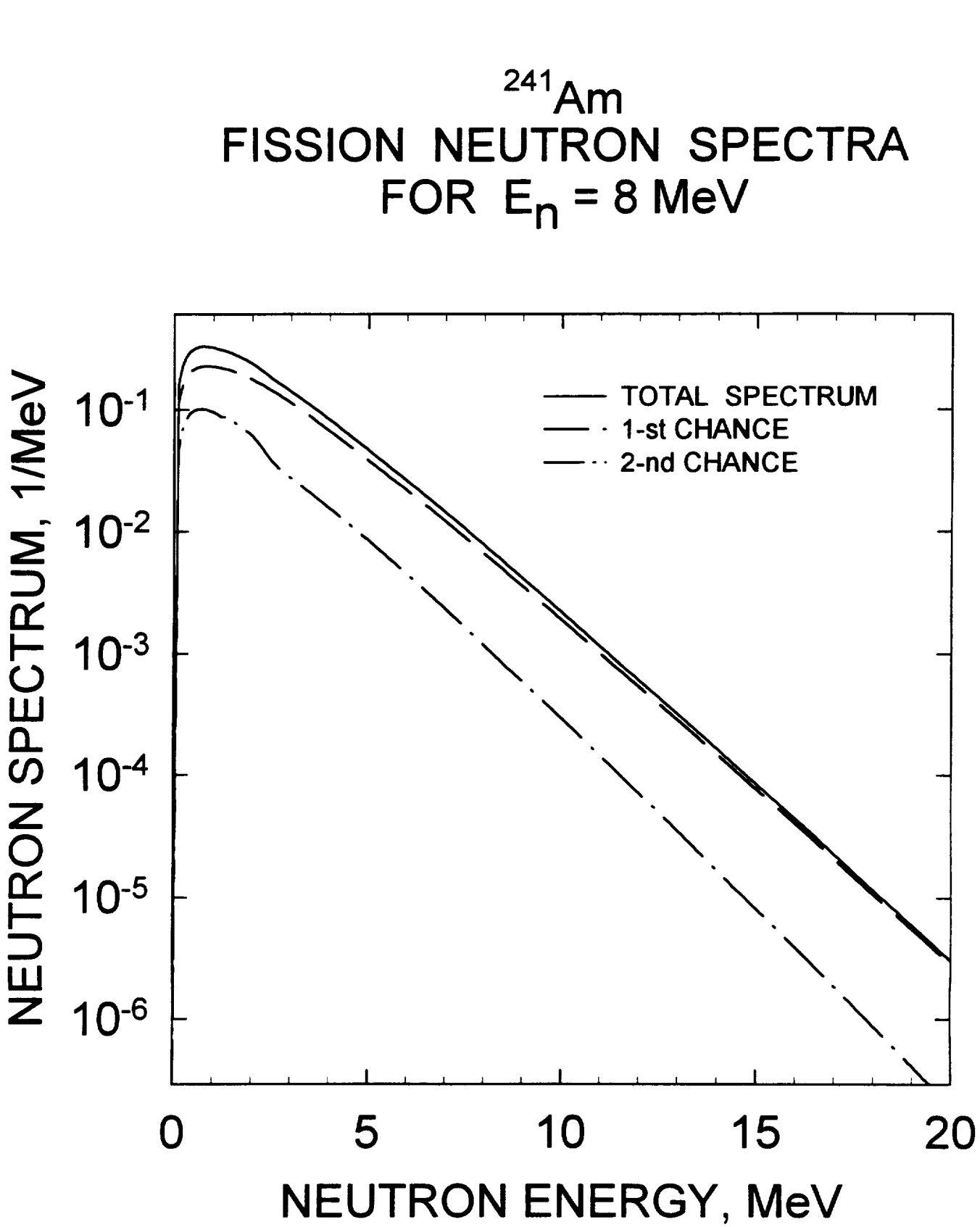
^{241}Am
FISSION NEUTRON SPECTRA
FOR E_n = 8 MeV
NEUTRON SPECTRUM, 1/MeV
10^{-1}
10^{-2}
10^{-3}
10^{-4}
10^{-5}
10^{-6}
TOTAL SPECTRUM
1-st CHANCE
2-nd CHANCE
0
5
10
15
20
NEUTRON ENERGY, MeV

FIG.5.12

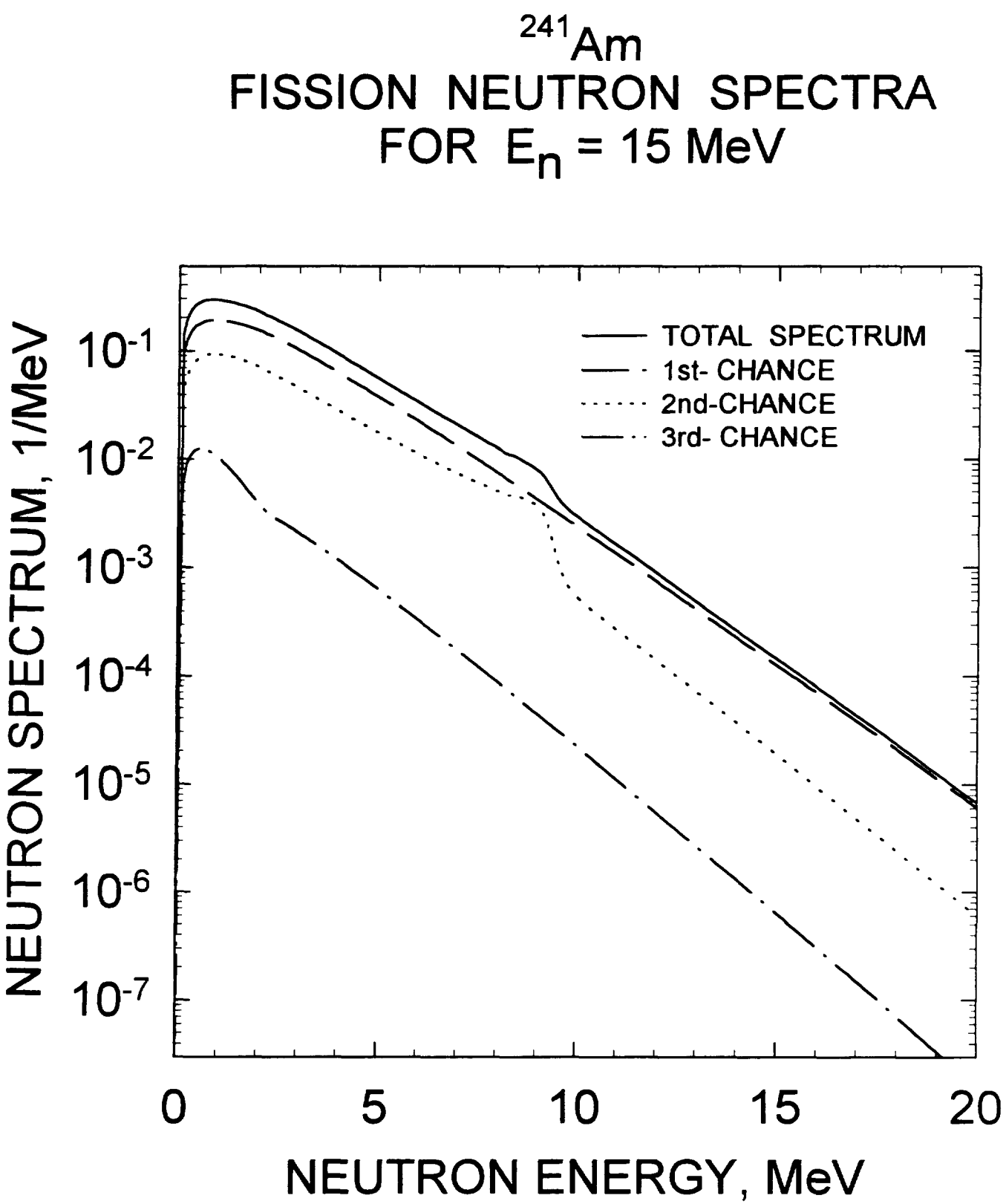
^{241}Am
FISSION NEUTRON SPECTRA
FOR E_n = 15 MeV
NEUTRON SPECTRUM, 1/MeV
10^{-1}
10^{-2}
10^{-3}
10^{-4}
10^{-5}
10^{-6}
10^{-7}
TOTAL SPECTRUM
1st- CHANCE
2nd-CHANCE
3rd- CHANCE
0
5
10
15
20
NEUTRON ENERGY, MeV

FIG.5.13

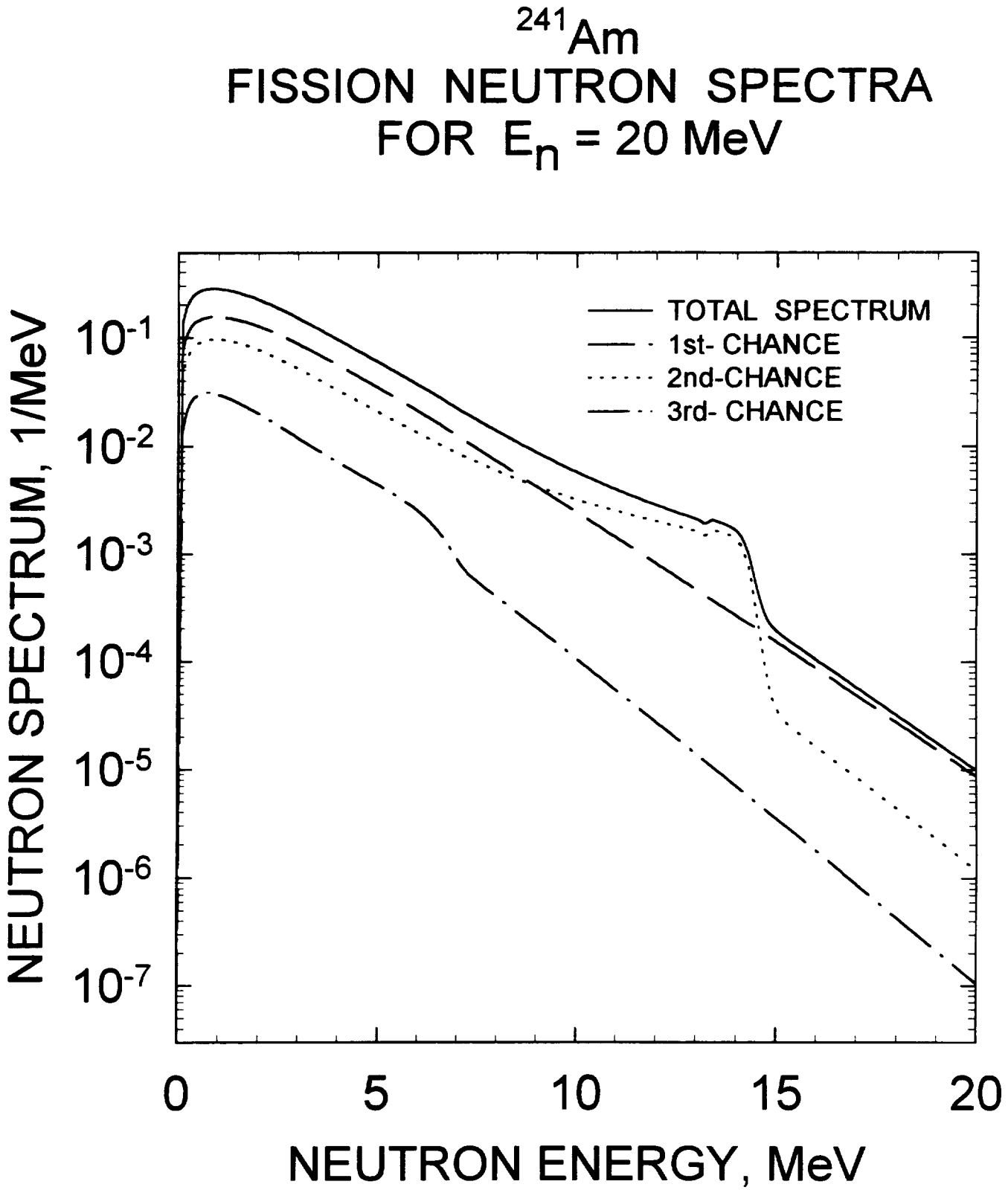
^{241}Am
FISSION NEUTRON SPECTRA
FOR E_n = 20 MeV
TOTAL SPECTRUM
1st- CHANCE
2nd-CHANCE
3rd- CHANCE
NEUTRON SPECTRUM, 1/MeV
10^{-1}
10^{-2}
10^{-3}
10^{-4}
10^{-5}
10^{-6}
10^{-7}
0
5
10
15
20
NEUTRON ENERGY, MeV

FIG.5.14

^{241}Am PROMPT NEUTRON MULTIPLICITY

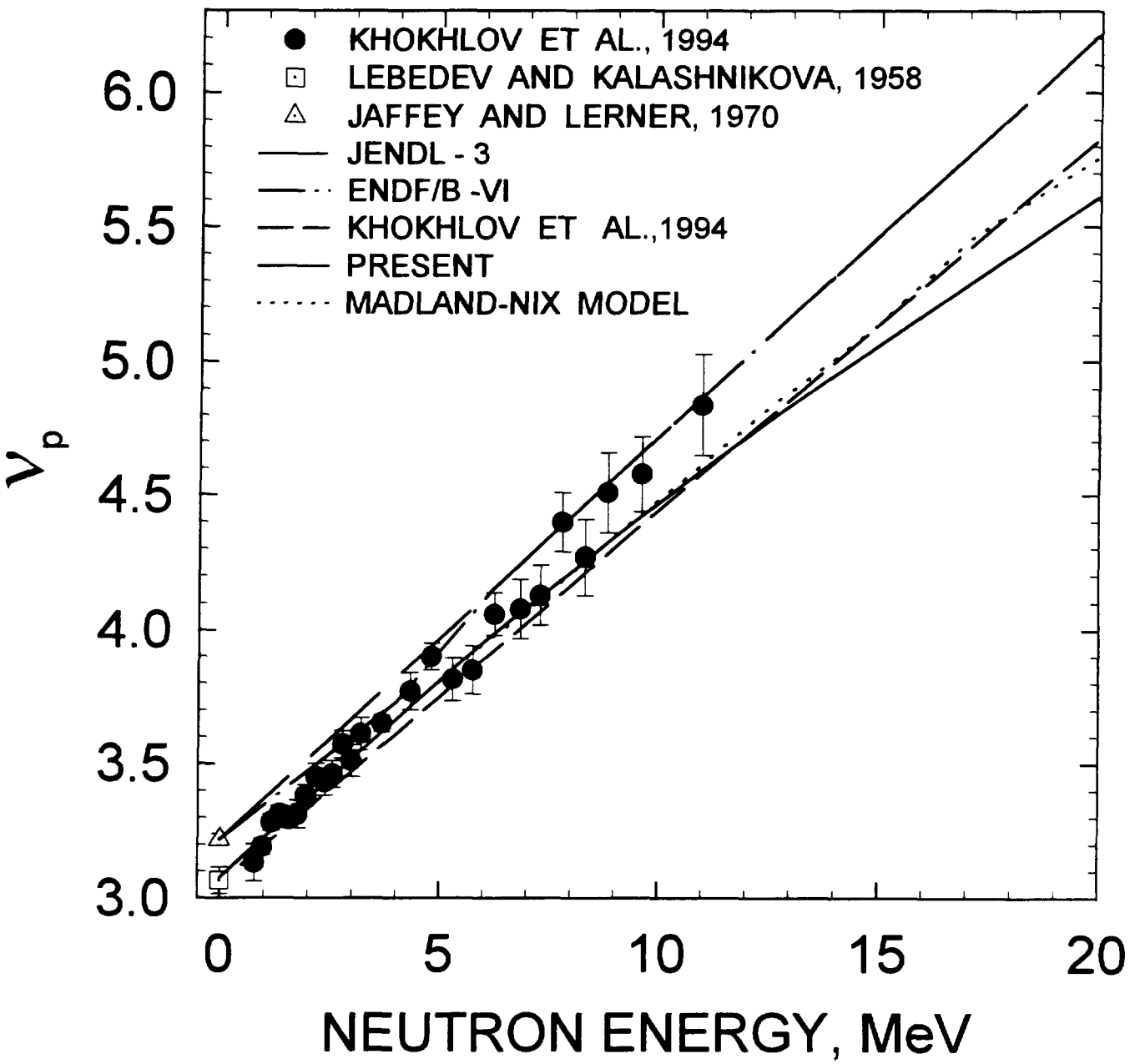

FIG.6.1

Nuclear Data Section
International Atomic Energy Agency
P.O. Box 100
A-1400 Vienna
Austria

e-mail, INTERNET: SERVICES@IAEAND.IAEA.OR.AT
fax: (43-1)20607
cable: INATOM VIENNA a
telex: 1-12645 atom a
telephone: (43-1)2060-21710

online: TELNET or FTP: IAEAND.IAEA.OR.AT
username: IAEANDS for interactive Nuclear Data Information System
username: ANONYMOUS for FTP file transfer
username: FENDL for FTP file transfer of FENDL files
For users with web-browsers: http://www.iaea.or.at